An Acoustic Sensor for Measuring Traffic Variables

by

Ramona Hui Tung

Submitted to the Department of Electrical Engineering and Computer Science
in partial fulfillment of the requirements for the degree of

Master of Science in Electrical Engineering

at the

MASSACHUSETTS INSTITUTE OF TECHNOLOGY

September 1994

Author ... .
Department of Electrical Engineering and Computer Science
June 6, 1994

Certified by.....
James K. Roberge
Professor of Electrical Engineering
Thesis Supervisor

Certified by.....
Anthony F. Hotz
Off-Campus Supervisor
Thesis Supervisor

Accepted by .....
Frederic R. Morgenthaler
Chairman, Departmental Committee on Graduate Students

An Acoustic Sensor for Measuring Traffic Variables

by

Ramona Hui Tung

Submitted to the Department of Electrical Engineering and Computer Science
on June 6, 1994, in partial fulfillment of the
requirements for the degree of
Master of Science in Electrical Engineering

Abstract

The Intelligent Vehicle-Highway System (IVHS) program requires a large number of sensors to accurately measure traffic data. A novel passive acoustic sensing scheme based upon a triple-aperture microphone array is proposed as an inexpensive, reliable alternative to other sensors under consideration. A single sensor exhibits the potential for monitoring several lanes of traffic simultaneously. An algorithm for determining vehicle speed and range from the microphone outputs is discussed and directions for future research are identified.

Thesis Supervisor: James K. Roberge
Title: Professor of Electrical Engineering

Thesis Supervisor: Anthony F. Hotz
Title: Off-Campus Supervisor

Acknowledgments

I would like to thank the MIT Lincoln Laboratory and Group 76 for their continual support of my work over the last four years (the last two of which were devoted to the research for this thesis). Special thanks go to Tony Hotz and Rob Gilgen who first suggested the use of microphones for traffic sensing, to Professor James K. Roberge, Dr. Richard Lacoss, and Professor Amar G. Bose who always made available their technical expertise and suggestions, and to Lenny Lopez who went above and beyond the call of duty to make sure the experimental work ran smoothly.

I am deeply indebted to Carl Much, the leader of Group 76, who consistently went out of his way to insure that I had everything I needed. I doubt that I will ever meet a more caring and supportive technical manager. I am also especially grateful to Tony Hotz for providing insight and intellectual stimulation (and exasperation...) in *all* areas (and for putting up with me as his first, and probably last, thesis student for the past two years). In addition, I would like to thank all the members of Group 76 (current and former) whose friendship and encouragement made working at Lincoln a real pleasure.

Last, but not least, I would like to thank my family and friends for believing in me. And finally, thanks to Avi, for giving me an incentive to finish...

Contents

List of Figures

List of Tables

Chapter 1

Vehicle Sensing

1.1 Objectives

Broadly stated, the proposed Intelligent Vehicle-Highway System (IVHS) is a national program which will use advanced technology to help solve transportation problems and improve safety. For example, some strategies for congestion management will attempt to optimize traffic flow by providing dynamic route guidance to vehicles based upon advance destination information from individual vehicles and real-time information from roadway sensors. Many sensors will be required for such applications and in order to minimize the cost of IVHS, low-cost sensors are desirable. Moreover, the sensors should be durable, require little maintenance, and remain insensitive to variable illumination, weather, and road conditions. However, they must provide accurate and reliable traffic information. Some important traffic data which must be measured includes detection of passing vehicles, vehicle location (lane determination), vehicle speed, and vehicle class.

1.2 Current Sensing Options

Sensing schemes currently under consideration for IVHS applications include visible and infrared video, "dead reckoning" (using the Global Positioning Satellite network), passive inductive (using buried loop detectors), ultrasonic, vehicle transponder, and

passive acoustic systems[3] [6]. These can be loosely subdivided into "continuous" and "discrete" sensors. The advantages and disadvantages of each of these is discussed briefly.

1.2.1 Continuous Sensors

"Continuous" sensors, which include video, infrared, and "dead reckoning" systems, are capable of monitoring long stretches of road with a single sensor. Through sophisticated image processing algorithms, visible light video systems detect and classify vehicles, as well as measure speed and estimate queue lengths. However, their accuracy and reliability is often hampered by poor lighting and weather conditions (fog, rain, snow). Alternatively, infrared cameras, which are relatively insensitive to variable lighting and weather conditions, can perform similar functions, but the considerable expense for cryogenic cooling makes them unattractive. Uncooled infrared arrays are under development and prototypes exist, but they remain more costly than most other sensors under consideration. A "dead reckoning" system would use the Global Positioning Satellite (GPS) network to report a vehicle's exact location. Such a system would be extremely accurate but would require each vehicle to be equipped with GPS or cellular communication equipment, thus putting a large share of the system cost on the users. In addition, an efficient communications link would be required for handling vehicle position reports. For many IVHS applications, it is more important to monitor traffic flow patterns rather than individual vehicles. Since the GPS network provides a higher level of precision than is necessary, it seems more practical to use a simpler, cheaper sensing system.

1.2.2 Discrete Sensors

"Discrete" sensors, which include passive inductive, ultrasonic, vehicle transponder, and passive acoustic systems, obtain traffic data by considering individual vehicles. Passive inductive systems use buried inductive loops to count passing vehicles. A pair of inductive loops closely spaced can also supply speed information. In contrast,

mounted above the roadway, ultrasonic sensors measure reflections of transmitted signals from a vehicle passing beneath the sensor to get estimates of vehicle height and length for classification. Vehicle speed is determined by measuring the Doppler velocity of the moving target. In vehicle transponder systems, vehicles are equipped with "transponders" that respond with a coded reply when a coded signal from an "interrogator" is received. The interrogator then measures the response delay and Doppler shift to determine range and speed. Additional information can be coded into the reply message, making transponders attractive for a wide range of IVHS applications from automating toll collection to providing driver information. Passive acoustic systems extract vehicle information from the outputs of microphone arrays directed toward the traffic. These outputs are correlated and processed to estimate parameters such as speed, range, bearing, and direction of travel.

An important issue for "discrete" sensors is cost (for the sensors, installation, and maintenance) since a large number of closely-spaced sensors are required to monitor traffic flow. Although presently widely used, inductive loops are expensive to install and maintain because they are large and must be buried. Most likely, for IVHS applications they will be augmented with other less expensive sensors. In an ultrasonic sensing scheme, the active transmitters consume power. Furthermore, the sensors require costly overhead mounting structures for installation. In vehicle transponder systems, the cost is shared between the traffic control system (interrogators and processors) and the users (transponders). Because the interrogators are active and the transponders can be either active[1] or passive[2], there will be some power requirements. Moreover, the high frequency radiation from the interrogators may raise health issues from the general public. Placement of the interrogators also requires consideration. The possibilities, which include mounting them overhead, building "toll booth"-like structures to house them, or burying them in the road, could be quite expensive.

Alternatively, passive acoustic systems, which are among the newest of the proposed sensing schemes, are of interest because the sensing elements are microphones

[1] By sending a digital message

[2] by reflecting a fraction of the interrogator power back to the source

which are inexpensive and widely available. In addition, the sensor package could be installed at the side of the road with minimal effort and equipment, which facilitates servicing. Conceivably, a sensing scheme which tracks vehicles with an array of closely-spaced microphones would prove an inexpensive, reliable, low-maintenance alternative to the methods mentioned earlier.

1.3 Proposed Sensing Scheme

This thesis explores the development of a passive acoustic sensor based upon a triple-aperture microphone array. The microphone outputs are correlated to estimate the delays (which will be denoted by τ) between the time a source signal is received at one microphone relative to the next. From the geometry of the problem, if the delay estimates are accurate enough, a vehicle's position and speed can be determined. Methods for improving the accuracy of the τ estimates and for removing biases in range and bearing estimates obtained from noisy delay estimates can be found in many underwater signal processing texts such as the one by Joseph C. Hassab [2].

When the proposal for this thesis was submitted on February 9, 1993, a literature search conducted at the MIT Lincoln Laboratory had not turned up any articles mentioning the use of microphones in vehicle sensing schemes. However, in April of 1993, AT&T announced it was developing a passive acoustic sensor (the SmartSonic^{TM} TSS) using technology from anti-submarine warfare research [4] [5]. Their sensor is based upon an array of 60 microphones in a package the size of a pizza box which is mounted overhead on existing fixtures along the side of the road. Using beamforming techniques, the sensor focuses on a 10' x 6' section of road (i.e.. one lane) and monitors the traffic flow through this square, concentrating on the frequency range from 4 to 6 kHz. It provides accurate traffic counts and occupancy for the lane under surveillance and is able to distinguish between larger vehicles (such as trucks and buses) and automobiles.[3] At the present time, AT&T is trying to expand the capabilities of its sensor to monitor two lanes and provide vehicle classification. Currently, the

[3]Based primarily on signal amplitude.

sensor is reported to cost around $2000.

In contrast, the passive acoustic sensor proposed in this thesis is composed of "off the shelf" components and primarily uses simple correlation techniques for processing. Experimental results indicate that the proposed sensor is capable of monitoring traffic simultaneously in *both* directions on a road with a single lane of travel in each direction. It further suggests that with additional processing, a single sensor will be able to monitor roads with *multiple* lane traffic in both directions. This issue will be pursued in the future. Vehicle classification has not been examined closely, but seems feasible with further processing. The potential of this passive acoustic scheme combined with its low cost make it an idea worth developing and considering as a viable alternative for IVHS applications.

Chapter 2

Sensor Components

2.1 Overview

The sensor package, which is installed at the side of the road a few feet off the ground, consists of an array of three microphones[1] and associated processing hardware. The outputs of the microphones are first amplified and bandpass-filtered before being digitized for processing. Processor architecture has not been investigated in detail, but is expected to be simple and inexpensive since current algorithms require only basic operations.

The use of accelerometers to detect vehicle vibration through the road bed was also explored but ultimately rejected. It was hypothesized that road vibration patterns could be analyzed to extract source vehicle information. To minimize transmission loss, accelerometers were glued to circular aluminum disks which were attached directly to the road surface with long carpentry nails. Unfortunately, the accelerometers used, which were quite sensitive, did not pick up any ground vibration at all. Seismic accelerometers, which are ten times more sensitive, are available but too expensive to consider. In retrospect, it appears unlikely that accelerometers would provide any information not obtainable from processing microphone outputs. Nevertheless, because they were a key component in the initial design, accelerometers will be included in

[1] Or "acoustic centers" if beamforming techniques are employed.

the description of the sensor design and evaluation phases.

2.2 Microphones

In the design of the passive acoustic traffic sensor, both ultrasonic and audible range microphones were considered. The current sensor algorithm depends solely on the outputs of audible range microphones. Nonetheless, data was collected from both types of microphones to allow development of future algorithms which might incorporate ultrasonic sensor outputs for improved accuracy and reliability. The benefits and disadvantages of each type of microphone are discussed briefly below.

It has been found that correlating the outputs of audible range microphones yields reliable speed estimates for relatively low sampling rates when the signal-to-noise ratio (SNR) is high. The fact that these microphones are inexpensive and widely available makes them even more interesting for IVHS applications. The main concern over audible range microphones is their sensitivity to a wide variety of background noise which could corrupt measurements. Some form of active filtering might be required for robustness in low SNR cases.

On the other hand, ultrasonic microphones (with a frequency range from 15-30 kHz) are attractive because they are especially sensitive to tire/road interface noise yet insensitive to most background noise. The drawbacks are that they are slightly more expensive, not as readily available, and require higher initial sampling rates and more sophisticated processing techniques. Yet ultrasonic microphones are worth examining because of the push in the automotive industry toward designing quieter vehicles. If electric cars ever become popular, vehicles will be virtually silent. Quiet vehicles may present difficulties for sensing systems focusing on audible emissions. However, ultrasonic microphones do not face this problem due to their sensitivity to tire/road interface noise. No matter how silent a vehicle is, as long as it has wheels it remains detectable by ultrasonic microphones.

2.2.1 Audible Range Microphones

A wide variety of microphones are commercially available for all types of acoustic applications. A number of criteria were considered in the selection of a suitable audible range microphone:

1. Cost
2. Bandwidth
3. Sensitivity
4. Flatness of its frequency response
5. Directivity (directional vs. omnidirectional)

Because the IVHS program will require large numbers of reliable traffic sensors, an inexpensive, sensitive microphone with a flat frequency response was sought. Furthermore, a wide bandwidth was desired because at the time, frequencies of interest had not been determined. Finally, directional (cardioid) microphones were preferred over omnidirectional microphones since the spatial region of interest (i.e., the road) lies directly in front of the array. Omnidirectional microphones introduce noise from other directions which would degrade performance.

On the basis of these criteria, two audible range microphones were selected. The first was a general-purpose omnidirectional electret microphone from Radio Shack (catalog # 270-090) shown on the left in Figure 2-1. This choice was based largely upon cost and immediate availability. The microphone proved fairly sensitive, although it was completely uncalibrated. The obscure frequency response curve which accompanied the sensor appears in Figure 2-2. Consequently, it was only used in a series of controlled tests to collect preliminary data. The second microphone was a low-cost, cardioid microphone from Sennheiser (model # KE 10-420) depicted on the right in Figure 2-1. As reflected by its frequency response curve in Figure 2-3, it meets the high sensitivity, wide bandwidth, and flat response requirements fairly well. These microphones were used to obtain traffic data from an actual road. Sensor

algorithm development and evaluation were conducted primarily with data from the Sennheiser microphones.

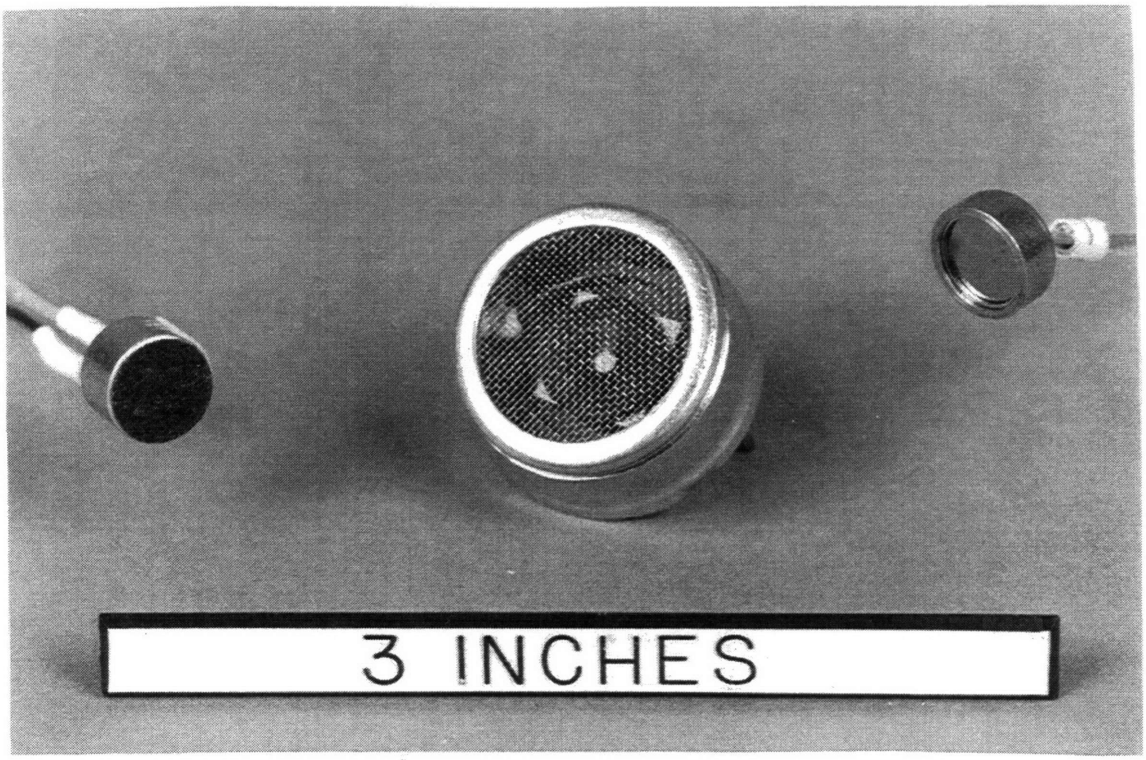

Figure 2-1: Photograph of microphones used to collect traffic data
(from left: Radio Shack 270-090, Murate-Erie MA23-L3-9, Sennheiser KE 10-420)

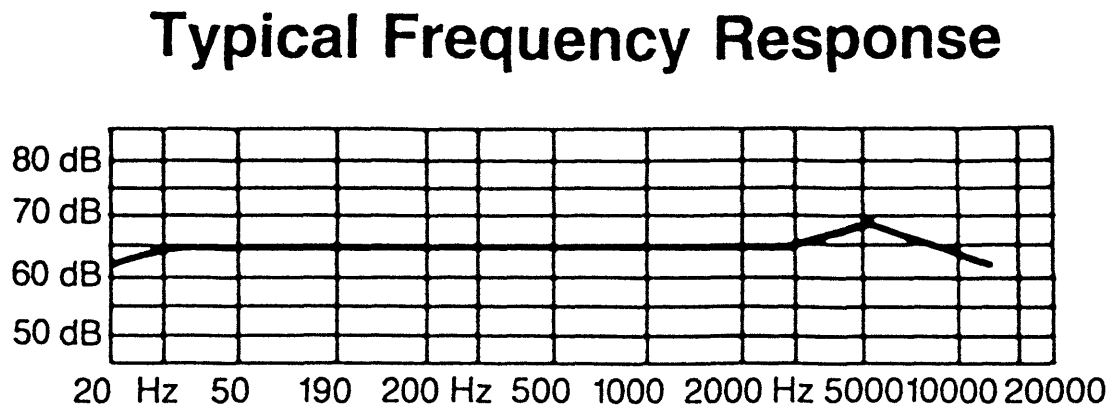

Figure 2-2: Frequency response of Radio Shack 270-090 microphones

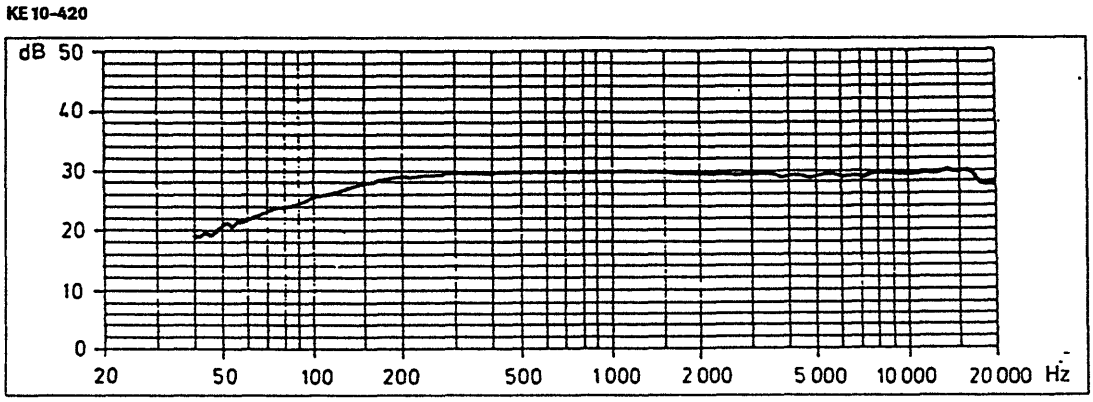

Figure 2-3: Frequency response of Sennheiser KE 10-420 microphones

2.2.2 Ultrasonic Microphones

There are several motivations behind the strong interest in ultrasonic microphones. Initially, they were considered in conjunction with the idea of tagging vehicles with acoustic identifiers (which is described in Appendix A). Likewise, there was speculation regarding the possibility of ultrasonic emissions from engine components. Moreover, from a signal processing standpoint, since the amount of ultrasonic background noise is minimal, algorithms focusing on ultrasonic frequencies would likely exhibit superior performance due to higher signal-to-noise ratios (SNR). With these ideas in mind, a low-range ultrasonic microphone whose frequency response overlapped the audible range was sought. Overlap was desired so that potentially interesting frequency bands would not be overlooked.

A survey of the market revealed only a few ultrasonic microphone manufacturers. Chief among these were the producers of precision instrumentation sensors (which were extremely expensive) and the manufacturers of ultrasonic imaging sensors. Most ultrasonic imaging sensors had frequency ranges which were greater than 40 kHz, but luckily, one was found which had a nominal frequency of 23 kHz and a bandwidth of 6 kHz centered about the nominal. This microphone was the Murata-Erie MA23-L3-9 depicted in the center of Figure 2-1. Five samples were procured before the part was discontinued in September 1993.

While examining the output of an ultrasonic microphone with an oscilloscope, some interesting observations were made. It was discovered that they are *extremely* sensitive to impulsive or abrasive sounds.[2] This observation indicates that the microphones should sense tire/road interface noise, although they are just as likely to detect pedestrians. Distinguishing a vehicle from a person is not difficult (see Section 3.2.2). To their advantage the ultrasonic microphones did not appear particularly sensitive to speech, planes, or wind (generated by a fan). All of these are factors which could degrade the performance of audible range microphones.

[2]Some examples of impulsive sounds are honking, clapping, coughing, or a door slamming. Abrasive sounds include scraping, rubbing the hands together, and scuffing the feet.

2.3 Accelerometers

An idea trading session sparked interest in two potential applications of accelerometers in the vehicle sensor. In one instance, accelerometers are directly attached to or embedded in the road bed to measure ground vibration patterns. If sensitive enough to detect ground vibration, they should at least be able to distinguish between large, heavy vehicles (such as trucks and buses) and smaller, lighter ones. In an alternative application, an accelerometer with a frequency range extending down to dc is mounted on a flexible membrane. By measuring air vibration it might theoretically serve as a low frequency "microphone".

There was a large assortment of accelerometers to choose from because of their extensive use in projects conducted at the MIT Lincoln Laboratory. Since signals from ground vibration were expected to be low frequency (up to a few Hz) with small amplitudes, the most sensitive accelerometers available were obtained. Cost was not a factor because sensors could be borrowed for determination of sensitivity requirements. Thus, some calibrated Sundstrand QA700 accelerometers (depicted in the center of Figure 2-4) with a sensitivity of 1 V/g (from dc to 300 Hz) were obtained for use in field tests. Though too expensive for use in an IVHS sensor, the QA700s permitted a qualitative evaluation of the feasibility and practicality of using accelerometers in a vehicle sensing scheme. PCB 336B04 piezoelectric accelerometers (seen on the right in Figure 2-4) with a sensitivity of 100mV/g (from 1 to 2000 Hz), were also placed on the road to collect vibration data. Despite lower sensitivity, they are more suitable for IVHS because of their cost.

For the low frequency "microphone", a lightweight accelerometer was required since it would be attached to a flexible membrane. The new ADXL50 accelerometer chip (displayed on the left in Figure 2-4) from Analog Devices was chosen because it was light, cheap, and able to measure accelerations down to dc. Its frequency response is provided in Figure 2-5.

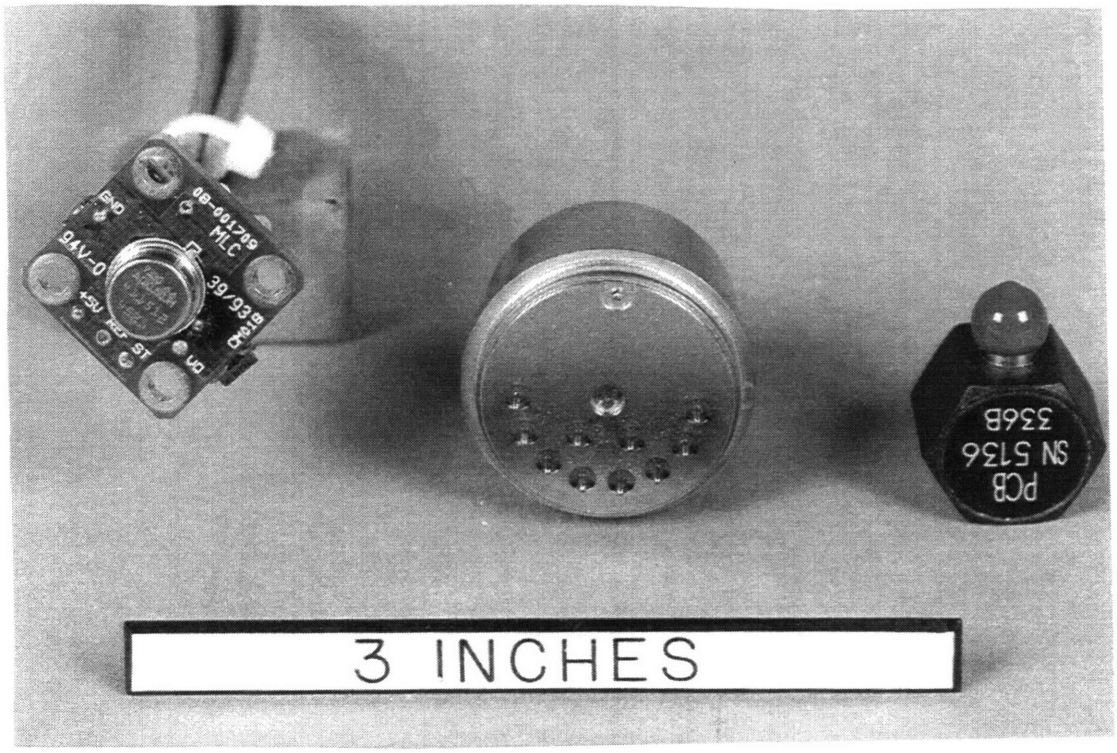

Figure 2-4: Photograph of accelerometers used to collect traffic data (from left: Analog Devices ADXL50, Sundstrand QA700, PCB 336B04)

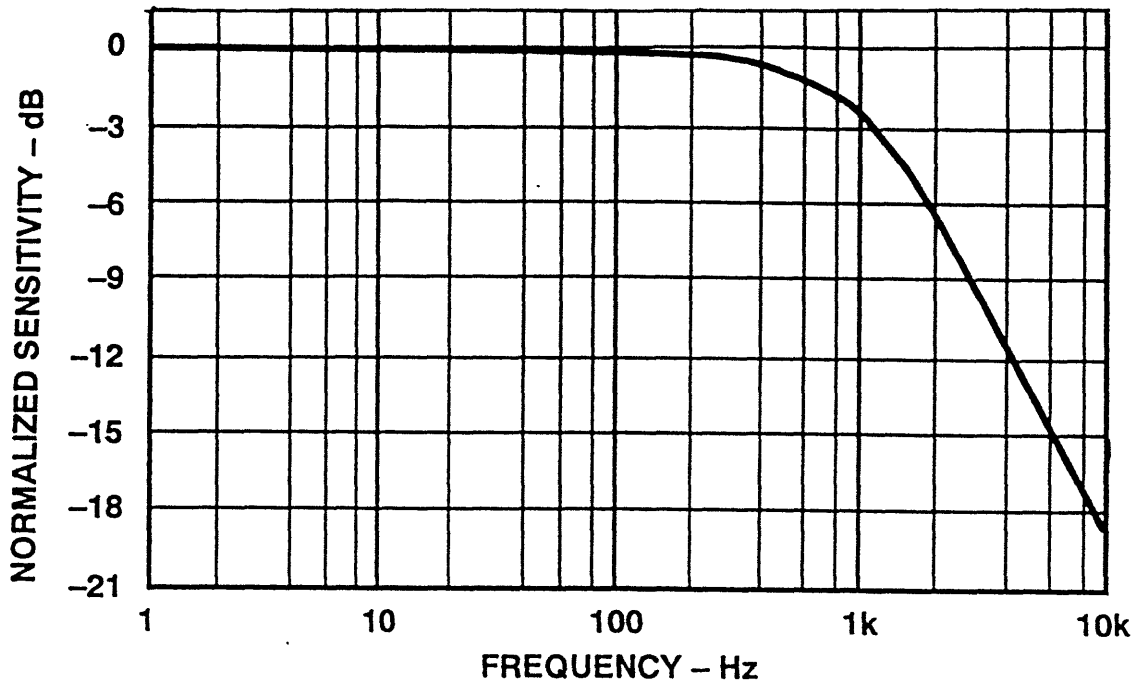

Figure 2-5: Frequency response of Analog Devices ADXL accelerometer

2.4 Amplifiers

The sensitivities of the microphones and accelerometers were enhanced with electronic amplifiers. For the Sundstrand and PCB accelerometers, signal conditioners were already available. However, ac amplifiers were designed and built for the microphones and the ADXL50 accelerometer.

The amplifier designs for the Radio Shack and Sennheiser microphones and the ADXL50 accelerometer exhibit the same structure. A block diagram of the amplifier appears in Figure 2-6. After appropriately powering the sensor, its output is ac coupled, amplified, then bandpass filtered to reduce noise. Circuit diagrams are provided in Appendix B in Figures B-1, B-2, and B-3.

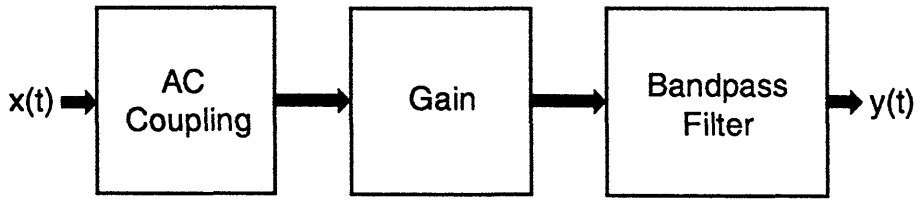

Figure 2-6: Block diagram of AC amplifier design

An amplifier design for the Murata Erie ultrasonic microphones was provided in the specification sheets. The design was modified slightly to avoid gain/bandwidth problems. The final circuit diagram appears in Appendix B in Figure B-4.

A photograph of one of the amplifier modules appears in Figure 2-7. This hardware realizes the amplifiers for five Sennheiser microphones and five ultrasonic microphones. In the future, all requisite amplifier hardware will be part of the sensor package.

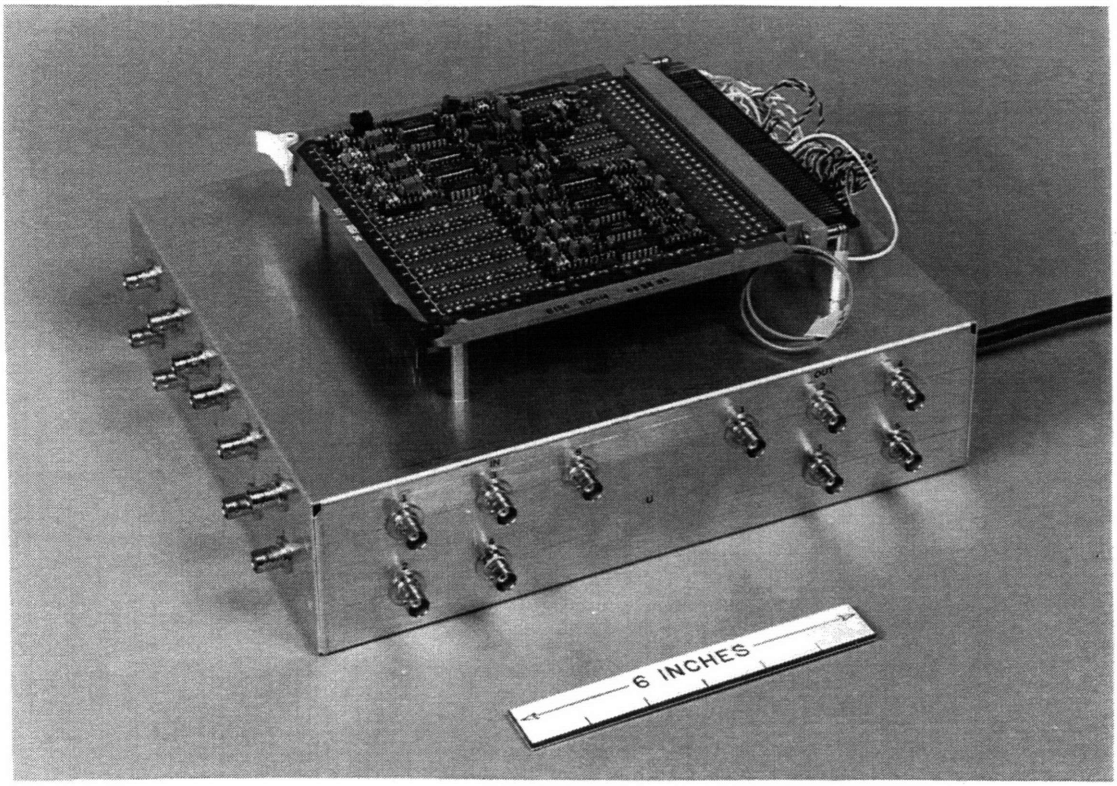

Figure 2-7: Photograph of amplifier module
(for 5 Sennheiser and 5 Murata-Erie microphones)

Chapter 3

Experimental Procedure

3.1 Test Plan

To get a sense of the bandwidth and shapes of the signals that would be detected on a real road, data was collected in a series of controlled experiments conducted on an experimental track at the MIT Lincoln Laboratory. The main facility of the MIT Lincoln Laboratory is located on Hanscom Air Force Base in Lexington, MA. Microphones and accelerometers were placed in various positions to detect vehicles traveling at constant speed, accelerating, braking, and honking. Analyzing this data provided insight which led to preliminary algorithm development and the decision to base the sensor on a triple-aperture microphone array. In addition, some general effects from acoustic noise sources such as planes, machinery, wind, and people (talking or walking by) were noted.

Following the controlled experiments, an array of both audible range and ultrasonic microphones was placed at the edge of the driveway of the MIT Lincoln Laboratory annex at 45 Hartwell Avenue to collect real traffic data. Located in Lexington, MA, Hartwell Avenue is one of the main roads that leads to Hanscom Air Force Base. It is a bidirectional roadway with two lanes of traffic on each side. Due to saturation of the audible range microphones on the first day of road testing, a gain stage was removed from their amplifiers and the experiment repeated on another day. In a third road test, the microphone configuration was altered to assess the performance of a

range estimation technique. Traffic was light on all three days during data acquisition.

Getting the data into a form which allowed it to be processed required several steps. In all instances, data was stored on beta tapes using a 14-channel Kyowa-Dengyo analog recorder. The recorder had a bandwidth of approximately 20 kHz when set at the fastest recording speed of 76 $\frac{cm}{s}$. The frequency response of the recorder was gauged by varying the frequency of a 4 volt peak-to-peak sinusoidal input and measuring the amplitude decay. The results are plotted in Figure 3-1. The recorded analog data was passed through an anti-aliasing filter (a Sallen-Key lowpass filter whose circuit diagram appears in Appendix B) before being digitized and stored using Lab Windows running on a PC. In practice, the data acquisition card allowed a maximum *total* sampling rate ($f_{s_{max}}$) of 85-90 ksps.[1] In the Lab Windows environment, data was viewed and sections selected for conversion to ASCII format. Finally, data analysis and algorithm development were conducted using Matlab.

3.2 Controlled Experiments

Three series of controlled experiments (Field Tests One, Two, and Three) were performed and are outlined in this section. The objectives of these tests were to:

1. Identify frequency range(s) of interest
2. Determine the number of sensors needed and suggest their placement
3. Qualitatively assess the sensitivity and range of uncalibrated microphones
4. Provide a starting point for preliminary algorithm development
5. Examine the effects of possible noise sources
6. Start a database for future algorithm development

The experiments performed and insights developed during the three Field Tests are described in the following subsections.

[1]Since the sampling scheme is multiplexed, the maximum sampling rate *per channel* is $\frac{f_{s_{max}}}{N}$, where N is the number of channels simultaneously sampled.

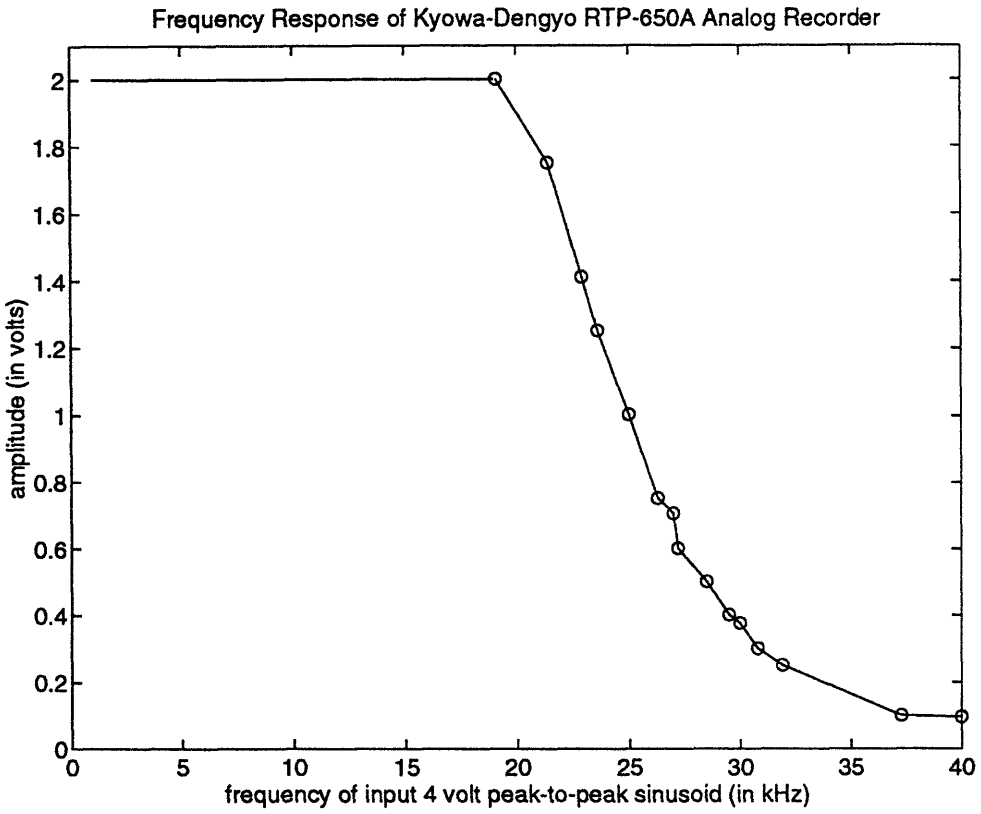

Figure 3-1: Approximate frequency response of the analog recorder

3.2.1 Field Test One

The first field test was conducted in an alley behind the high bay of Building I at the MIT Lincoln Laboratory. The test site was convenient and offered few distractions from other vehicles. The acoustic noise environment that day included some machinery noise from the building's ventilation system, light wind in the alley, and a few random noises like doors slamming and people walking. The experimental configuration is detailed in the drawing of Figure 3-2. An assortment of sensors were placed along the side of the "road" to collect data.

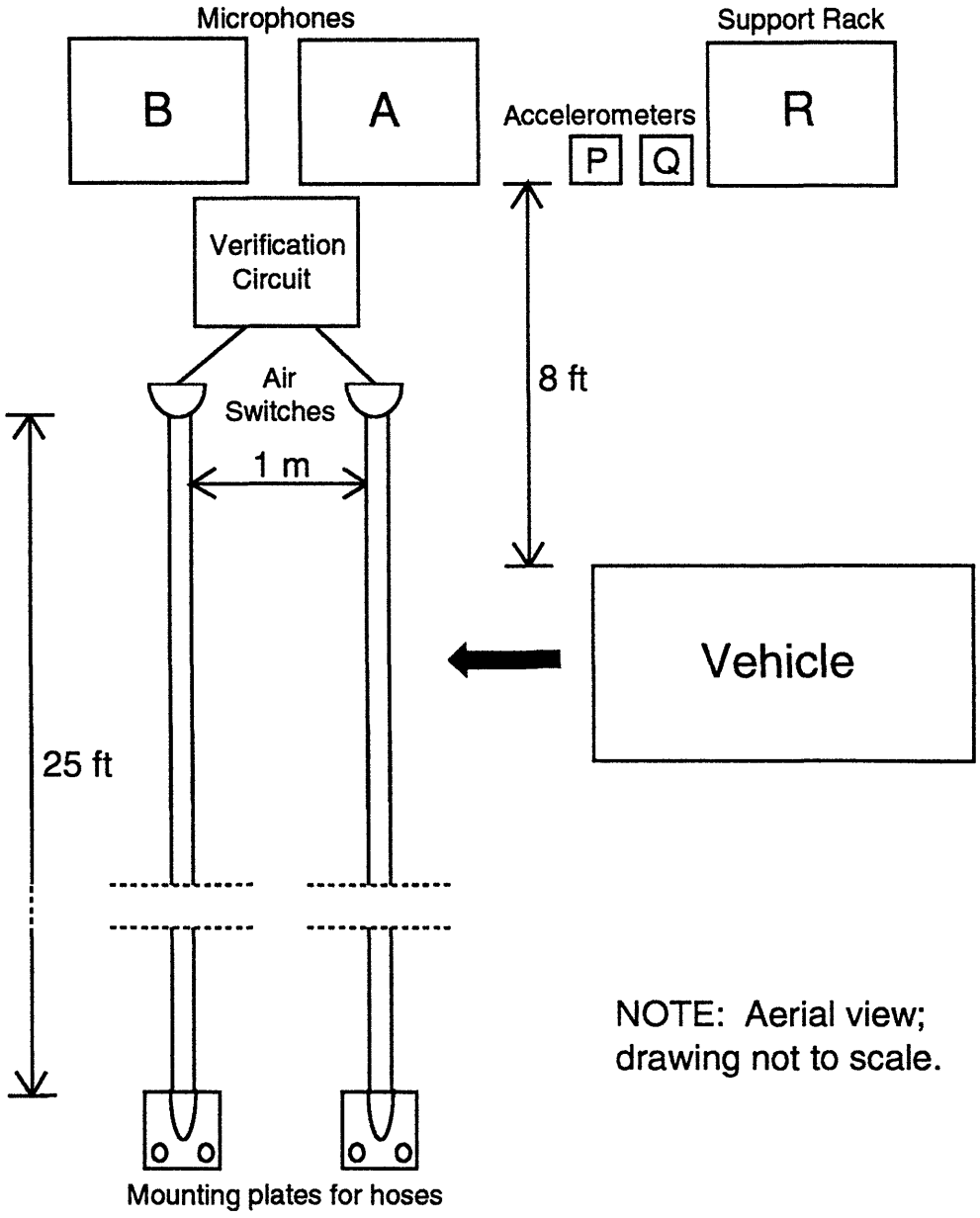

Figure 3-2: Experimental configuration for Field Test One

The microphones were placed in the fixtures labeled as A and B in Figure 3-2. Both assemblies had the structure displayed in Figure 3-3. Mounted at the top of a hollow aluminum pole (which provided support) was an 18-inch diameter radar dish with an omnidirectional Radio Shack microphone at its focal point. The parabolic reflectors were included for two reasons: to make the microphones directional and to determine if their use would greatly improve measurements. Halfway down the pole, three microphones spaced 4 inches apart were positioned on a mounting box (Radio Shack in Assembly A, ultrasonic in Assembly B). The mounting boxes for both arrays are shown in Figure 3-4. The box was attached to the pole using tie wraps. At the base of the assembly was a mount that was attached to the pavement with long carpentry nails.

The verification system used for Field Test One was comprised of a pair of air hoses spaced one meter apart and associated digital circuitry. An air switch at the end of each hose provided a low TTL pulse when a vehicle's wheels ran over the hose. The outputs of the two air switches were routed to the verification circuit which is described in Appendix C. Essentially, each signal is debounced, then fed into a simple finite-state machine which starts a counter when the front wheels cross the hose at A and stops it after they cross the hose at B. Knowing the distance between the hoses and the time it took to cross both of them gives the speed of the vehicle.

Accelerometers were placed in triaxial mounts labeled P (for PCB) and Q (for QA700) in the diagram of Figure 3-2. The mounts were attached to the road with long carpentry nails. The direction of the measurement axes are identified in Figure 3-5. Along with the microphone amplifiers and analog recorder, the signal conditioners for the accelerometers were found on the rack labeled R.

During Field Test One, a vehicle was driven past the sensors at a distance (R_y) of about 8 feet. Henceforth, the vertical range component, R_y, will denote the perpendicular distance between the sensor array and the lane of travel. Several experiments were conducted, some in which the vehicle was traveling at constant speeds, others where the vehicle was accelerating or braking. A few trials also included the vehicle honking. Two different vehicles, a Subaru XT6 and a Toyota pickup truck, were

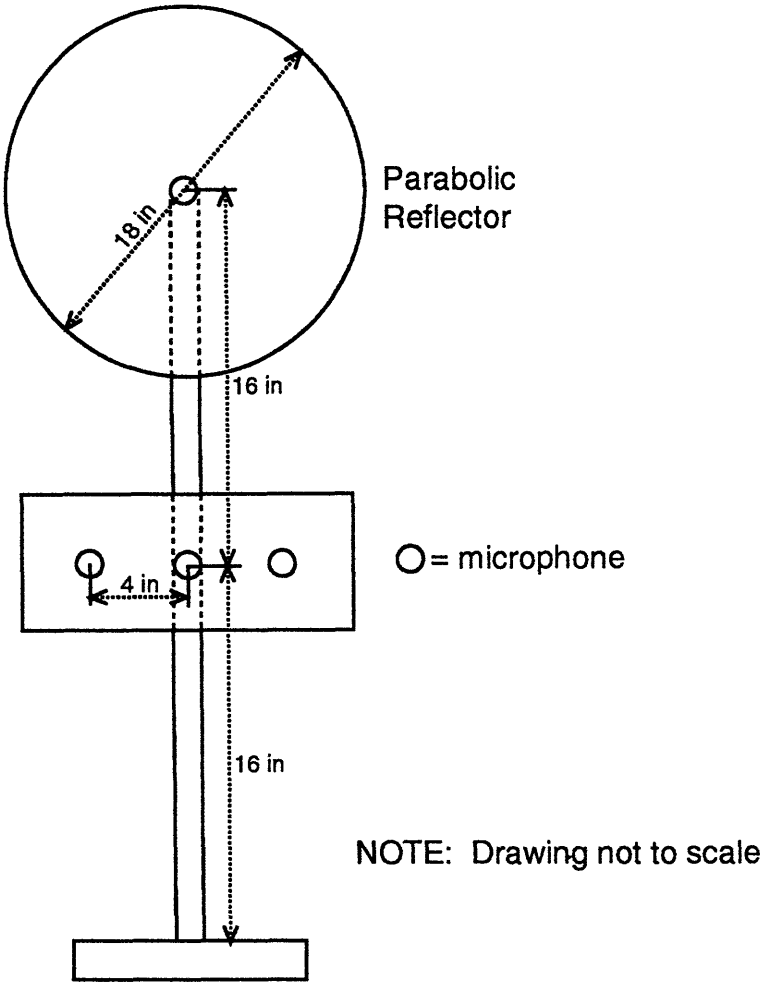

Figure 3-3: Microphone assembly for Field Test One

driven for comparison. The primary goals of Field Test One were to identify frequency bands of interest and begin a database of basic "traffic" situations to be used for algorithm performance evaluation.

In the spectra for both vehicles, signal power is dominant for frequencies up to 8 kHz as seen in Figure 3-6. However, in the band between 8-15 kHz, noise seems to be the major contributor. Surprisingly, examination of the outputs of the ultrasonic microphones, reveals significant signal power in the range from 15-27 kHz (refer to Figure 3-7. It is uncertain whether there is signal power at frequencies greater than 27 kHz because the frequency response of the ultrasonic microphones begins to roll off at

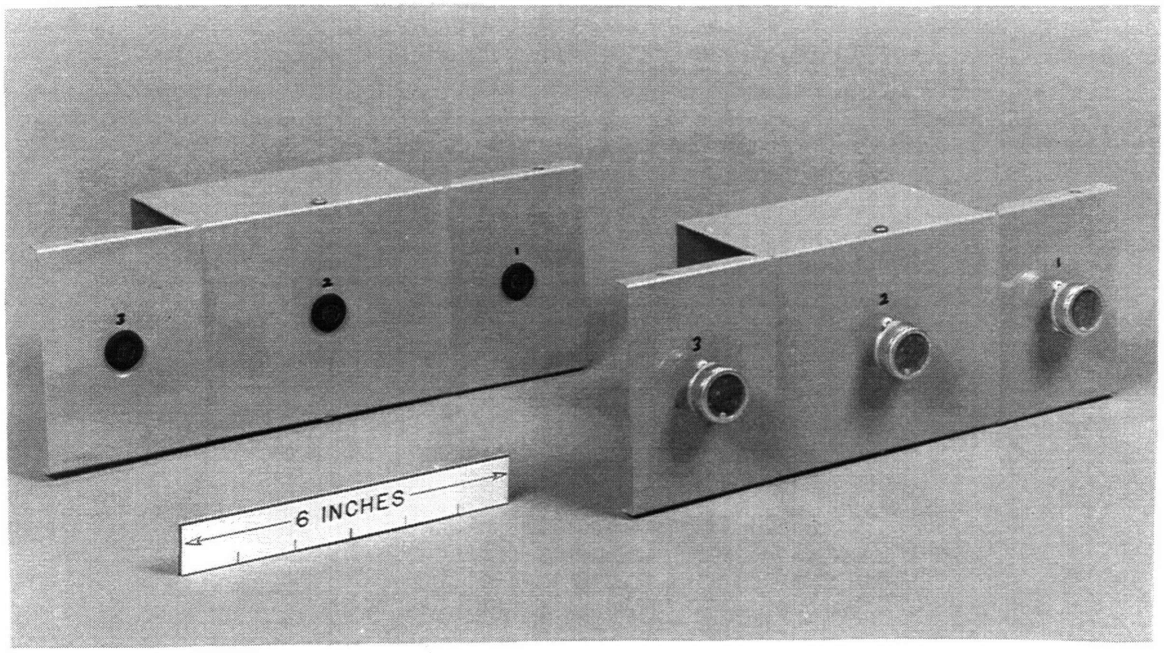

Figure 3-4: Microphone mounting boxes

26 kHz *and* the analog recorder rolls off at 20 kHz.[2] Originally, it was hypothesized that this energy was due to the wind generated by the moving vehicle. However, it was later discovered during Field Test Two that most of the energy at the high end of the spectrum is likely due to tire/road interface noise.

Closer examination of the regions where signal power is dominant does not reveal obvious peaks which can be tracked. This is probably due to the large number of *distributed* acoustic sources in a vehicle, such as the engine in the front and the muffler in the back. Furthermore, if a vehicle proceeds rapidly through the spatial detection zone (especially in the nearest lane), the associated Doppler shift can be large and difficult to track. The difficulty of tracking wideband Doppler shifts led to consideration of alternate processing techniques such as wavelets, short-term Fourier

[2]Signal power up to 27 kHz appears significant enough to be detectable even though the equipment bandwidth is less than 27 kHz.

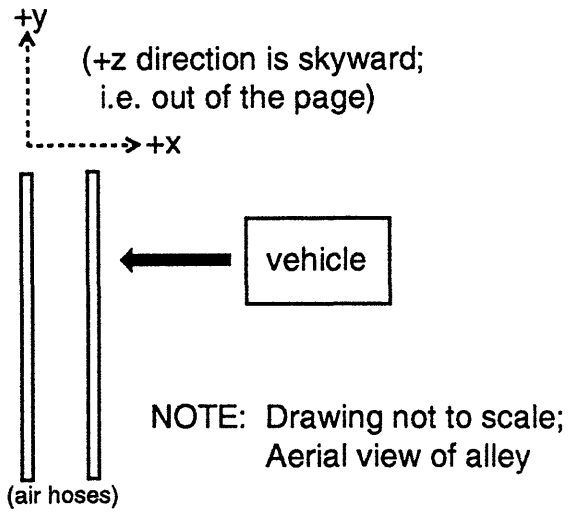

Figure 3-5: Accelerometer measurement axes for Field Test One

transforms, and time correlation.

The speed estimation algorithm which focuses upon tracking the change in time delay between a pair of microphones (refer to Section 4.4) was applied to the data set. The delay in signal arrival time between two spatially separated microphones will be denoted by τ. In Field Test One, the vertical range component (R_y) was known and a three-element array was unnecessary. The shapes of the τ vs. time curves obtained from correlating the outputs of the Radio Shack microphones were exactly as expected, which was promising. There is a tradeoff between using longer correlation windows, which yield smoother curves but are more likely to violate the assumption of quasi-stationarity, and shorter windows, which yield noisier but more accurate curves. For the sampling rate of 35 kHz, using 1000 point correlation windows (overlapped by 500 points) to measure τ returned fairly accurate speed estimates when the τ vs. time plot was fitted with a fifth-order polynomial.

A curve generated using a 1000 sample correlation window (for $f_s = 35$ kHz) with 50% overlap between windows is shown in Figure 3-8. It corresponds to an experiment where the Subaru XT6 was driven by at a constant speed of 14.53 mph (according

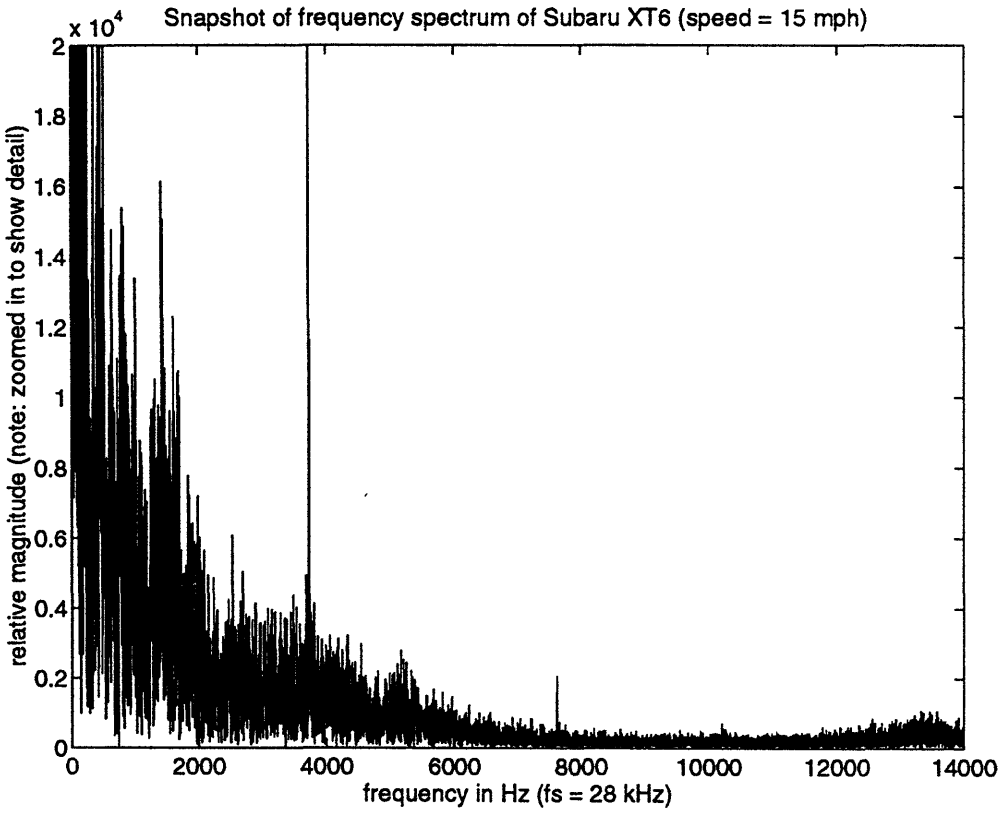

Figure 3-6: Spectrum of the Subaru XT6 as measured by a Radio Shack microphone (snapshot)

to the verification system). Since R_y was very short during Field Test One, *two* τ vs. time curves were distinguishable. These were attributed to acoustic sources in the front (such as the engine and front wheels) and rear (such as the muffler and rear wheels) of the vehicle. After discarding noisy values, a fifth-order polynomial curve-fit yielded speed estimates of 11.27 mph for the front acoustic sources and 14.00 mph for the rear. The separated curves for each set of acoustic sources (augmented with τ estimates from the second and third largest peaks) appear in Figure 3-9.

These speed estimates should be taken as an indication of algorithm *potential* rather than precision. In retrospect, there were several factors which could have degraded the τ estimates ($\hat{\tau}$): aliasing, machinery noise, echoes, the omnidirectional microphones, and the nearness of the sensors to the source. Anti-aliasing filters were not included in the analysis sequence until road test data was analyzed. Consequently,

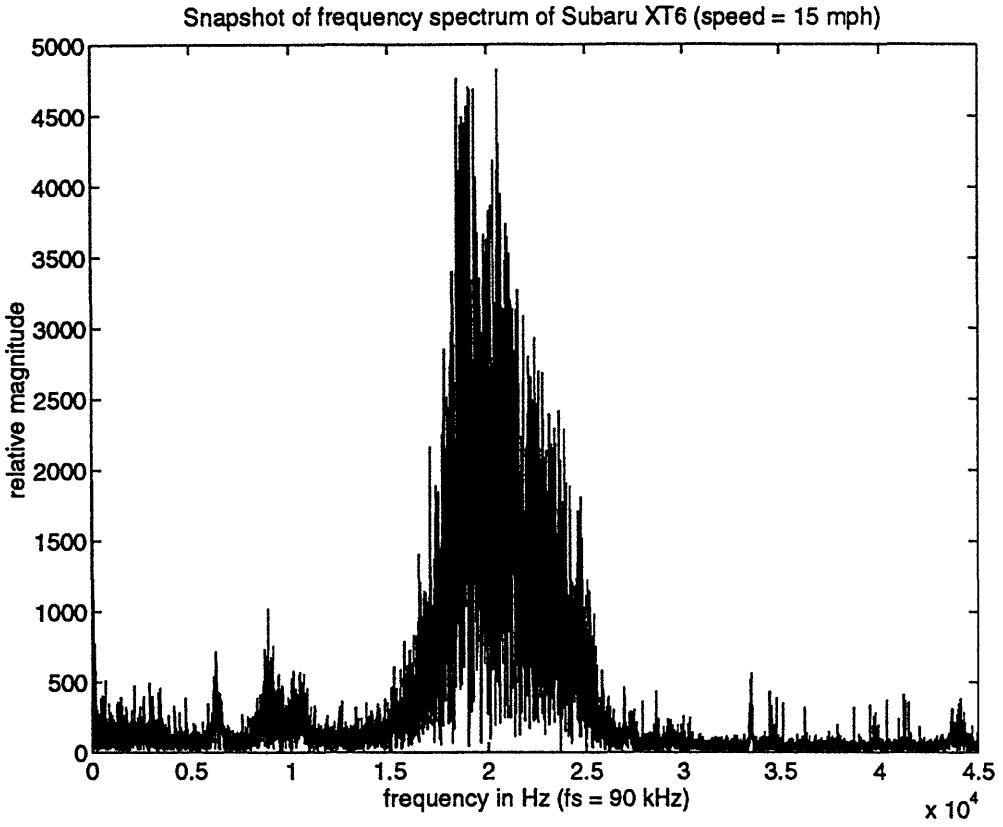

Figure 3-7: Spectrum of the Subaru XT6 as measured by an ultrasonic microphone (snapshot)

in the sampled data from Field Tests One and Two[3], frequencies above 17.5 kHz were aliased down to baseband. As noted earlier, there is a considerable amount of high frequency energy from 17-27 kHz due to tire/road interface noise. Quite possibly, the Radio Shack microphones detected the high frequency contributions, especially since the sensors were situated so close to the lane. To investigate this theory, data from the above experiment was resampled using anti-aliasing filters. The new τ vs. time plot from the filtered data was similar to the original obtained from the unfiltered data. Furthermore, the spectra from both sets of data were nearly identical. Hence, it seems safe to assume that the frequency response of the Radio Shack microphones falls off well below 17 kHz. The remainder of the Radio Shack microphone data from Field Tests One and Two was *not* resampled.

[3]Field Test Three was conducted *after* Road Test Two.

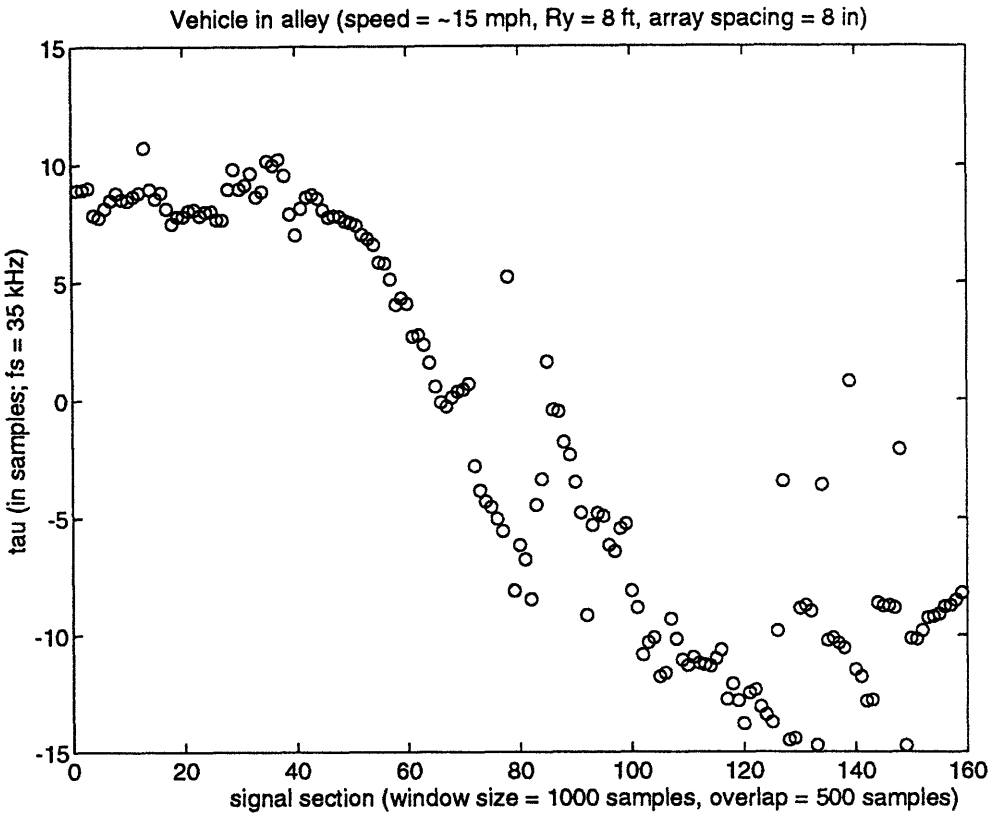

Figure 3-8: τ vs. time for the Subaru XT6
(using only dominant peaks)

There appeared to be a strong low frequency component in the audible range data (at 40 Hz for the car and at 50 Hz for the pickup truck). At the time, it was uncertain whether the "spike" was due to signal or noise power since the frequency response of the microphones was unknown. Nonetheless, in retrospect, it appears that it could be a *signal* component since its magnitude increases as the vehicle approaches and decreases as it departs. The peak did not appear to shift in frequency while the vehicle was in the detection zone which suggested that it might be noise. However, for low frequencies, the Doppler effect (which is a function of frequency) is very small and would *not* be detectable with the given frequency resolution. Currently, it is suspected that it *is* a signal component which warrants further consideration.[4] Determination

[4]For the construction vehicle from Field Test Two, a spike appeared at 80 Hz.

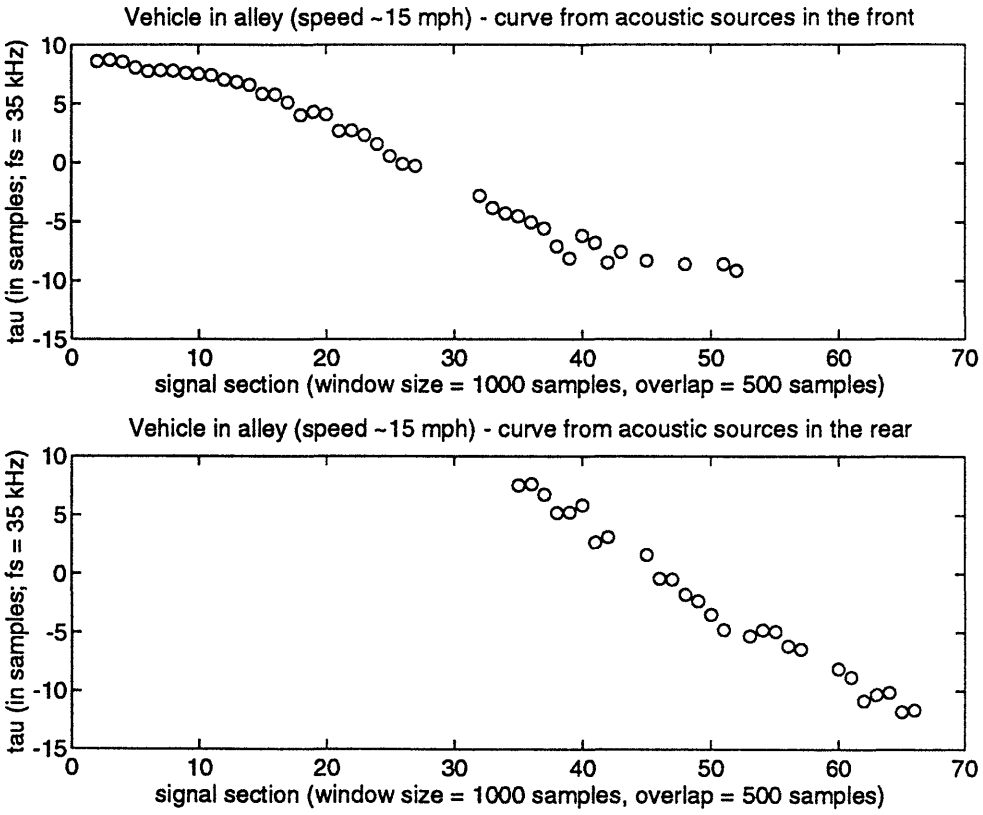

Figure 3-9: Separated curves for acoustic sources in front and rear of Subaru XT6 (after addition of supplemental points)

of whether the spike is definitely due to signal or noise is left for the future.[5]

The large mean squared-errors (MSE) in some of the $\hat{\tau}$ from this data set probably resulted from the close proximity of the sensors to the source and from echoes in the alley. As the vehicle/sensor separation is narrowed, the time interval over which the assumption of quasi-stationarity is valid becomes shorter. Furthermore, the omnidirectional nature of the microphones allowed them to detect sounds from *behind* the array, which included machinery noise and echoes from the wall directly behind the microphones.

With regard to the ultrasonic data (sampled at 45 ksps), the time delay estimates

[5]During the road tests, a two-pole highpass filter with a cutoff frequency of 80 Hz was included which effectively rejected this frequency component along with other noise. The highpass filter was included because the frequency response of the Sennheiser microphones used in the road tests was limited at the low end to 50 Hz.

were much worse. This could have arisen from several factors. First, since there was no anti-aliasing filter applied, frequency components above 22.5 kHz were aliased into the baseband. Furthermore, because the frequencies of interest are high relative to the sampling rate, the number of samples/cycle for a given frequency is very low (3 or less). Thus, inaccuracies from discrete correlation should be expected. Theoretically, if the sampling rate was increased so that the number of samples/cycle was much larger, the $\hat{\tau}$ should improve. The same effect is achieved by bandpass filtering the data from 15-30 kHz then sampling at 30 ksps. In this way, the frequencies from 15-30 kHz will be shifted down to baseband (0-15 kHz) which effectively raises the number of samples/cycle. The algorithm is applied to the bandshifted signal to yield better delay estimates. This idea and others are presently under investigation.

The accelerometers seemed to detect very little motion from the vehicles. Since it is more likely that an accelerometer would sense vertical motion rather than lateral motion when a vehicle passes, a triax seemed unnecessary. Hence when the traffic on Hartwell Avenue was measured, only one accelerometer sensing translational motion was placed on the road.

Strangely enough, the PCB accelerometers pointed in the y and z directions *were* able to detect a vehicle's horn very faintly. It is suspected that the accelerometers were detecting *air* vibration rather than ground vibration. This sparked interest in the possible use of accelerometers for measuring low frequency air vibration since the Sennheiser microphones are not very sensitive to frequencies below 50 Hz. The ADXL50 sensor on a flexible membrane during Road Test One was a crude attempt to realize such a low frequency microphone.

Finally, it was noted that the radar dishes did not seem to offer much improvement for the Radio Shack microphones. They provided only a slight gain increase. Nonetheless, it is possible that they would improve the performance of the ultrasonic sensors. The focusing effect of the dish might provide enough gain to noticeably increase their limited detection range. However, because of the short wavelengths of the frequencies involved, reflections would likely introduce random phase shifts which would make time delay estimation difficult.

3.2.2 Field Test Two

The second field test was conducted on a side street that runs perpendicular to the alley used in the first field test. This wide, open site was chosen for several reasons: to avoid echo problems, to allow more distance between the sensors and the source (for larger R_y), and to provide enough space for vehicles to be driven by at different distances. The main objectives of this test were to roughly estimate the range capabilities of the microphones, measure a sample vehicle's "resting" spectrum by letting it idle by the microphones, and examine signals from possible noise sources.

Since only microphones were considered in this test, the structure in the diagram of Figure 3-10 was nailed to the pavement. Both audible range (Radio Shack) and ultrasonic microphones were included because the final sensor design might involve a hybrid of both. The two microphone mounting boxes from Field Test One (from Figure 3-4) were attached with tie wraps to a hollow aluminum pole for support. The pole was connected to an optical mount which was attached to the pavement with nails. The ultrasonic microphones, which are more sensitive to tire/road interface noise, were positioned closer to the ground at a height of 16 inches. However, they were not placed too near the ground to avoid multipath problems from signals bouncing off the pavement. The Radio Shack microphones were placed at a height of 26 inches.

While viewing the outputs of the ultrasonic microphones with an oscilloscope, their extreme sensitivity to abrasive noise was discovered when a pedestrian walked by. As an indication of their sensitivity, they were able to detect a person scraping his feet on the ground 20 feet away. Since sensitivity to pedestrians would introduce noise to the measurements, several instances of a person walking by from various positions were recorded for future reference.

With the audible range microphones, a person can easily be distinguished from a car since their spectral characteristics are different. For the person walking, the detected signal is primarily due to interface noise. Examining short-term Fourier transforms (STFTs) of windowed sections reveals that the spectral shape and magnitude stay fairly constant. In contrast, due to the large number of distributed acoustic

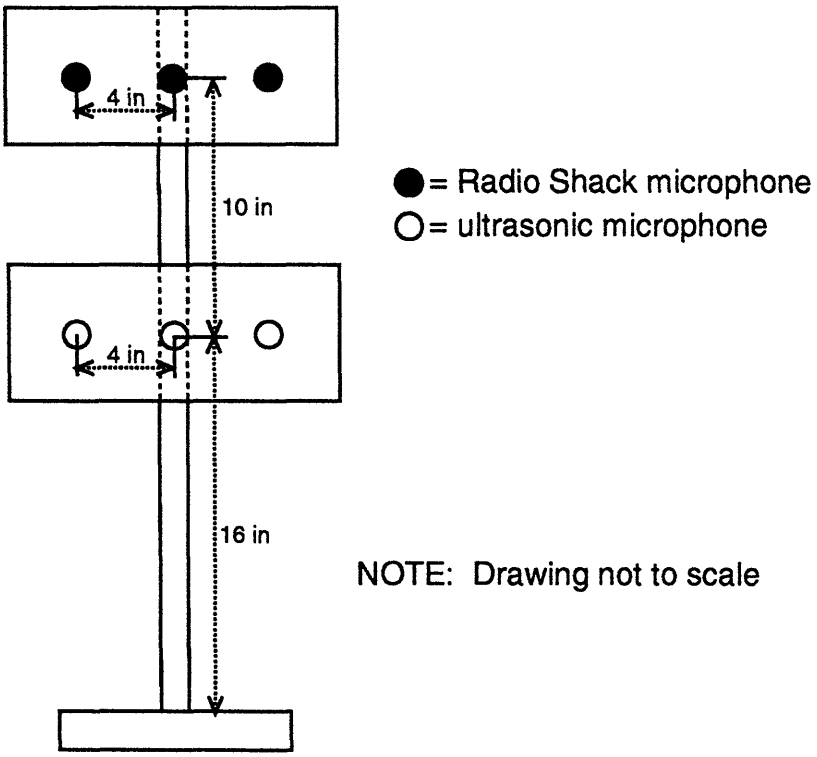

Figure 3-10: Microphone assembly for Field Test Two

sources on a vehicle, its spectral shape varies and its magnitude tends to increase as the vehicle is approaching and decrease as it departs. As the vehicle departs, however, the STFT plots tend to assume a shape similar to that of a person walking.

Data from airplanes flying overhead was also collected. The ultrasonic microphones were not sensitive their presence. This is explained by the fact that in the air, higher frequencies are attenuated faster than low frequencies. The Radio Shack microphones did detect the planes, which poses a potential problem for vehicle tracking. At worst, there might be a few missed detections while a plane is overhead. However, since vehicles will be much closer than the airplane, they should be the dominant sources and the delay estimates will likely reflect their motion more than the plane's motion. The effect of plane noise can be reduced by replacing each microphone in the array with a cluster of microphones and using beamforming techniques to generate

a narrow-beam "acoustic center". Improved τ estimates are obtained by examining the delays between the effective acoustic centers.

Another objective of Field Test Two was to get an idea of the spectrum of various engine components. A few trials were run with a sample vehicle (the Toyota pickup truck) idling directly next to the microphones in a few different positions. Data was collected with the vehicle directly facing the microphone array (head on) and with the left front wheel directly next to the array. In retrospect, since people drive on the right side of the road in the United States it would have been better to place the vehicle's *right* front wheel next to the array. However, this can easily be done later if it becomes necessary. Though the current vehicle tracking algorithm does not depend on the contents of the vehicle's acoustic spectrum, the data was obtained for future reference. In Field Test Three, a vehicle (the Subaru XT6) with its tailpipe next to the array was recorded.

In another series of tests, sensor range capabilities were studied while the Toyota truck was driven by at distances of approximately 10, 20, and 30 feet. The Radio Shack microphones performed well; the speed estimates obtained from correlating their outputs appeared reasonable. However, they were not be verified because vehicle speed was not recorded (since only range effects were investigated in this field test). The ultrasonic microphones also proved capable of detecting the vehicle 30 feet away. This is promising since it is desirable for the passive acoustic sensor to be able to monitor multiple-lane roads which may have lane widths of 8 feet or more. Range capabilities might be extended with further amplification or focusing, but this has not been determined.

A typical τ vs. time curve obtained from correlating two Radio Shack microphones is shown in Figure 3-11. This curve was generated using a correlation window of 5000 points with an overlap of 2500 points with a sampling rate of 35 kHz. It was obtained from an experiment where the Toyota truck was driven by the array at a distance of 30 feet. A speed estimate of 13.5 mph was returned, which appears reasonable. It was noted that the τ vs. time curves in general were much smoother than those obtained from Field Test One due to the increased source/array distances (which increased

stationarity over the correlation windows). Furthermore, due to the increased R_y the vehicle remained in the detection zone for a longer period of time, generating more points for the τ vs. time curve (for more accurate curve-fitting) and allowing use of longer correlation windows if desired.

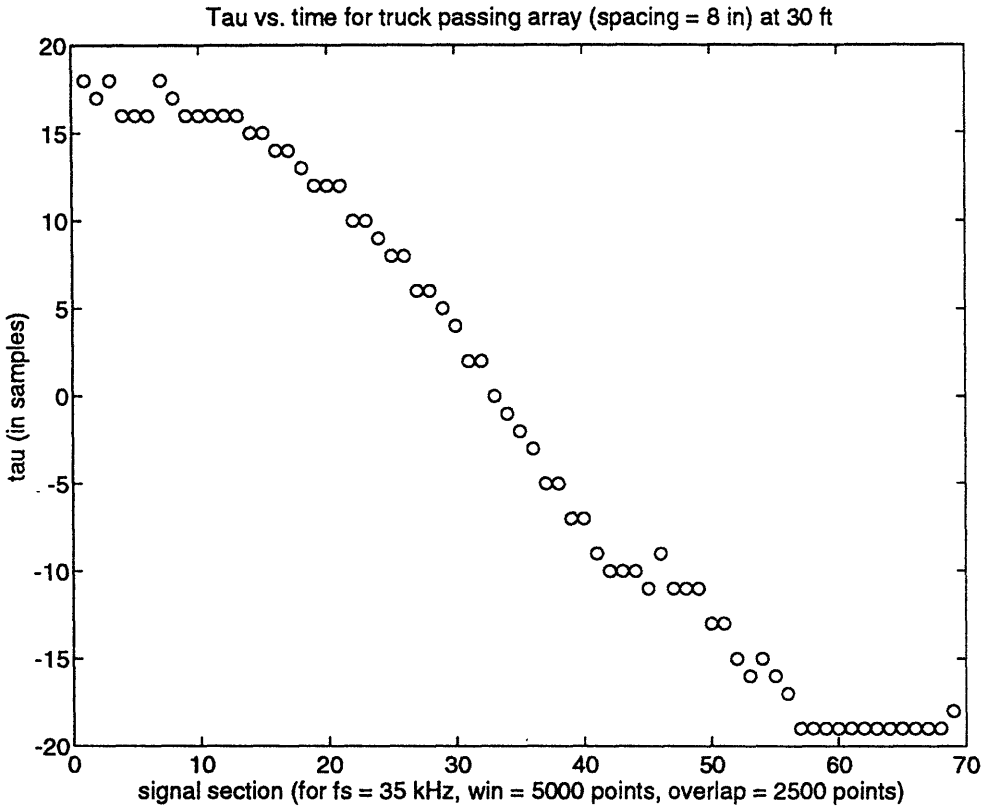

Figure 3-11: τ vs. time plot for pickup truck passing array at 30 ft

Since a Honda EX1000 generator would be providing power for the upcoming road tests, there was some concern whether its presence would contribute significant background noise. When the array outputs were examined with an oscilloscope, it appeared that the generator raised the background noise levels of both sets of microphones, though the ultrasonic only slightly. Standing in front of the generator seemed to block most of the acoustic power, so for the road tests, sound deadening material was placed in front of it. The generator was not used in Field Tests One or Two.

One final important observation from Field Test Two was made when a construc-

tion vehicle drove past the array in the opposite direction that the truck had been traveling. Its crossing was recorded (the truck was not in the field) and the correlation technique applied. In comparing the τ vs. time curves of the construction vehicle and the truck, they had similar shapes as expected. However, their slopes were of *opposite* sign, indicating they had been traveling in opposite directions! This observation agreed well with theory and strongly supported the notion that bidirectional traffic could be monitored with a single sensor. It also demonstrated that determining a vehicle's direction of travel would be trivial. Cases involving bidirectional traffic were examined using data from the road tests.

Upon completion of Field Test Two, the stage was set for analyzing real traffic data. A preliminary algorithm had been developed which involved correlating the outputs of a pair of microphones over short observation intervals to obtain time delay estimates ($\hat{\tau}$). After plotting the $\hat{\tau}$ vs. time, it was shown experimentally that the speed of the vehicle is proportional to the slope at the inflection point, as expected from theory. When the range of the vehicle is known, the algorithm yields an accurate speed estimate. However, a reliable means for determining range must be formulated. Methods involving triangulation using a colinear three-sensor array are nonlinear and highly sensitive to noisy time delay estimates. Extended Kalman filtering (EKF) techniques, which compensate for noisy measurements, are suggested for improving the range and bearing estimates from triangulation. Alternatively, a lesser-known algorithm pinpoints the source's location on a conic axis (LOCA) using time delay estimates from an array of three *noncolinear* sensors. Even though LOCA is also sensitive to noisy $\hat{\tau}$, it yields more promising range estimates than triangulation. These three range finding techniques are discussed in greater detail in Section 4.5.

3.2.3 Field Test Three

In order to observe the contribution of tire/road interface noise to the ultrasonic spectrum, a vehicle was allowed to "coast" past the microphone array in neutral with the engine off during Field Test Three. The sensors for the experiment were the lower three-element microphone arrays (Sennheiser audible range and ultrasonic) from Road

Test Two (refer to Figure 3-16). The arrays were located approximately three feet from the road. Since the engine was off, the microphones' outputs primarily reflected tire/road interface noise. Examination of the output of one of the ultrasonic sensors revealed a signal that had the same general characteristics (bandwidth, bandshape, amplitude, time envelope shape) as those seen in other tests where the engine was on. During Field Test Two, the spectra of idling vehicles (which predominantly reflected engine noise) which were positioned directly next to the ultrasonic microphones also exhibited ultrasonic energy. However, it is suspected that when vehicles are more distant, the contribution of engine noise to the ultrasonic spectrum will be much smaller.

Viewing the contribution of the tire/road interface noise in the audible spectrum suggested an interesting avenue to pursue in the future. Examination of STFTs of overlapping short segments of the audible range data revealed a spectrum whose magnitude increased then decreased as the vehicle coasted by as expected. The bandwidth was approximately 8 kHz. Despite the dynamics of the spectrum as the vehicle passed, the frequencies in the band from 6 to 8 kHz remained distinct from the rest of the spectrum (see Figure 3-12). When STFTs of data from the road tests were analyzed for comparison, the spectra exhibited the same dynamic property of increasing as the vehicle approached and decreasing as it departed. However, as a vehicle neared the array, the power in the range from approximately 5 to 8 kHz (depending on the vehicle type) would suddenly increase then decrease as the vehicle moved out of range. Presumably, these power "bursts" were shorter in duration than the one observed in Field Test Three because the vehicles on the road were farther away and traveling more rapidly. The power burst provides an indication that a vehicle is approaching the array and is near the "inflection" point (which is the point where the vehicle is directly in front of the array). It is thought that these bursts are due to audible range tire/road interface noise. If this is the case, it might be worthwhile to try frequency domain processing techniques to see if an alternative method to measure speed can be found by focusing on this band. If speed can be determined in this manner, then employing the correlation technique would provide

lane information (R_y) and direction of travel.

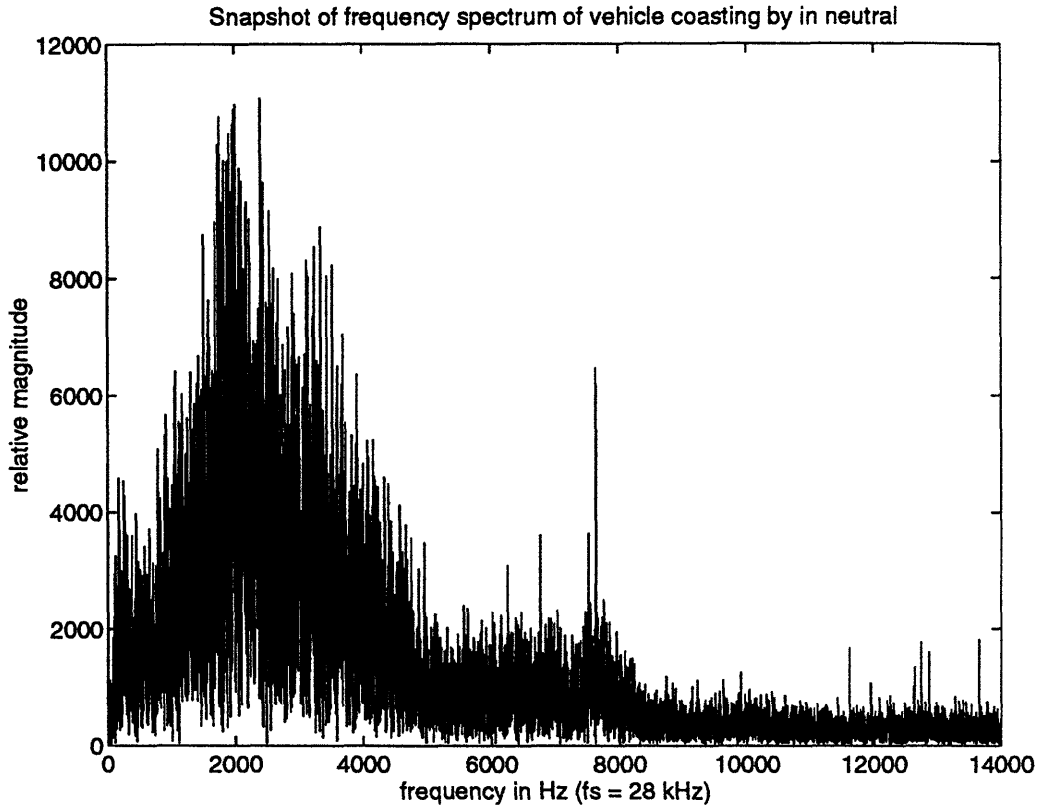

Figure 3-12: Spectrum of vehicle coasting by in neutral (snapshot)

The car coasting by in neutral was easily tracked by the audible range microphones using the correlation technique. This suggests that in the future, tracking "quiet" vehicles with audible range microphones should not pose a problem. On the other hand, a problem arose when the τ vs. time plot was viewed. Two essentially parallel curves were evident, one for each axle, as seen in Figure 3-13. Apparently, because of the nearness of the array, the axles were separated enough that each set was tracked independently. Hence, trucks and other long vehicles with widely separated axles might be miscounted as two vehicles if they pass too closely to the array. This could be avoided by increasing the distance from the array to the road (Y_0), but this might hurt the performance of the correlation algorithm since SNR is lower and estimate biases will amplify as range is increased. Furthermore, increasing the distance would not be practical for the short-range ultrasonic microphones. A better approach would be to

analyze the data in the frequency domain to see if long trucks can be distinguished from two closely spaced vehicles by their acoustic signature.

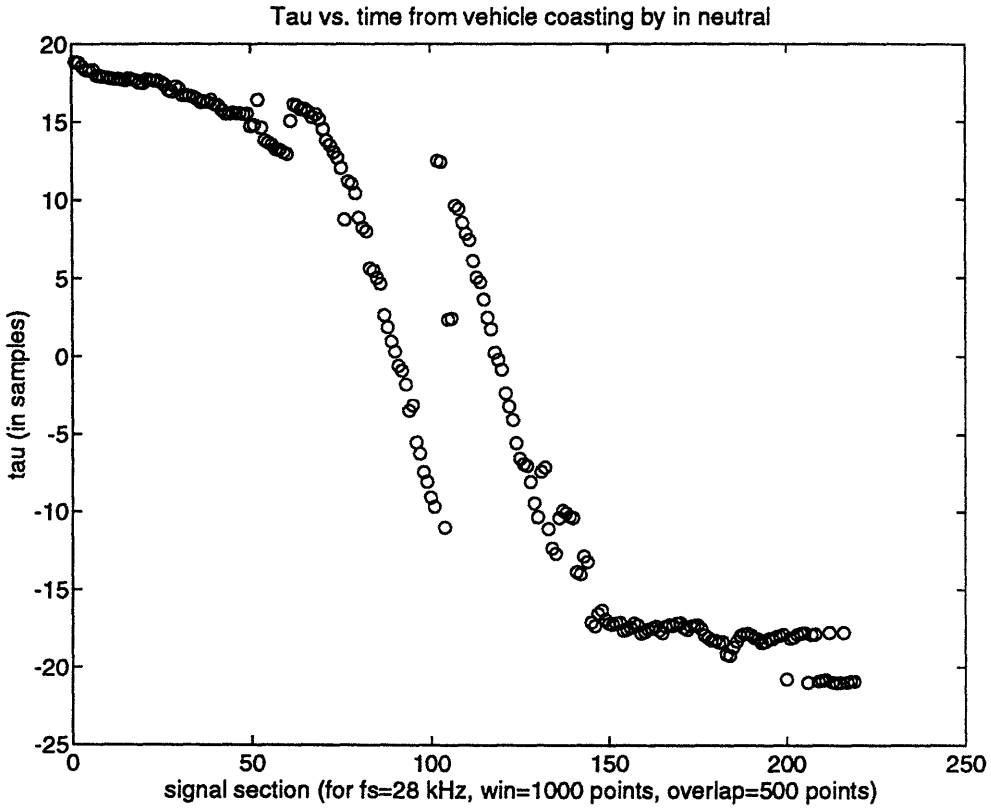

Figure 3-13: A τ vs. time plot obtained from a vehicle coasting by in neutral

In addition to the vehicle coasting experiment, data for the vehicle database was also collected. A vehicle idling with its tailpipe by the microphone array was recorded to get a measure of the contributions of the acoustic sources toward the rear of a vehicle. Also, to simulate a situation which could arise in a major traffic jam, a trial was conducted which involved a sequence of starting the ignition, idling the engine, then turning it off. This data is kept for future reference.

3.3 Road Tests

Three road tests (Road Test One, Two and Three) were conducted with the goal of measuring traffic flow on Hartwell Avenue. As mentioned previously, Hartwell

Avenue is a bidirectional roadway with two narrow lanes of traffic in each direction. The amount of traffic flow varies, but is usually light to moderate except at rush hour. During the road tests traffic was fairly light. In the busiest segments, short streams of vehicles crossed each other from both directions, though there were usually no more than two vehicles in the detection zone simultaneously. Though not the best location to view a wide variety of traffic conditions, Hartwell was a good choice for initial road tests because the data contained an assortment of vehicle types and basic traffic situations which provided a good starting point for testing the proposed algorithm. In the future, more interesting traffic situations such as stop-and-go traffic, steady streams of traffic in both directions (and in multiple lanes), tunnel traffic, and multi-lane high-speed traffic are slated for investigation.

A video camera maintained a record of the traffic flow and provided a means of verifying vehicle speed and range estimates. The camera shutter speed was set at 1/1000 second to avoid smearing in the images, and a clock kept track of elapsed time for synchronization purposes. Ten lines spaced one foot apart were painted at the edge of the driveway and kept in the field of view of the camera. Vehicle speed was approximately found by counting the number of lines a vehicle passed in a certain number of frames. For vehicles in the far lanes, it was more difficult to determine speed because of their distance from the measurement lines. If necessary, a more accurate verification scheme (such as radar) could be used for future performance analysis, with continued use of video for synchronization.

3.3.1 Road Test One

On February 17, 1994, the first set of real traffic data was acquired from Hartwell Avenue during Road Test One. The sensors, which were placed near the end of the driveway of the MIT Lincoln Laboratory annex at 45 Hartwell Avenue, included an array of ultrasonic and audible range (Sennheiser) microphones, the ADXL50 accelerometer to detect low frequency air vibration, and a QA700 accelerometer to measure translational ground vibration. The sensor configuration is displayed in the diagram of Figure 3-14. Using the analog recorder, their outputs were stored on beta

tapes which could hold about 4 $\frac{1}{2}$ minutes of data each. During Road Test One, five tapes of data were obtained.

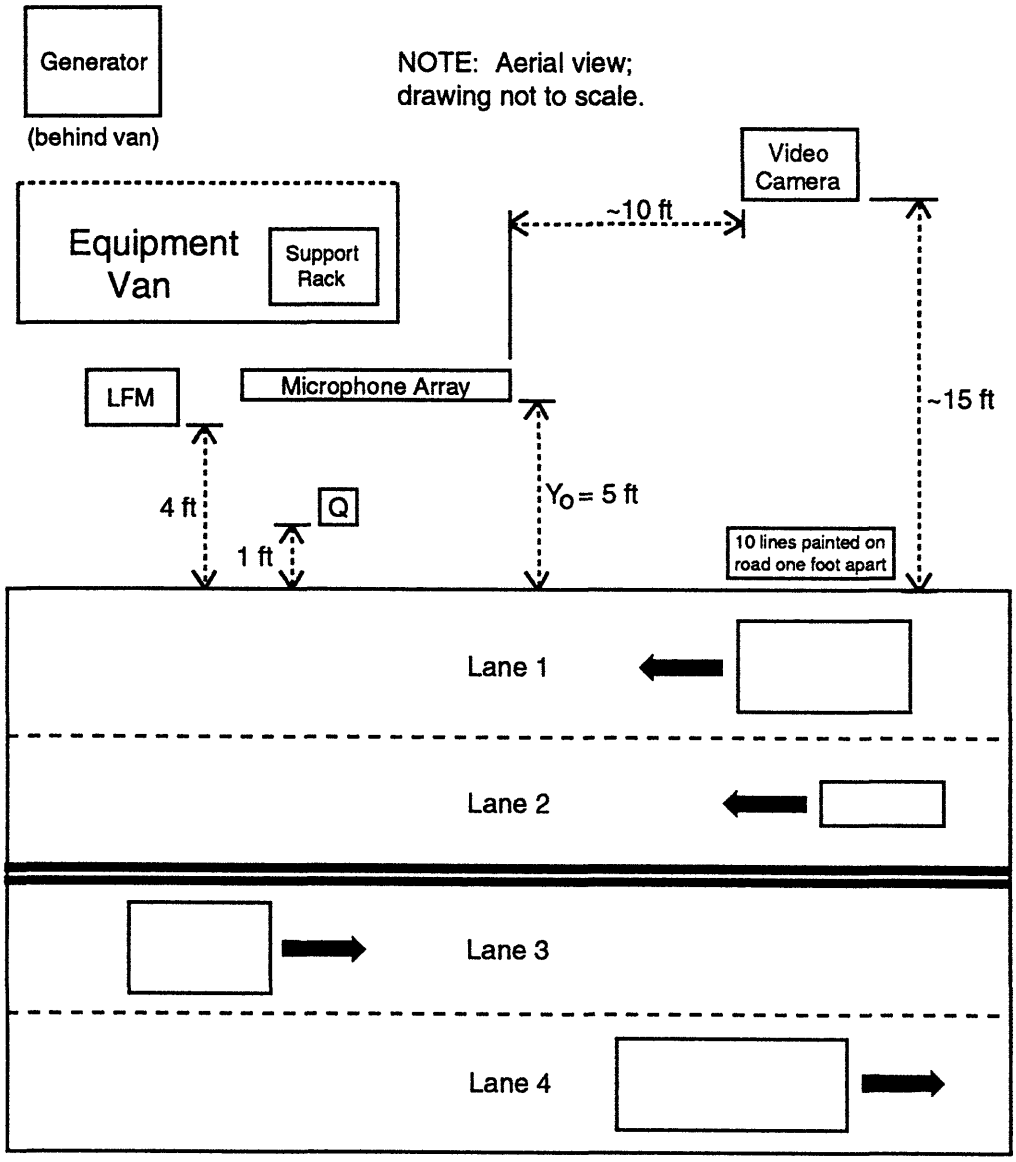

Figure 3-14: Experimental configuration for Road Test One

The microphone array was comprised of six audible range (Sennheiser) and six ultrasonic microphones. Each ultrasonic microphone was matched with an audible range microphone to form a *pair element*. A photograph of a pair element is provided in Figure 3-15. The pair elements were attached to a 2x4 foot screen with screws. Sound deadening material was attached to the back of the screen to minimize the effect of noise sources behind the array. A screen was chosen because it allowed pair elements to be moved around easily to accommodate configuration changes. During the first road test, the pair elements were grouped to form three two-element arrays at heights of one, two, and three feet with an intersensor spacing of twenty inches. Three arrays were included for redundancy and to determine if array height had an effect on measurements (which has not been investigated yet). A diagram of the microphone array for Road Test One appears on the left in Figure 3-16. The array was situated five feet from the road because of the short range of the ultrasonic microphones. Hereafter, the perpendicular distance of the array from the road edge will be designated as Y_0.

The low frequency accelerometer/microphone (designated by LFM in Figure 3-14) proved difficult to implement. A suboptimal configuration was assembled rather quickly. A large balloon served as the flexible membrane upon which the accelerometer was mounted. The original intent was to leave the balloon as a flat rubber sheet with the accelerometer attached to its face. However, in this mounting scheme, the accelerometer's sensitive axis would be pointing skyward, which is not the direction of choice. If the accelerometer were rotated so that its axis of sensitivity were directed toward the road as desired, it would be difficult to mount it to the rubber sheet without cutting a hole in it.

A compromise was reached by inflating the balloon and affixing the accelerometer to its side. The balloon was suspended in an open 2x2x2 foot cardboard box which was turned on its side so that the open end faced the road. Located four feet from the road edge, the box acted as a wind shield by blocking cross wind which could move the balloon. Strings tied to the balloon were threaded through tiny holes in the top and bottom of the box to hold it in place. The ADXL50 accelerometer (with

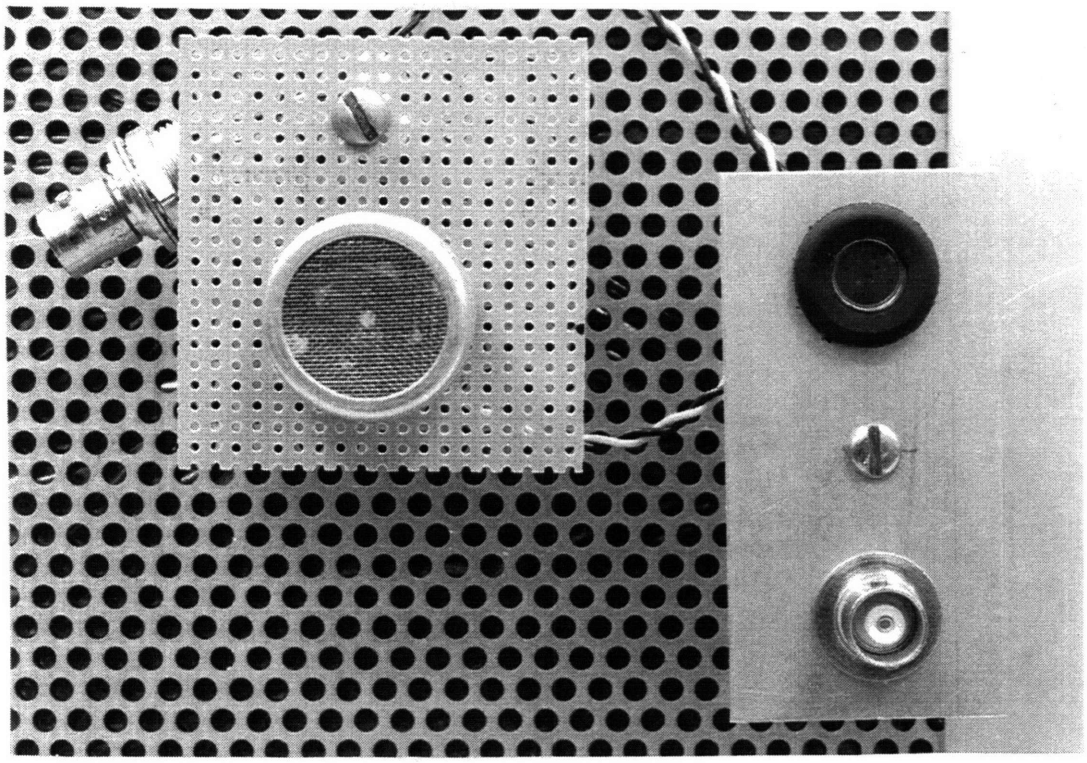

Figure 3-15: Photograph of a microphone pair element

its sensitive axis directed toward the road) was mounted on the side of the balloon with tape. Since the balloon would often rotate from the weight of the accelerometer and its cable, the opposite surface of the balloon was attached to the box with a strip of tape to restrict torsional motion. Obviously, the balloon still twisted (which makes this a suboptimal configuration), but the tape helped. The entire assembly is illustrated in Figure 3-17. A superior design would have aligned the accelerometer's axis of sensitivity with the axis of flexibility of a membrane restricted to linear motion in *one* direction. With the balloon, this did not seem feasible.

The QA700 accelerometer (denoted by Q in Figure 3-14) which measured $\frac{3}{4}$ inch in diameter was glued to a circular aluminum disk of the same diameter which was attached to the pavement with a long carpentry nail. Short of burying the accelerometer and pouring concrete to bond it to the road shoulder, this seemed the best way to attach the accelerometer to the pavement with minimal damping. The QA700 was

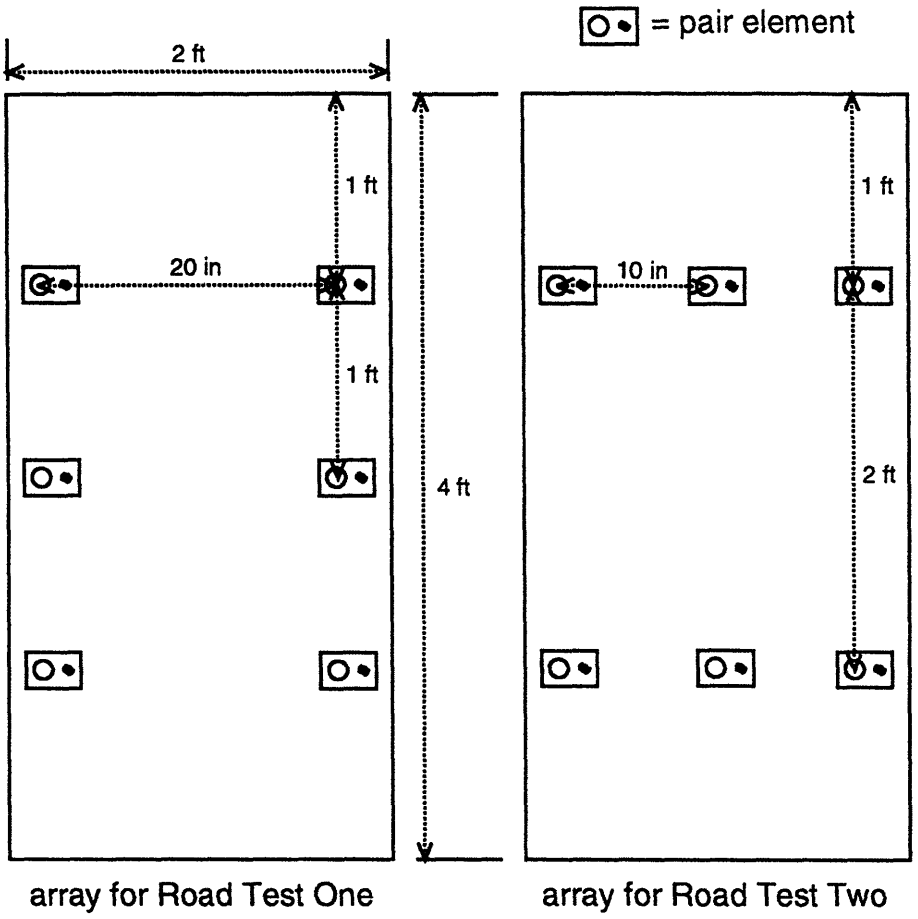

Figure 3-16: Microphone arrays for Road Test One and Two

placed as close as possible to traffic at a distance of about two feet from the road edge.

Since the sound level by Hartwell Avenue was higher than expected, the excessive amplification of the Sennheiser microphones caused the recorder to saturate. Consequently, a gain stage (x11) was removed from the Sennheiser amplifiers and a second road test conducted. The signals from the ultrasonic microphones and the accelerometers were unaffected by the saturated audible range data.

The ultrasonic microphone data was examined and a few qualitative observations made. First, it was noted that the microphones were capable of detecting vehicles in the farthest lane, which corresponded to a range of approximately 35 feet. In addition, because of their insensitivity to background noise, they are useful for identifying time

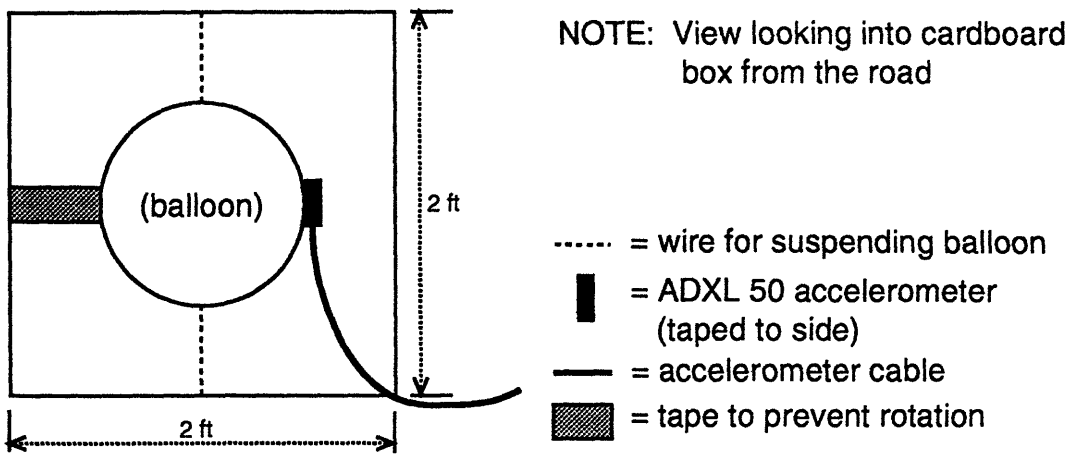

Figure 3-17: Low frequency microphone assembly

intervals of interest (so a processor does not have to operate if there is no vehicle present). Furthermore, it is thought that ultrasonic sensors are likely to be more useful in tunnels than audible range microphones since high frequencies are attenuated more rapidly than low frequencies both in air and upon incidence. Hence, they are less susceptible to multipath problems.

The sampled output from a single ultrasonic sensor tracking four vehicles on Hartwell Avenue is shown in Figure 3-18.[6] The four vehicles detected in this interval were a pickup truck (in lane 4), a Federal Express van in (lane 1), a car (in lane 4), and another pickup truck (in lane 4) respectively. In this instance, arrivals were spaced far enough apart that the number of vehicles could be counted by viewing the time domain signal. In general, this will not be the case since multiple vehicles will usually be present in the detection zone. Nonetheless, intervals of interest for processing can be identified from the time domain signal. Selective processing of intervals of interest would be useful during periods of little or no traffic.

Application of the correlation technique to estimate delays between the ultrasonic sensors yielded useless noisy results (for the sampling rate of 45 ksps). Again, this is attributed to a low sample/cycle ratio for the frequencies of interest and aliasing

[6]The amplitude is expressed in LabWindows "sampling units". 400 sampling units is equivalent to one volt.

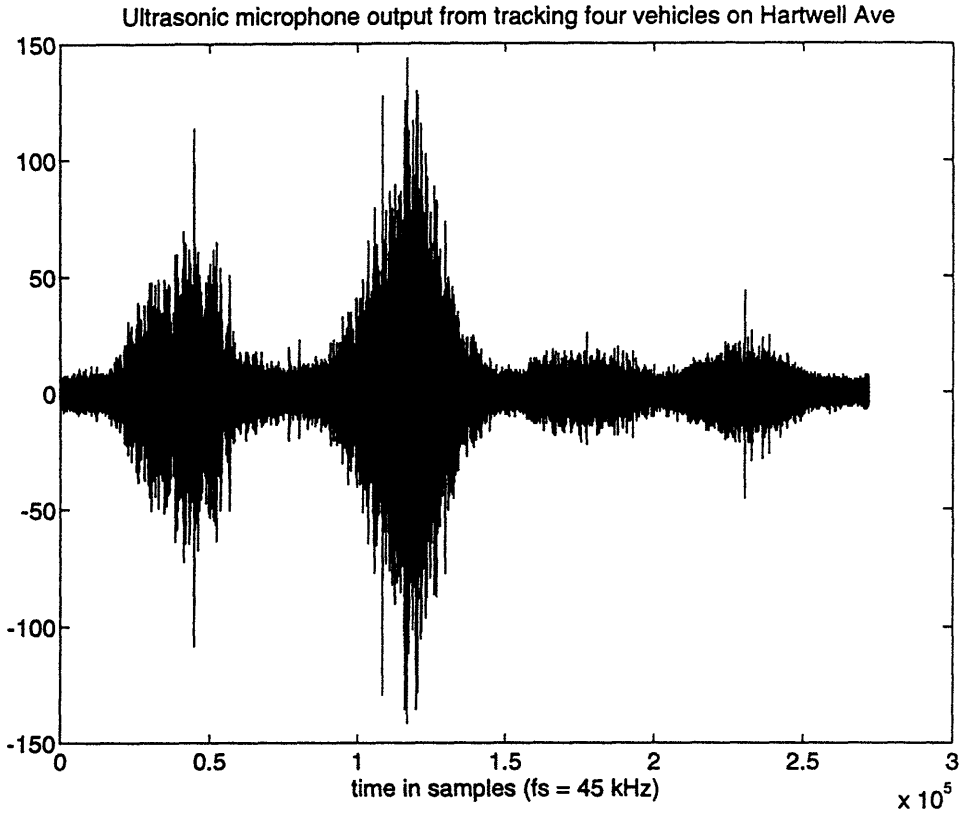

Figure 3-18: A typical time domain plot from an ultrasonic sensor

of frequencies above 22.5 kHz down to baseband. It remains to be seen if a higher sampling rate would improve results. If so, then methods of shifting the frequencies of interest down to baseband accurately should be investigated.

The outputs of both accelerometers did not offer any useful information. Presently, the idea of sensing road vibration as an aid for monitoring traffic variables has been set aside. With regard to the low-frequency "microphone", interesting results might be attained with an improved configuration. However, this again appears doubtful and unnecessary.

3.3.2 Road Test Two

The second road test took place on March 16, 1994, in the same location and under similar conditions as Road Test One. Only the microphone array was employed to collect data. The revised experimental set up is shown in Figure 3-19. The locations

of the microphones on the screen were altered in Road Test Two. The two-element arrays were replaced with three-element arrays so that triangulation techniques could be applied for range and bearing estimation. The pair elements were regrouped to form two colinear three-element arrays with an intersensor spacing of ten inches. These arrays were attached to a screen at heights of one foot and three feet. A diagram of the new configuration appears on the right in Figure 3-16 and a photograph of the final assembly is provided in Figure 3-20.

The distance of the array from the road edge (Y_0) was extended from 5 feet to 16 feet for improved stationarity over the processing windows. Since the angular rate of change of a vehicle's bearing ($\frac{d\beta}{dt}$) decreases as Y_0 is increased, the assumption of quasi-stationarity holds over a larger number of correlation windows which yields better τ and $\frac{d\tau}{dt}$ estimates. However, the tradeoffs for enhanced stationarity are lower SNR (which impairs delay estimation) and poorer range and bearing estimates from the triangulation and LOCA algorithms. Statistical analyses of the effects of target motion on delay estimates and of noisy delay measurements on range and bearing estimates would help optimize the choice of array parameters such as Y_0 and intersensor spacing.

The ultrasonic data in Road Test Two was not analyzed because the increase in Y_0 yielded much lower signal levels than Road Test One. Vehicles in the farthest lane were barely detected. If ultrasonic microphones are employed in the future, they should be placed as close to the road as possible. In addition to the range problem, data was not obtained from three of the microphones because of equipment failure. These things considered, the ultrasonic data from Road Test One should be used for algorithm development and evaluation.

3.3.3 Road Test Three

The third road test was conducted on May 19, 1994, in the same location as the first two road tests. The main objective of this experiment was to assess the performance of the LOCA range estimation algorithm described in Section 4.5.2. This time, only the six Sennheiser microphones were employed, and the array configuration was altered so

that different geometries could be compared. The 2x4 foot screen was rotated so that its holes faced skyward, and the sensors were mounted *above* it[7] and directed toward the road. This mounting scheme allowed variation of the Y_0 of individual microphones to produce noncolinear arrays. A diagram of the revised sensor configuration appears in Figure 3-21. Three microphones were kept in a colinear arrangement in the "front" (i.e. closer to the road) with unequal spacing to provide $\frac{d\tau}{dt}$ estimates. The other three sensors were positioned "behind" the colinear array at various Y_0 so the LOCA technique could be evaluated using various microphone location and spacing patterns. The overall test configuration is depicted in Figure 3-22.

When using the LOCA technique, greater accuracy is expected from sensors which are positioned farther apart. Larger spacing reduces the effect of vehicle motion on the τ estimates. For this reason, relatively wide intersensor separation was chosen to test the performance of the LOCA algorithm given *better* τ estimates than expected. In practice, intersensor spacing will be smaller due to size limitations. If the final range estimates using the data from Road Test Three are promising, the LOCA ranging algorithm will be re-evaluated with data from smaller arrays more suitable for IVHS. The performance of the LOCA algorithm using data from Road Test Three is discussed in Section 4.5.2.

[7] At a height of 16 inches.

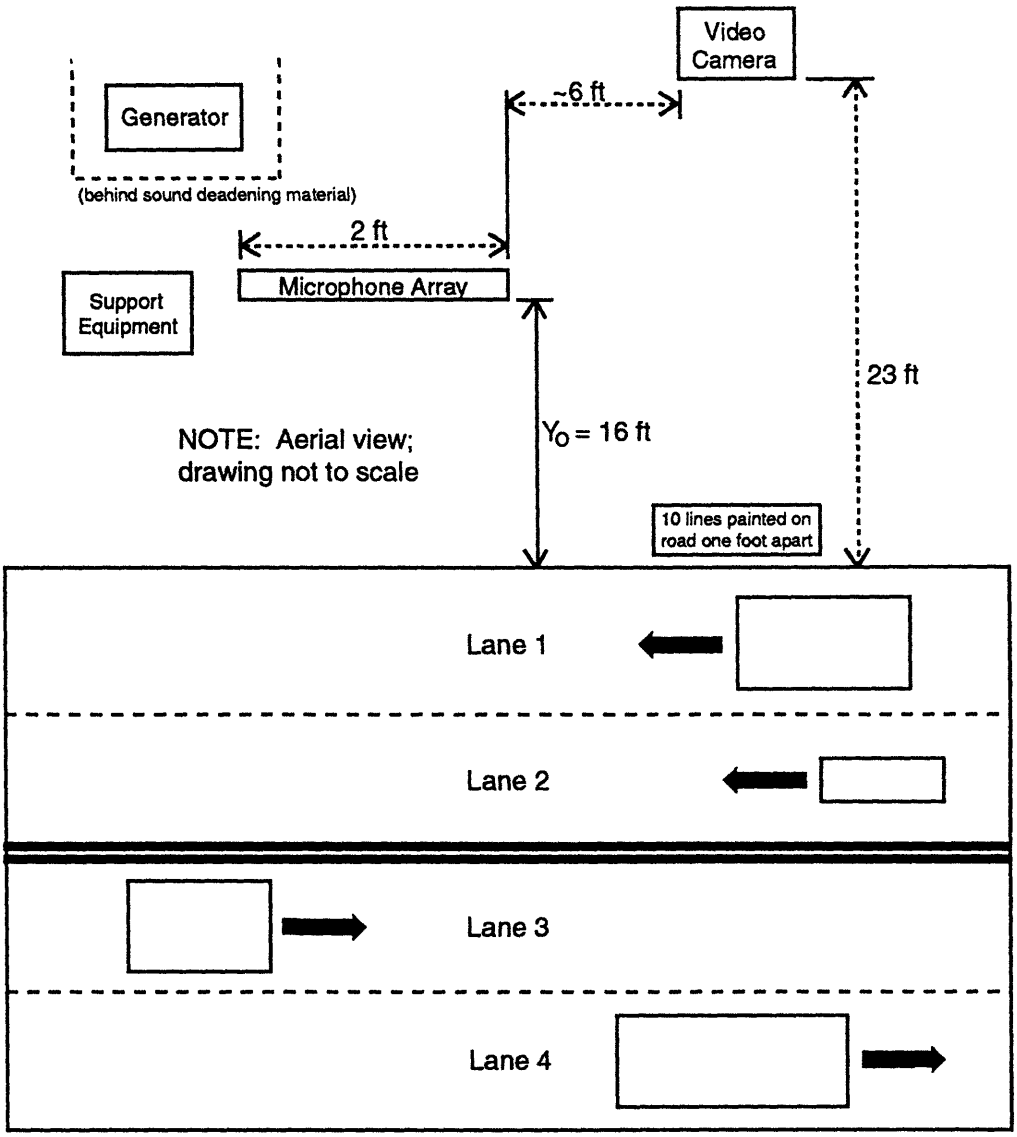

Figure 3-19: Experimental configuration for Road Test Two

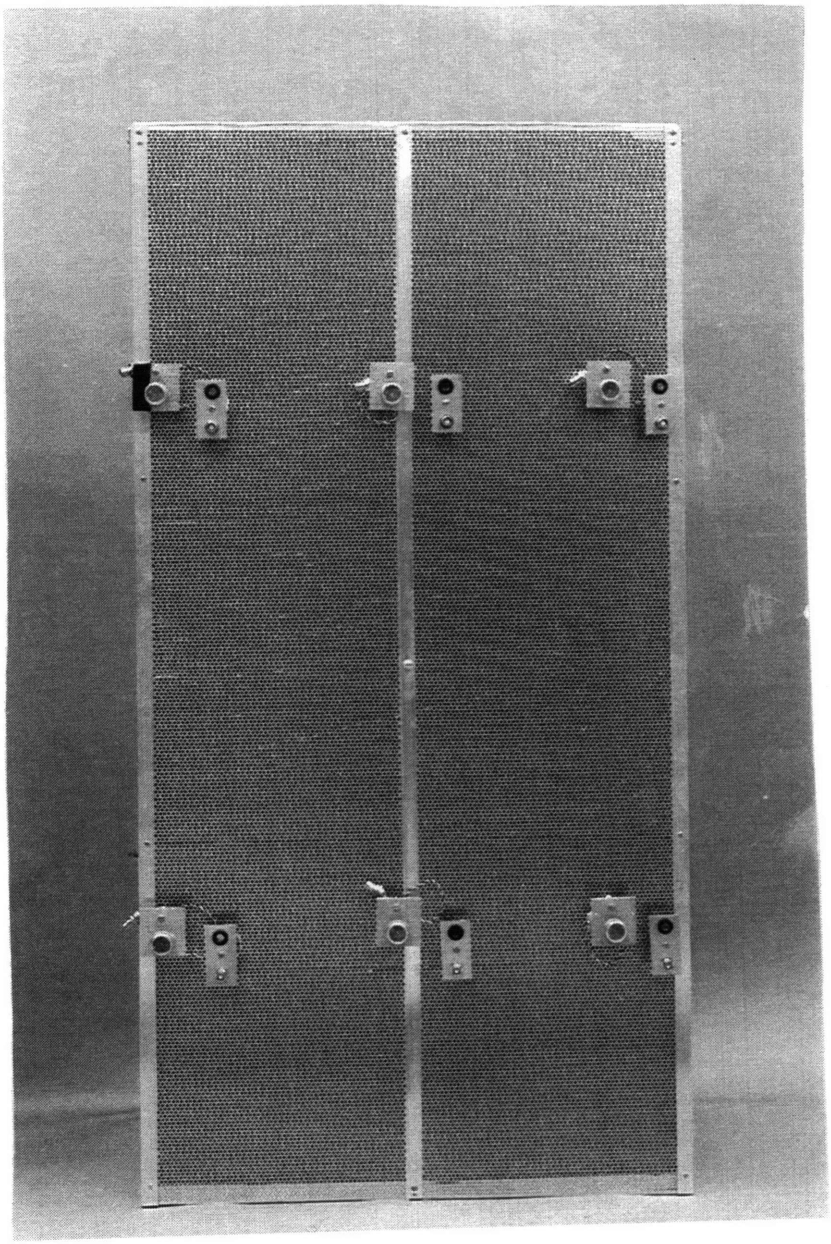

Figure 3-20: Photograph of microphone assembly for Road Test Two

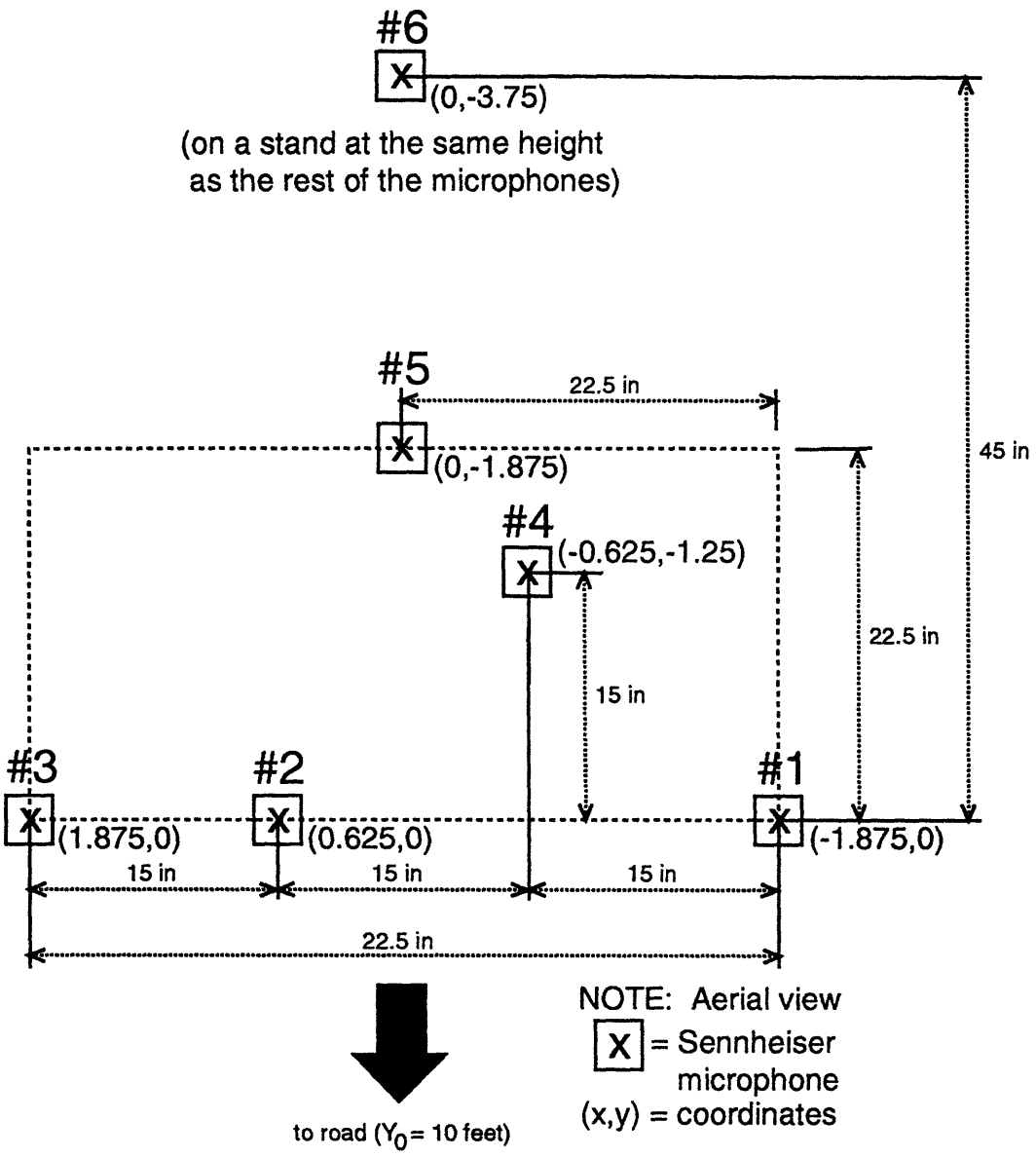

Figure 3-21: Microphone configuration for Road Test Three

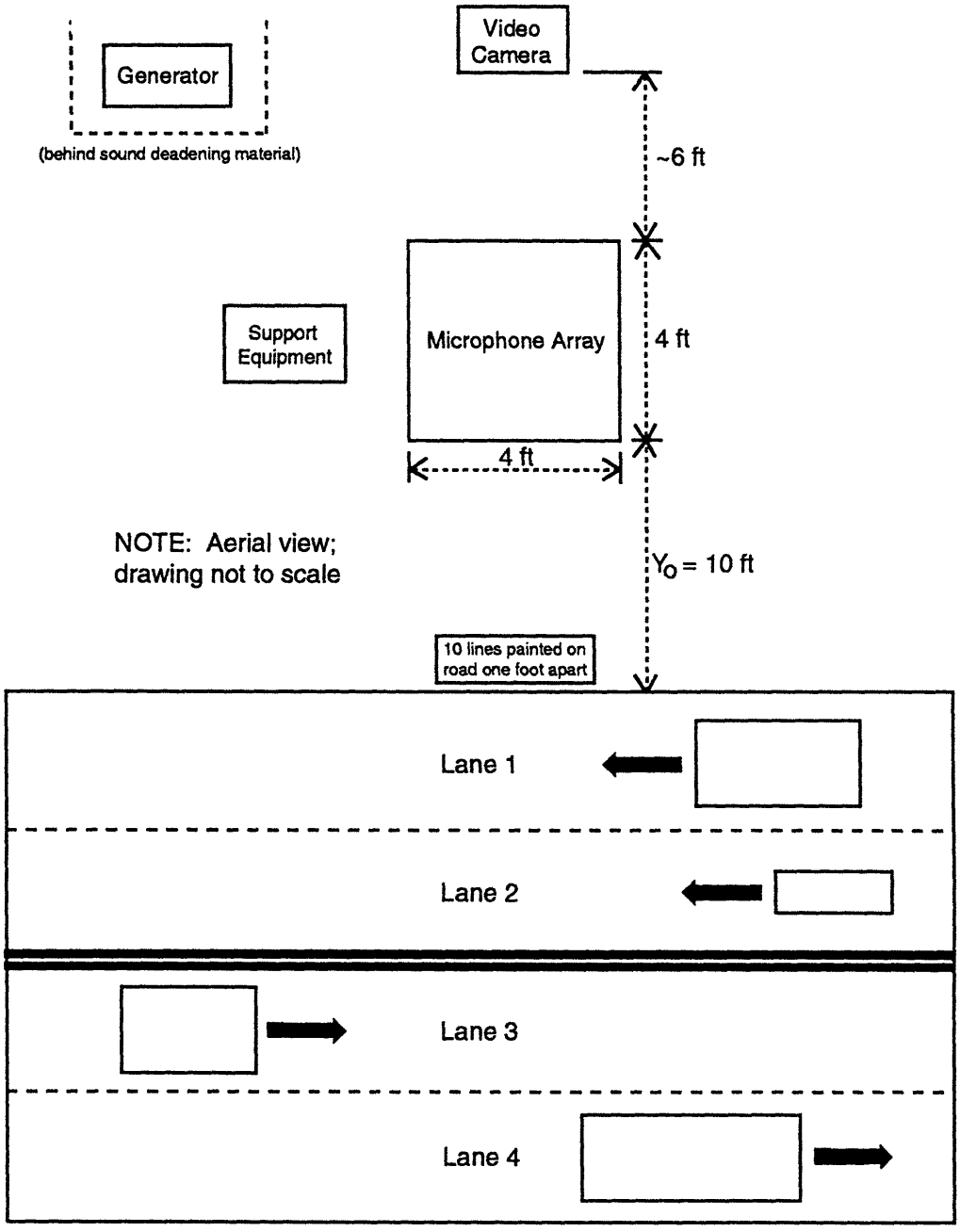

Figure 3-22: Experimental configuration for Road Test Three

Chapter 4

Sensor Algorithm

4.1 Basic Theory

At the heart of the passive acoustic vehicle sensor is the triple aperture microphone array. By correlating the outputs of the three pairs of microphones to estimate the true time delays between them (τ_{12}, τ_{23}, and τ_{31}), a vehicle's range (R) and bearing (β) can be computed.[1] Finding the vertical range component (R_y), which is the perpendicular distance between the vehicle's trajectory and the array, permits lane determination. Moreover, by plotting the delay *estimates* ($\hat{\tau}$) vs. time for a pair of microphones which are "parallel" to the road[2], vehicle speed can be calculated using the slope ($\frac{d\hat{\tau}}{dt}$) at the inflection point and R_y. The sign of $\frac{d\hat{\tau}}{dt}$ indicates the direction of travel. Henceforth, a caret ($\hat{}$) placed over a variable name emphasizes that it is an estimate.

4.2 Time Delay Estimation

Theoretically, when two spatially separated microphones are simultaneously regarding a single source, their outputs will be identical except for a time delay which is

[1] Several techniques for determining a vehicle's position are described in Section 4.5.

[2] A pair of microphones is considered parallel to the road if the line connecting their locations is parallel to the road. *All* of the $\hat{\tau}$ vs. time plots shown in this thesis were obtained from pairs of microphones which were parallel to the road.

proportional to the difference in the acoustic path lengths. It is this time delay (designated as τ) which must be measured. Cross-correlating the outputs of the two microphones in continuous time yields an accurate measure of τ if the source signal is distinct.[3]

In the case of vehicle sensing, two factors inherently degrade τ estimates: use of discrete cross-correlation and source motion. If the number of samples per cycle ($\frac{f_s}{f}$) for the frequencies of interest is not large, discrete-time correlation will *not* be a good approximation of continuous-time correlation. In addition, since the $\hat{\tau}$ obtained from discrete correlation are measured in integral multiples of the sampling period ($T_s = \frac{1}{f_s}$), quantization errors ranging between $\pm\frac{T_s}{2}$ are introduced.[4] Both of these effects can be reduced by increasing the sampling rate. A more serious contributor of estimation noise is source motion, which attributes non-stationarity to the problem. It is widely known that the acoustic spectrum of a moving vehicle will exhibit Doppler shifts. This is equivalent to saying that the τ measured between two stationary microphones tracking the source will be *time-varying*. To satisfy quasi-stationarity, cross-correlations must be performed over short observation windows to estimate instantaneous time delays. Short windows increase the probability of error because signals are less distinct. Furthermore, since the vehicle is in motion, the $\hat{\tau}$ for a given correlation window will be some average of the true τ values over that window.

Fortunately, since a vehicle's trajectory is limited to passing in front of the array broadside, the theoretical τ vs. time curve is dependent *only* on geometric quantities and the speed of the vehicle. Further analysis demonstrates that speed can be determined from the slope of this curve at the inflection point ($\frac{d\tau}{dt}\Big|_{\tau=0}$). This idea is the key to the speed estimation algorithm described in Section 4.4. This thesis demonstrates that curve fitting the estimates obtained from overlapping correlation

[3]The term distinct can be loosely interpreted as wideband. Distinct signals have autocorrelation functions which are distinguished by a narrow, high-valued mainlobe, and small sidelobes (the ideal being an impulse function). This trait is desirable since the algorithm searches for the peak of the cross-correlation function to determine τ.

[4]Quantization error is reduced by performing a parabolic curve fit through the points surrounding a correlation peak. The fractional offset of the parabola's peak is added to the original $\hat{\tau}$ for an improved estimate.

windows yields a good enough approximation to the true τ vs. time curve that reliable speed estimates can be obtained.

4.3 Block Diagram of Algorithm

A block diagram of the current algorithm is supplied in Figure 4-1. The algorithm depends on three major factors: estimating the true time delays between pairs of microphones, processing the delay estimates to obtain intermediate parameters, and calculating speed from the intermediate parameters. The notation τ_{ab} is adopted to represent the time delay between microphone a and b.

Initially, the outputs of the three microphones (played back through the analog recorder) are passed through anti-aliasing filters (AAF) before being sampled (A/D). Once sampled, the signal sequences are passed through an optional prefilter before cross-correlation. The prefilter could be a statistical filter like those commonly used in underwater signal processing [2]. Since passive sonar signal processing relies heavily on correlating the outputs of hydrophones for target parameter determination, a great deal of research has been directed toward the design of statistical filters for the sole purpose of improving delay estimates. The reader is directed toward the book by Joseph C. Hassab [2] and other underwater signal processing literature for a deeper discussion of prefilter selection. Prefilters were not considered in this investigation.

Following the prefiltering stage, the microphone outputs are cross-correlated to yield raw estimates of the time delays between respective pairs. The size of the correlation window and amount of overlap between successive estimates are user-defined parameters. For each window, the index of peak of the cross-correlation within a window of $\pm\Delta$ samples determines the time delay. Δ should be chosen large enough to accomodate $\hat{\tau}$ corresponding to the *farthest* vehicle positions in the detection zone.[5] In order to reduce the effect of quantization noise on the τ estimates, a parabola is fitted to the correlation peak value and its two surrounding values. The

[5]These positions are determined by R_y of the farthest lane and the directivity of the microphones (β_{max}). For simplicity, the detection zone is assumed to be a section of a circle specified by the range and angular directivity of the microphones.

fractional offset of the parabola's peak is added to the integral sample delay for an improved estimate.

Once sequences of raw delays are obtained, they are analyzed to find sections of interest where a vehicle might be present. Several general observations indicate a vehicle's presence:

1. The time domain signals of both the audible range and ultrasonic microphones exhibit an envelope shaped like an "eye". Qualitatively, this is due to increasing sound level as the vehicle approaches and decreasing sound level as it departs.

2. Likewise, the energy in the frequency regions of interest (below 8 kHz and from 15-27 kHz) tends to increase as the vehicle approaches and decrease as it departs.

3. The τ vs. time curve has a distinctive shape indicative of a passing source. Figure 4-2 shows a theoretical τ vs. time curve expected from two microphones[6] tracking a vehicle (traveling at 40 mph from $\beta = -60°$ to 60°) from a distance of 25 feet. A vehicle traveling in the opposite direction would generate a curve of similar shape but opposite slope.

Originally, during the field tests regions of interest were selected by viewing the signal in the time domain. Processing was begun when the signal amplitude began to increase above the level of general background noise. However, since there was a constant flow of traffic on Hartwell Avenue while road data was collected, the microphone outputs were continually cross-correlated. Regions of interest were determined by visually examining the τ vs. time plots from a pair of microphones for distinctive shapes.

[6]The microphones are assumed to be parallel to the road and separated by 10 inches. A sampling rate of 28 kHz with a correlation window size of 1000 points (with an overlap of 500 points between windows) was entered in the calculations.

Figure 4-1: Block diagram of current algorithm

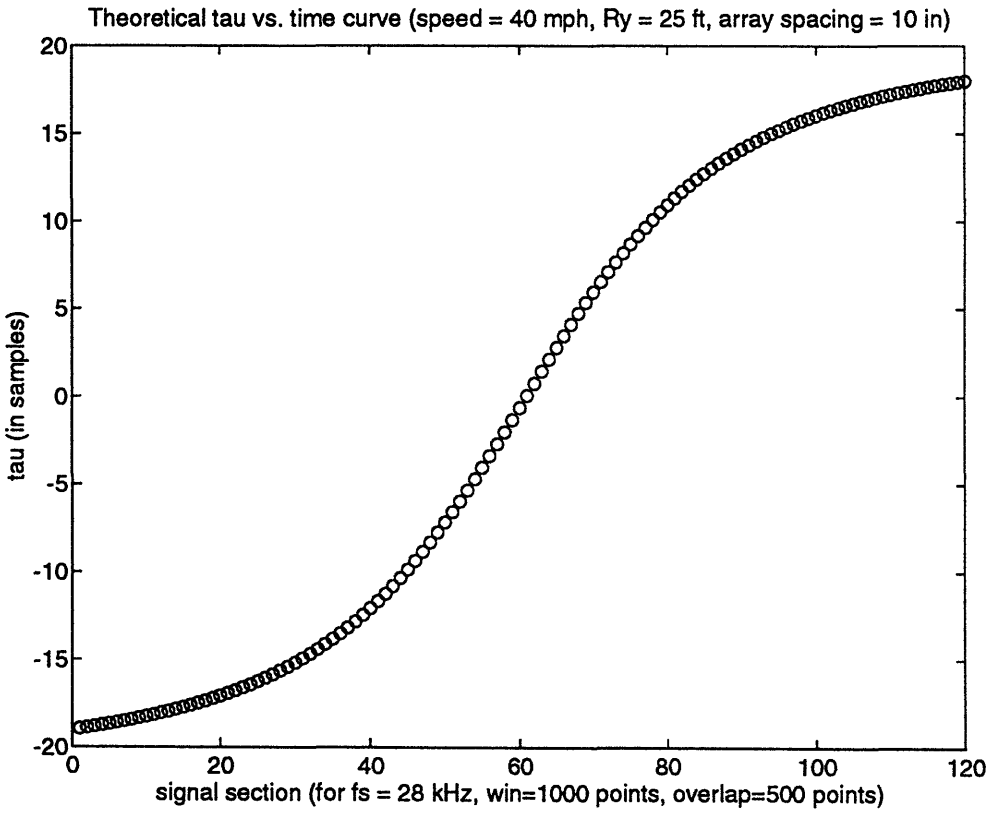

Figure 4-2: A sample theoretical τ vs. time curve

A typical plot obtained from correlating real traffic data from a pair of Sennheiser microphones parallel to the road is shown in Figure 4-3. Disregarding obvious noisy values, it is evident which regions indicate the presence of a vehicle (or vehicles) and which are predominantly noise. In the future, a quantitative measure of determining regions of interest could be found by first curve fitting the data and tracking the derivative of the τ estimates (which would also provide the slope at inflection points). Currently, however, the τ vs. time curves for each vehicle are separated by visual inspection. This works extremely well in instances where at any given time the detection zone contains only one or more vehicles traveling in the *same* lane. In instances where two vehicles are passing each other from opposite directions, their τ vs. time curves overlap. This reduces the number of points available for curve fitting since the $\hat{\tau}$ tend to reflect the motion of the dominant source. Tracking secondary peaks of the correlation functions provides supplemental points which result in better curve fits. For cases involving vehicles traveling side-by-side in different lanes, but headed in the same direction, a reliable method has not been found for separating the curves which reflect each vehicle's motion. Multiple vehicle situations are discussed in greater detail in Section 4.6.

Once a curve is separated and smoothed with polynomial curve fitting (fifth-order in this case), the slope of the derivative at the inflection point ($\frac{d\tau}{dt}\Big|_{\tau=0}$) for a microphone pair *parallel* to the road is computed. The sign of the slope, which specifies direction of travel, is noted. For an equally-spaced colinear array[7] (where microphone 2 is in the center), the interpolated τ vs. time curves for τ_{12} and τ_{23} should yield the same $\frac{d\tau}{dt}\Big|_{\tau=0}$ and their average can be taken. Likewise, $\frac{d\tau_{13}}{dt}\Big|_{\tau=0}$ should be half of $\frac{d\tau_{12}}{dt}\Big|_{\tau=0}$ and $\frac{d\tau_{23}}{dt}\Big|_{\tau=0}$.

Before speed can be determined, R_y must be found. Currently, three methods for determining R_y are under consideration: triangulation (as a special case of hyperbolic range difference location), the Location On the Conic Axis (LOCA) algorithm, and extended Kalman filtering (EKF). These techniques are discussed in greater detail in Section 4.5. In triangulation, the $\hat{\tau}$ from a colinear microphone array (where micro-

[7] A colinear array is employed when vehicle position is computed by triangulation.

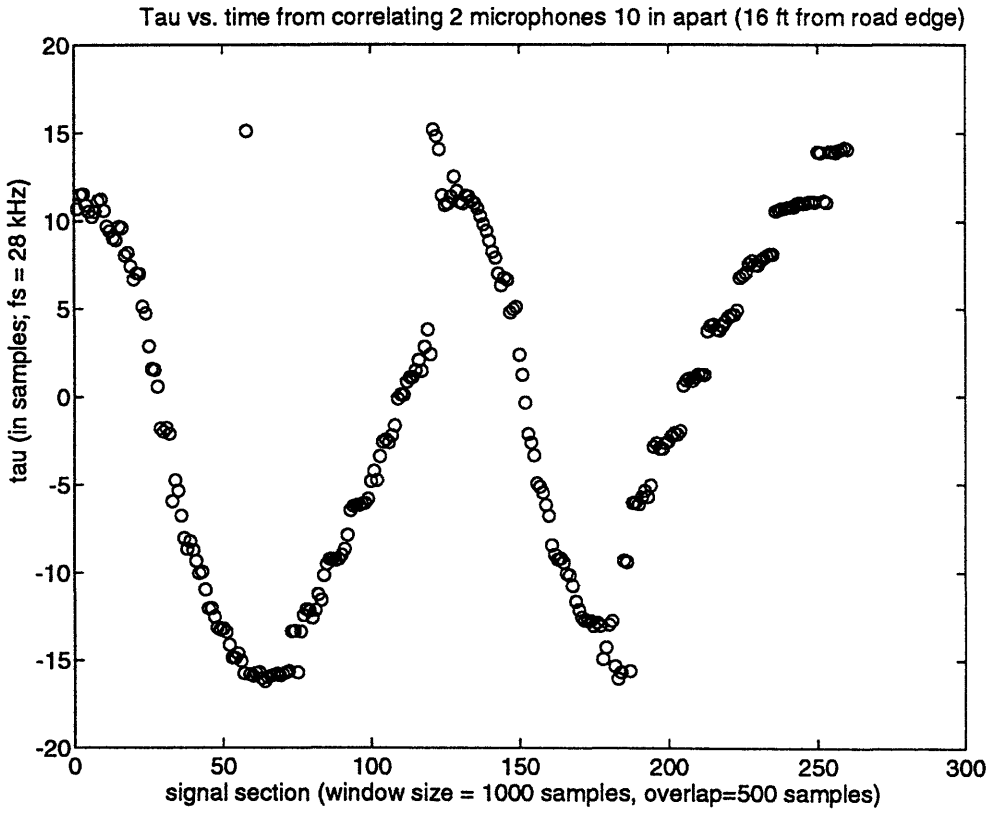

Figure 4-3: A τ vs. time plot obtained from a pair of microphones

phone 2 is in the center) are obtained. When a vehicle is present, its range (R) and bearing (β) can be calculated from τ_{12} and τ_{23} if they are known exactly. However, as the noise on the $\hat{\tau}$ increases, $\hat{R}$ and $\hat{\beta}$ become extremely biased. In addition, if the ratio of the array spacing to the vertical range ($\frac{s}{R_y}$) is small, the ideal method becomes unreliable. With the LOCA algorithm, delay estimates from a *noncolinear* microphone array are measured. For a given time slice, the time delays identify a linear line of position upon which the source is located. By treating the sensor "coordinates" as points of a conic whose axis is the line of position, the vehicle's location is fixed as one of the foci. The performance of the LOCA technique is also affected by errors in the $\hat{\tau}$, although it does not appear as sensitive as triangulation. Finally, EKF (which accounts for measurement errors) is under investigation for determining range (and speed) by modeling the nonlinear system dynamics and linearizing about a nominal trajectory. EKF is widely used in underwater signal processing for target

localization.

Once R_y and $\frac{d\tau}{dt}\Big|_{\tau=0}$ are found, vehicle speed is determined from Equation 4.3 which is derived in Section 4.4. There was good agreement between experimental results and actual vehicle speeds obtained from the verification systems when R_y was known.

4.4 Speed Estimation

The speed estimation algorithm was inspired by the geometry of the problem. Two parameters must be obtained from the data: the slope of the τ vs. time curve at the inflection point ($\frac{d\tau}{dt}\Big|_{\tau=0}$) and the vertical range component (R_y) of the vehicle. Once these values are determined, speed ($\frac{dx}{dt}$) can be found using Equation 4.3 whose derivation follows. Refer to Figure 4-4 for definition of relevant dimensions (x, s, R, R_y). An equally-spaced colinear array is assumed for demonstration. All distances are expressed in units of feet.

First, a pair of microphones which is parallel to the road is chosen; in this case, microphones 1 and 2. Considering the vehicle as an aggregate quasi-stationary source emitting one signal, let the time delay between its arrival at microphones 1 and 2 be defined as τ_{12} (in samples). Then it follows that:

$$\frac{\tau_{12}}{f_s} + T_d = \frac{R - R_1}{c} = \frac{\sqrt{R_y^2 + (x+s)^2} - \sqrt{R_y^2 + x^2}}{c} \tag{4.1}$$

where c is the speed of sound in air (= 1130 $\frac{ft}{s}$), f_s is the sampling rate (in Hz), and T_d is a sampling delay.[8]

This equation defines the theoretical shape of the τ vs. time curve. By computing the mean squared-error (MSE) of the difference between the curve obtained from the data and the expected results, a quantitative measure of the estimation error can be

[8] T_d is an additional delay that arises from the multiplexed sampling scheme of the A/D card. Since there are 3 channels, the sampling delay between microphones 1 and 2 (or 2 and 3) is $\frac{1}{3f_s}$. Between microphones 1 and 3 it is $\frac{2}{3f_s}$.

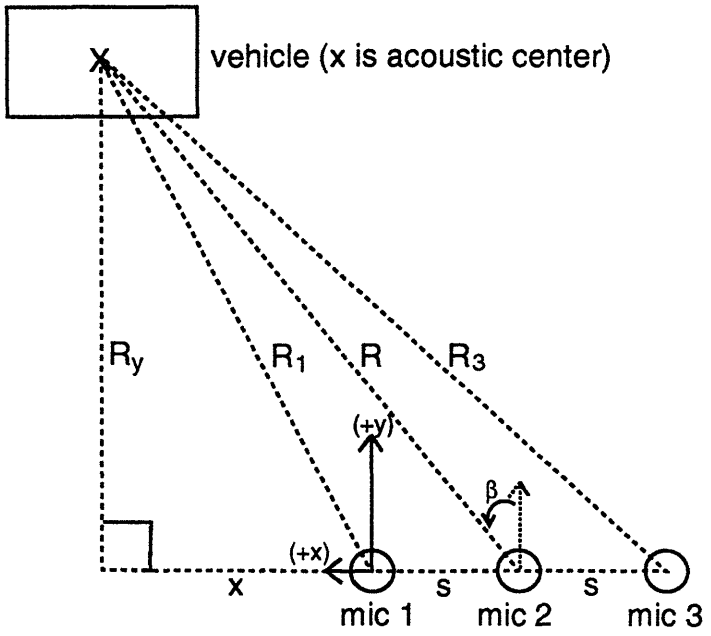

Figure 4-4: Geometry of vehicle tracking problem

found.[9] However, this error measure should not be relied on too heavily because in generating the theoretical plot several major assumptions are made:

1. The vehicle is traveling at a constant speed and vertical range (R_y) throughout the detection zone.

2. The actual vehicle speed and vertical range are known accurately and used to generate the theoretical curve.

3. The array is in the far-field, so the vehicle can be treated as a point source for acoustic emissions.

These assumptions may or may not be true for a given situation. Nonetheless, it is interesting to observe how factors such as background noise, non-stationarity, variable

[9]Here the MSE = $E[(\hat{\tau}_{12} - \tau_{12})^2]$.

speed, distributed acoustic sources on the vehicle, interference from other vehicles, and curve fitting (for approximating the continuous τ vs. time curve) affect delay estimates.

Taking the derivative with respect to time of Equation 4.1 and rearranging terms yields:

$$\frac{d\tau_{12}}{dt} = \frac{f_s}{c}\frac{dx}{dt}\left[\frac{x+s}{\sqrt{R_y^2+(x+s)^2}} - \frac{x}{\sqrt{R_y^2+x^2}}\right] \tag{4.2}$$

The inflection point of the curve occurs when the vehicle is directly in front of the midpoint between the microphones. Theoretically, this is also the point where $\tau = 0$, the range (measured from the midpoint of 1 and 2) is R_y, and x = -$\frac{s}{2}$. If Equation 4.2 is considered at the inflection point, the results simplify dramatically:

$$\frac{dx}{dt} = \frac{c}{f_s s}\sqrt{R_y^2+\frac{s^2}{4}}\left.\frac{d\tau_{12}}{dt}\right|_{\tau=0} \tag{4.3}$$

If $\left.\frac{d\tau_{12}}{dt}\right|_{\tau=0}$ and R_y can be obtained from the data, the vehicle's speed can be calculated using this equation. $\left.\frac{d\tau_{12}}{dt}\right|_{\tau=0}$ can be found directly from either $\hat{\tau}$ vs. time curve. Fortunately, R_y is theoretically obtainable from the $\hat{\tau}$ between respective microphone pairs.

4.5 Range Estimation

4.5.1 Localization with Hyperbolic RDL

For a three-element array, the range and bearing of a source can be pinpointed from geometry if the time delays between two pairs of microphones are known precisely [2]. This is a technique known as hyperbolic range difference location (RDL) [7]. For each pair of microphones, τ is equal to the difference in target range measured from two spatially distinct positions divided by the speed of sound. The line of position curves corresponding to constant τ (or range differences) are *hyperbolic* in two-dimensional space. A source's (x,y) location is pinpointed by the intersection of the hyperbolas corresponding to $\hat{\tau}$ from at least two spatially separated pairs of microphones.

In theory, source location can be deduced from the τ estimates from any two of the three pairs of microphones. However, for an equally-spaced colinear array with microphone 2 in the center, τ_{12} and τ_{23} are chosen to exploit symmetry. Because of the linear geometry of the array, range (R) and bearing (β) can be found directly from τ_{12} and τ_{23}. This is the method of triangulation. For simplicity of notation, (τ_{12}, τ_{23}) will be refered to as (τ_1, τ_2). In this case, the estimates of R and β will be referenced to the center microphone as indicated in Figure 4-4. Once again, Figure 4-4 should be consulted for definition of relevant dimensions (R, R_1, R_3, s).

The time delays (τ_1 and τ_2) are related to geometric quantities by the following equations:

$$\tau_1 = \frac{R - R_1}{c} = \frac{1}{c}\left[R - \sqrt{R^2 + s^2 - 2sRsin(\beta)}\right] \tag{4.4}$$

$$\tau_2 = \frac{R_3 - R}{c} = \frac{1}{c}\left[-R + \sqrt{R^2 + s^2 + 2sRsin(\beta)}\right] \tag{4.5}$$

These equations can be manipulated to solve for R and β in terms of the time delays:

$$R = \frac{s^2 - 0.5c^2(\tau_2^2 + \tau_1^2)}{c(\tau_2 - \tau_1)} \tag{4.6}$$

$$\beta = sin^{-1}\left[\frac{c}{2s}(\tau_2 + \tau_1) + \frac{c^2}{4sR}(\tau_2^2 - \tau_1^2)\right] \tag{4.7}$$

In the case of vehicle sensing, the source is in the far-field (R >> s) and the equations simplify to:

$$\hat{\beta} = sin^{-1}\left[\frac{c}{2s}(\tau_2 + \tau_1)\right] \tag{4.8}$$

$$\hat{R} = \frac{s^2 cos^2(\hat{\beta})}{c(\tau_2 - \tau_1)} \tag{4.9}$$

Because the dependence of $\hat{R}$ and $\hat{\beta}$ on τ_1 and τ_2 is nonlinear, errors in the time delay estimates lead to extremely biased estimates. Since the signals are wideband, the correlation time interval (T_{win}) is large compared with the correlation time of signal and noise which results in $\hat{\tau}$ which are nearly unbiased and nearly Gaussian. By assuming that the $\hat{\tau}$ are unbiased and jointly Gaussian, a second-order Taylor expansion of the expressions for $\hat{R}$ and $\hat{\beta}$ about the true time delays provides estimates

of the biases ($\hat{R}_{bias}$, $\hat{\beta}_{bias}$) [2]:

$$\hat{R}_{bias} = \frac{s^2 cos^2\beta}{c(\tau_2 - \tau_1)^3}(\sigma_{n_1}^2 + \sigma_{n_2}^2 - 2\mu_{12}) \tag{4.10}$$

$$\hat{\beta}_{bias} = \frac{1}{2}\left(\frac{c}{2scos\beta}\right)^2 tan\beta(\sigma_{n_1}^2 + \sigma_{n_2}^2 - 2\mu_{12}) \tag{4.11}$$

where $\sigma_{n_1}^2$ and $\sigma_{n_2}^2$ are the variances of $\hat{\tau}_1$ and $\hat{\tau}_2$ and μ_{12} is the covariance of ($\hat{\tau}_1$, $\hat{\tau}_2$). As detailed by Hassab in [2], estimates of the variances can be calculated from SNR(ω), the signal-to-noise ratio as a function of frequency. Finally, the predicted biases can be subtracted from $\hat{R}$ and $\hat{\beta}$ to yield better estimates.

Determining a good measure of SNR was not simple. A method which involved partitioning the power spectral density (PSD) into signal and noise contributions was investigated. For the audible range microphones, the power below 8 kHz was considered signal power, S(ω), while the power in the frequencies above 8 kHz was attributed to noise power N(ω). Assuming white noise, the average of the power above 8 kHz was taken to represent the noise power *per frequency*, N(ω). SNR(ω) was simply S(ω) divided by N(ω). However when this value was used for bias removal, the bias decreased but did not disappear.[10] A better method of measuring SNR(ω) could improve performance, but perhaps a whole new approach should be tried.

4.5.2 Range Determination Using the LOCA Technique

A lesser-known range difference location (RDL) algorithm fixes source location on *linear* lines of position using τ estimates from groups of three noncolinear sensors (designated as *triads*) [7]. Described in a paper by Ralph O. Schmidt in 1972, for a given triad, the LOCA (Location On the Conic Axis) technique regards each sensor position as a point on a conic (ellipse or hyperbola), with the source location constrained to be one of the foci on its major axis. The conic axis (x_0, y_0) is a line of position defined by the differences in range between the three pairs of microphones

[10] None of the range estimates were even close, although the bearing estimates appeared reasonable.

(δ_{12}, δ_{23}, and δ_{31}):

$$[x_1\delta_{23} + x_2\delta_{31} + x_3\delta_{12}]x_0 + [y_1\delta_{23} + y_2\delta_{31} + y_3\delta_{12}]y_0 = [\delta_{12}\delta_{23}\delta_{31} + a_1^2\delta_{23} + a_2^2\delta_{31} + a_3^2\delta_{12}] \tag{4.12}$$

where $a_n^2 = x_n^2 + y_n^2$, (x_n, y_n) are the coordinates of microphone n, and $\delta_{ab} = \frac{c}{f_s}\tau_{ab}$.[11] A typical microphone arrangement is shown in Figure 4-5.[12] The foci are defined by the conic axis and the locations of the three microphones. They can easily be found after the microphone coordinate system is rotated so that the x-axis is aligned with the conic axis. Determining which focus represents the correct vehicle location is trivial since array geometry and approximate lane distances (and vehicle trajectories) are known apriori. For hyperbolas, the focus corresponding to a position in front of the array is selected. For ellipses, the focus associated with *positive* time delays (in Equation 4.12) is the true location. Another method of identifying source location and resolving ambiguity involves finding a second line of position using a different set of three microphones. The source coordinates are now specified by the intersection of the two conic axes.

Presently, analysis of sample data from Road Test Three indicates that the LOCA method using delays from a single triad[13] shows promise for accurately measuring R_y, but appears extremely sensitive to fractional offsets in the delay estimates. This observation is supported by simulations using computer-generated "perfect" time delay estimates. As expected, when the LOCA algorithm is used with theoretical τ values, the vehicle's position is reported perfectly. In the microphone coordinate system, the trajectory is a line at R_y. However, when these values are offset by even a small fractional value, the position estimates become biased. Depending on the signs of the three fractional offsets, the reported trajectory tends exhibit two basic shape patterns, examples of which are shown in Figures 4-6 and 4-7. The particular fractional

[11] The effects of noise on the $\hat{\tau}$ can be reduced by subtracting the average of the sum of the three delay estimates ($\frac{1}{3}[\tau_{12} + \tau_{23} + \tau_{31}]$) from each $\hat{\tau}$. In the case of noiseless measurements, the sum should equal zero.

[12] A specific triad geometry from Road Test Three will be referenced as "triad abc" where a,b,c are microphones in coordinates (x1,y1), (x2,y2), and (x3,y3) respectively. The coordinates (specified in feet) for locations a,b,c were provided in Figure 3-21.

[13] Where source location is pinpointed as a conic focus.

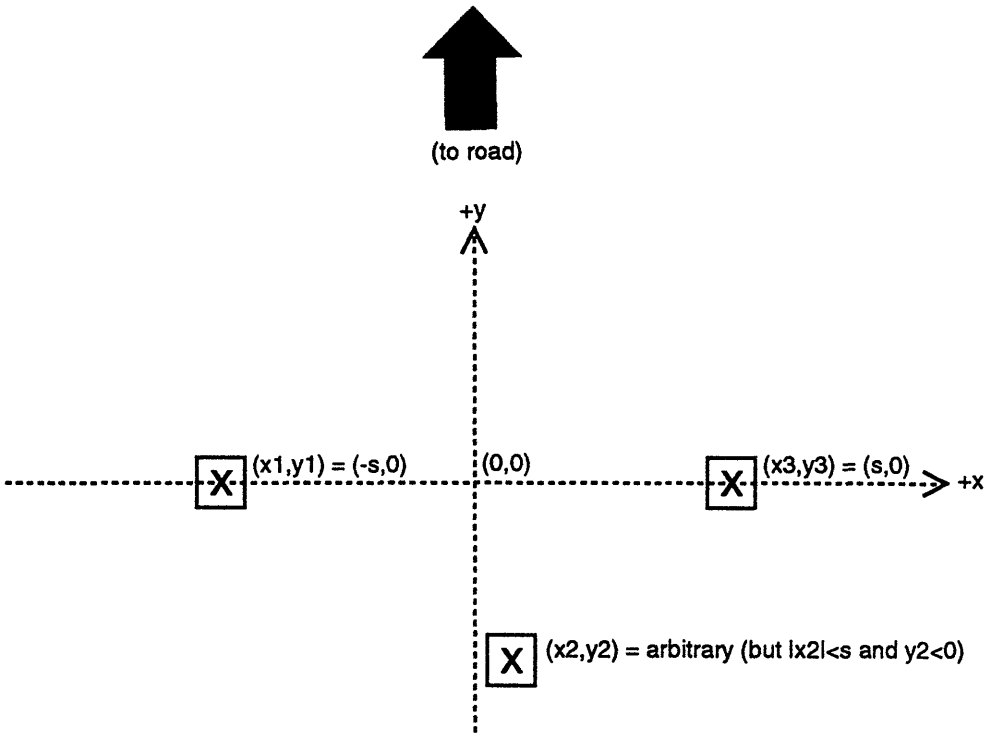

Figure 4-5: Typical microphone configuration used with the LOCA algorithm

offsets chosen for the examples reflect possible offsets which are introduced by the multiplexed sampling scheme of LabWindows (depending on the order the channels are sampled). The "compensated"[14] trajectories returned by the LOCA algorithm tended to exhibit the shape of Figure 4-7, although some seemed to be a combination of both of the basic shapes.[15] Despite inaccuracies in computing a vehicle's *trajectory*, some of the R_y values calculated for a given sample vehicle were correct. In Figure 4-8, R_y estimates from conic foci are compared with those obtained from the intersection of two conic axes.

[14]For fractional sampling delays. Fractional offsets $(\delta_a, \delta_b, \delta_c)$ for a few different sampling orders were tried. $(\delta_a, \delta_b, \delta_c)$ are the compensations for $\tau_{ab}, \tau_{bc}, \tau_{ca}$ respectively for triad abc. An trajectory assuming no sampling offsets (compensation of zero) was also computed.

[15]Biases are either introduced by incorrect compensation for the multiplexed sampling scheme of LabWindows (which is being investigated) or because the τ values obtained from cross-correlation (including the parabolic peak fit) are only *approximate* since the vehicle is in motion.

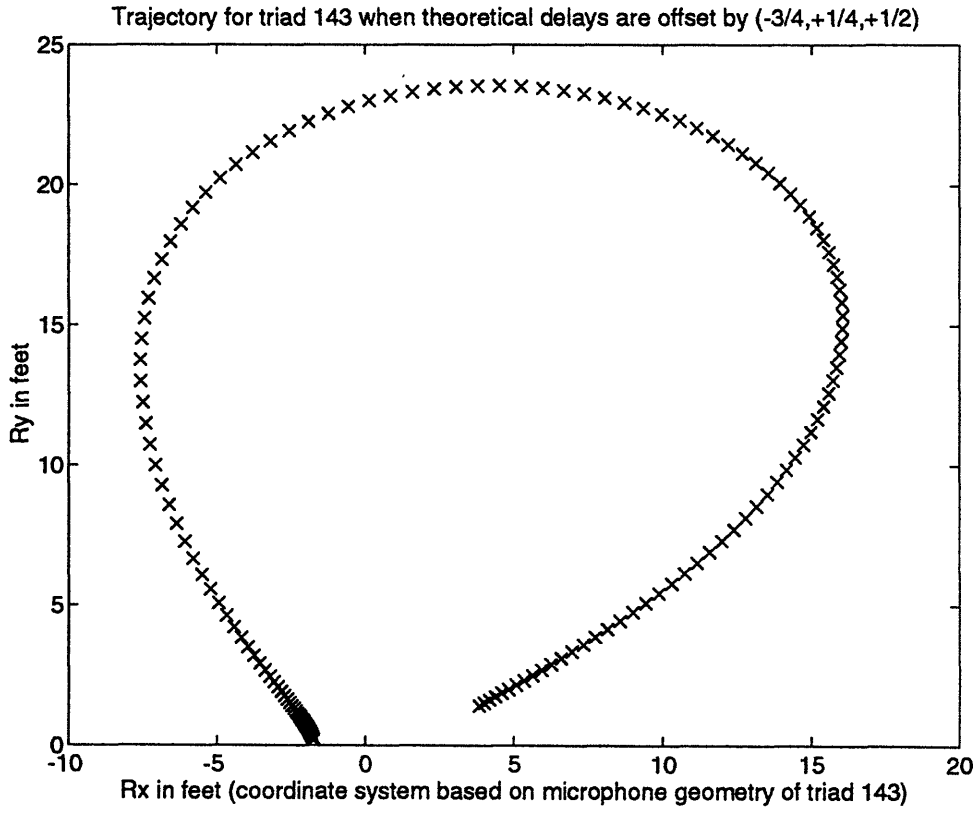

Figure 4-6: A basic trajectory shape returned by LOCA when the theoretical τ values are offset

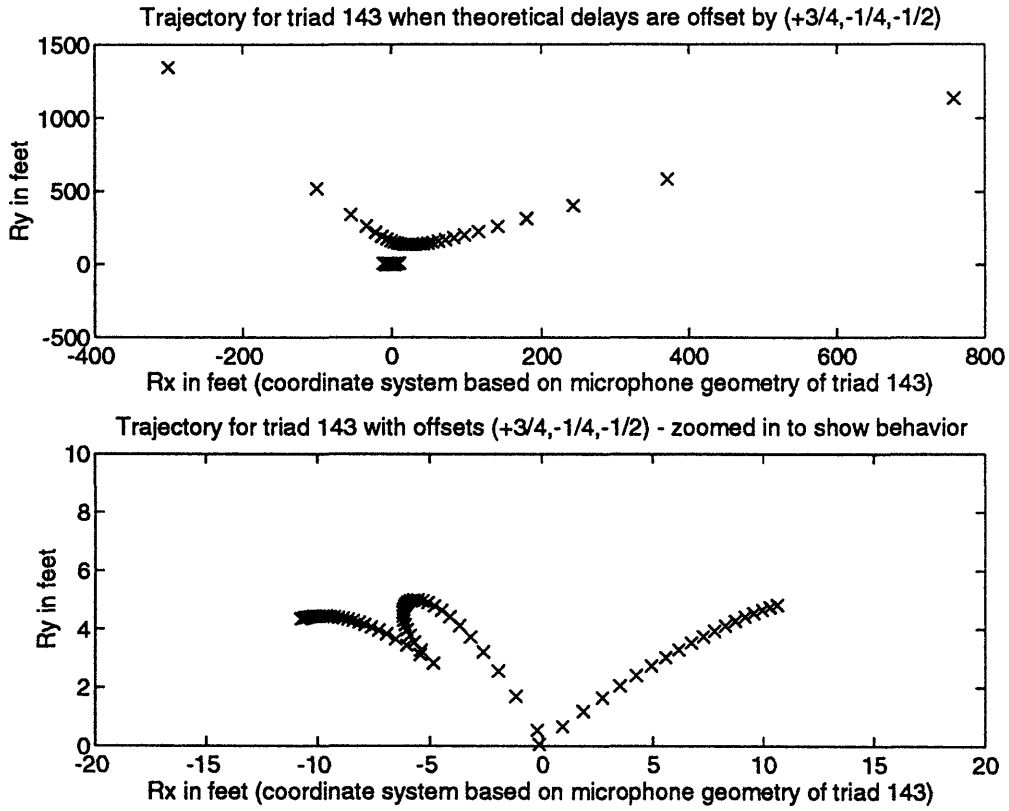

Figure 4-7: Another basic trajectory shape returned by LOCA when the theoretical τ values are offset

Determining source location from the intersection of lines of position (conic axes) for two triads will probably be less sensitive to τ estimation error than fixing location as a conic focus.[16] When the LOCA technique is applied with four microphones, the vehicle's position is theoretically found from the intersection of conic axes corresponding to two of the microphone triads. With four microphones, the two triads considered have two microphones in common. As a result, the calculated lines of position are nearly identical, so small errors in the slopes of the conic axes (obtained from the $\hat{\tau}$) yield large positioning errors. Once again, because the $\hat{\tau}$ were not perfect, an inaccurate trajectory was obtained from experimental data, although some of the $\hat{R}_y$ were correct. Positions determined from the intersection of conic axes corresponding to two widely separated triads (using six microphones) should prove less sensitive to noisy $\hat{\tau}$. This theory should be examined in the future using a better sampling scheme than the one provided by LabWindows.

The $\hat{R}_y$ obtained from a group of four microphones (in positions 1,2,3,4 of Figure 3-21) tracking a semi in lane 4 are provided in Figure 4-8. Range estimates from finding the conic foci for triads 142 and 143 are compared with those from the intersection of conic axes of the same two triads. The true value of R_y was approximately 40 feet and is indicated by a solid line. A correlation window of 1000 samples (for f_s = 22500 Hz) was chosen to generate the $\hat{\tau}$ with an overlap of 500 samples between windows. Each signal section reflects the estimates from one correlation window, and the time between successive estimates is $\frac{500}{22500}$ (= 0.022) seconds. The R_y estimates are provided in *chronological* order as the vehicle passes through the detection zone, although the vehicle is headed in the *negative* x direction of the microphone coordinate system.

Though many incorrect values were reported, the LOCA algorithm shows some potential for measuring R_y. Current research efforts are still concentrated upon using LOCA for determining range (using different array geometries). In the future, extended Kalman Filtering (EKF) techniques, which account for measurement noise,

[16]However, a combination of the two methods can always be employed if more than one triad is available.

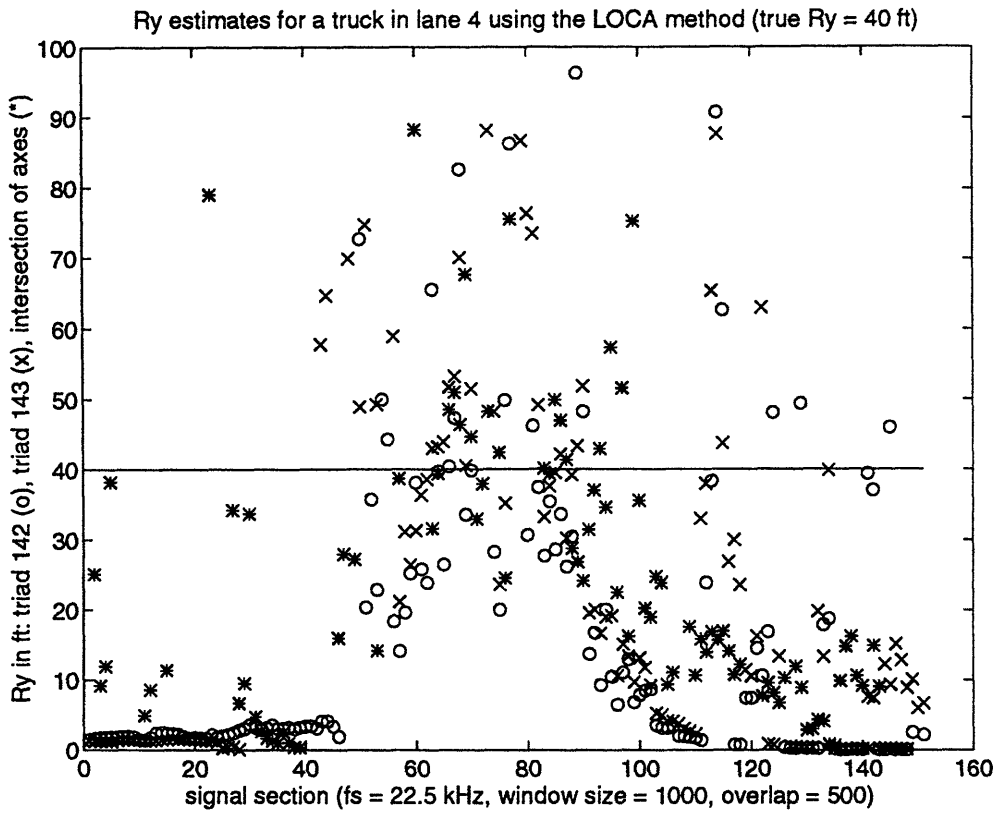

Figure 4-8: $\hat{R}_y$ returned by LOCA for single triads (focus) vs. two triads (intersection) (for a truck in lane 4 at a distance of 40 feet - R_x values were ignored)

may be used to support (or replace) LOCA in generating dependable $\hat{R}_y$. EKF is described in the following subsection as a third alternative for determining range.

4.5.3 Source Tracking With the Extended Kalman Filter

The Kalman filter is a standard technique for tracking parametric (state) changes using sensor measurements and a model of system dynamics. Kalman filtering minimizes the perceived error between *actual* sensor measurements and *predicted* measurements by using a feedback loop which drives the error to zero. The result is the minimization of a quadratic cost function where weighting is provided by "confidence" matrices for both the system model and measurements. When the system is nonlinear, a linear model is obtained by performing a Taylor series expansion about a nominal trajectory. The chosen trajectory is traditionally the previous state, so the

extended Kalman filter (EKF) effectively estimates parametric *changes* rather than the actual states.

For vehicle tracking, since range (R) and bearing (β) can be determined from the $\hat{\tau}$ from two microphone pairs in a colinear array, an EKF can be designed to monitor the changes in these parameters (or R_x and R_y) while the vehicle is in the detection zone. Possible choices for state vectors include [R,β,$\frac{dR}{dt}$,$\frac{d\beta}{dt}$][17] or [R_x,R_y,$\frac{dR_x}{dt}$,$\frac{dR_y}{dt}$][18]. Depending on the array geometry, location measurements from either hyperbolic RDL or LOCA are combined with position predictions from the system model to generate the new state vector. A well-designed EKF will generate more accurate position estimates than either hyperbolic RDL or LOCA alone because it compensates for measurement errors. As a bonus, vehicle speed can be obtained as one of the states ($\frac{dR_x}{dt}$)! The effectiveness of EKF for different array geometries will be investigated in the future once statistical analyses of τ estimation noise are completed.

4.6 Multiple Vehicles

When $\hat{\tau}$ vs. time curves for individual vehicles can be separated, the algorithm returns excellent results. Therefore, for each distinctive region of the $\hat{\tau}$ vs. time curve, the number of vehicles present must be determined. The problem becomes more challenging when multiple vehicles are simultaneously present in the detection zone. These cases are examined in greater detail in this section.

Curves from vehicles passing each other from opposite directions are easily identified. For observation windows where both vehicles are in range, the $\hat{\tau}$ reflect the motion of the *dominant* source. The overall $\hat{\tau}$ vs. time curve *alternates* between points that represent the motion of one vehicle or the other. A demonstration plot obtained from real data is shown in Figure 4-9. When the curves for the two vehicles are separated (with noisy values discarded), the plots in Figure 4-10 are obtained. "Missing" data points in Figure 4-10 make curve fitting difficult and inaccurate.

[17] Which corresponds to the hyperbolic RDL technique.
[18] Which corresponds to the LOCA method.

In these cases, the motion of the secondary source is often indicated by τ estimates corresponding to *other* peaks of the cross-correlation function (usually the second or third largest peak). These values can be used to supplement the original $\hat{\tau}$. In Figure 4-11, the plot from Figure 4-9 was augmented with τ estimates from tracking the second and third largest peaks of the cross-correlations within a window of ± 30 samples. The $\hat{\tau}$ from the largest peak are denoted by 'o', with the second by 'x', and the third by '+'. Obviously, a great deal of noisy values are introduced by plotting *all* the τ estimates from tracking the first three peaks. Consequently, appropriate supplemental points were visually selected and included, which yielded the graph of Figure 4-12.

A more formal procedure for selecting supplemental points is suggested below:

1. Beginning with the original $\hat{\tau}$ obtained from the peak, the curves are separated. A non-visual method for doing this has not been developed yet.

2. Obvious noisy (impulsive) values are discarded by performing polynomial fits over the "smooth" sections of the curve. Points which are greater than δ from the fitted curve are rejected as noise. If necessary, this step can be repeated until the fitted curves don't change very much. Usually only one iteration is sufficient.

3. Consider one vehicle's τ curve. Supplemental values are only necessary in the large "blank" intervals where the other vehicle dominates. The τ estimates from tracking the next largest peak are examined for this interval. If they are *within* some ϵ of the fitted curve, they are kept. All other values are discarded.

4. The process is repeated (steps 2-4) with as many τ estimates from other peaks as desired. Tracking three peaks yielded good results in this case.

After the supplemental points are added, each curve is fitted and the slope (and sign) at the inflection point found. The speeds calculated from the augmented τ estimates agreed well with the values from the verification system.

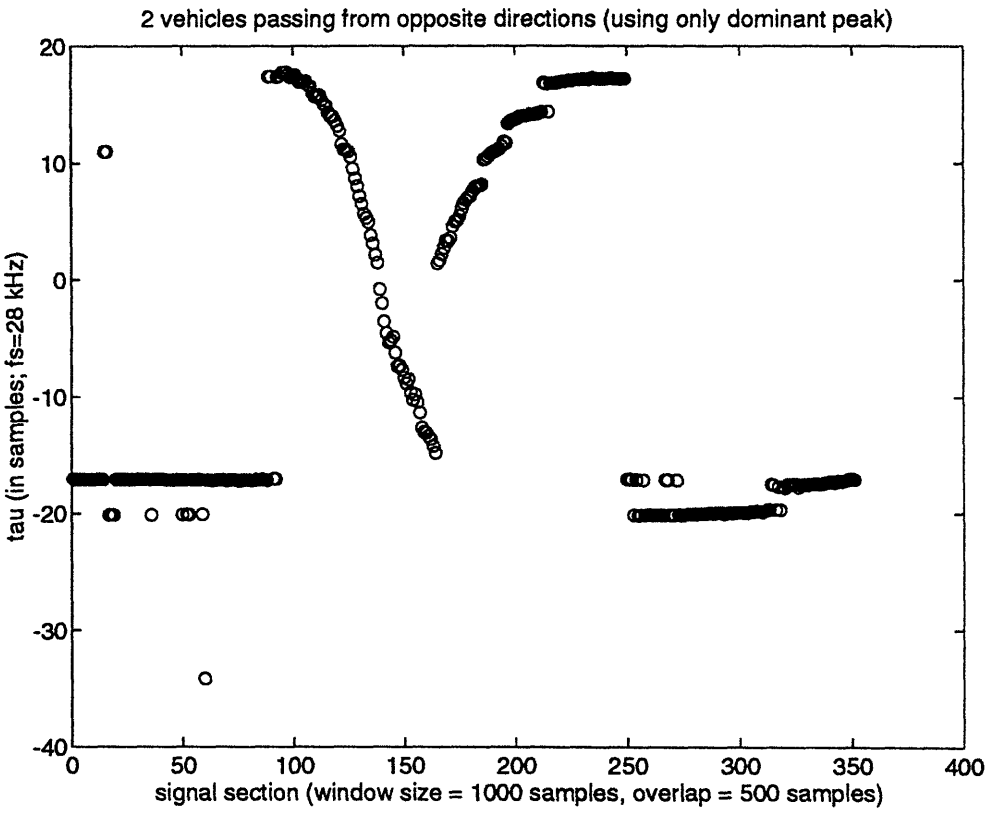

Figure 4-9: τ vs. time for two vehicles crossing from opposite directions (before supplemental points are added)

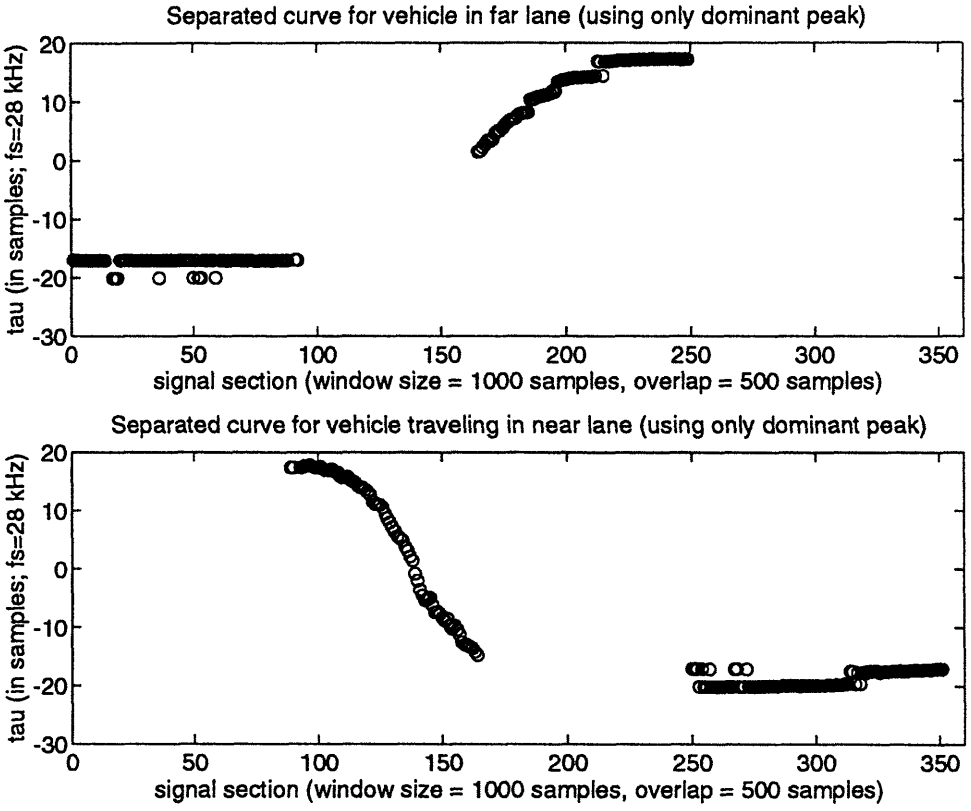

Figure 4-10: Separated curves for two vehicles crossing from opposite directions (before supplemental points are added)

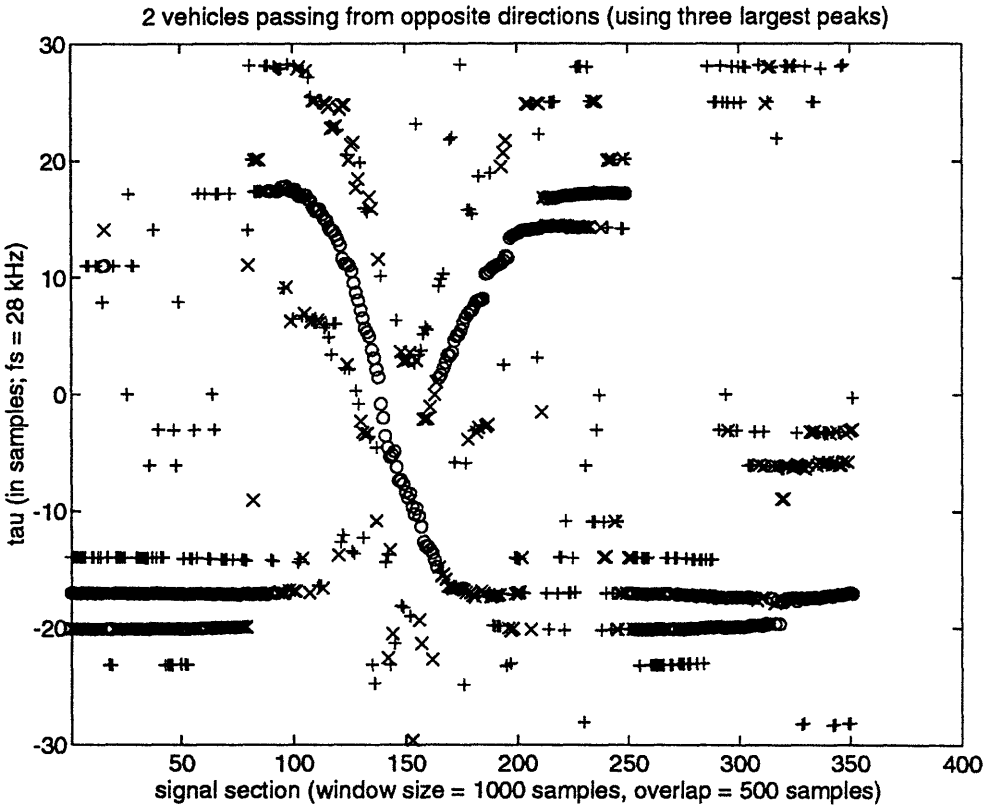

Figure 4-11: τ vs. time for two vehicles crossing from opposite directions (after addition of supplemental points)

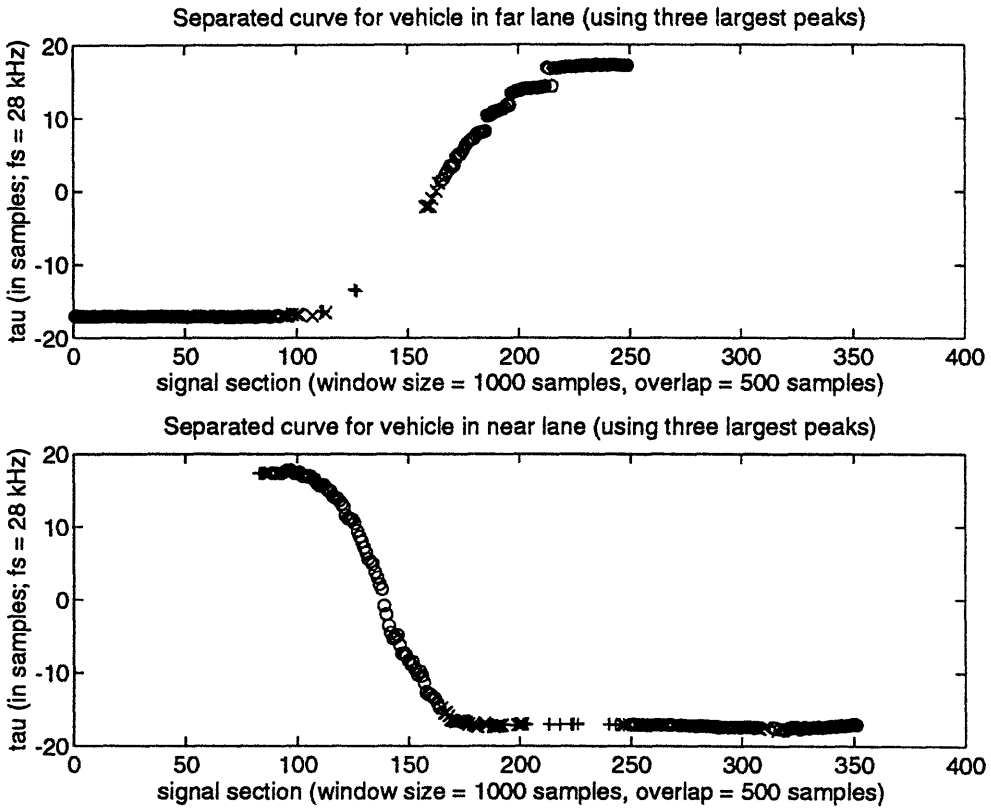

Figure 4-12: Separated curves for two vehicles crossing from opposite directions (after addition of supplemental points)

When vehicles are following each other closely, part of the τ vs. time curve of the leading vehicle is masked by $\hat{\tau}$ reflecting the motion of the next vehicle. An example of this is shown in the τ vs. time plot of Figure 4-13. Once again, when supplemental points from tracking the second and third largest peaks of the correlation function are inserted, the curve fit (and subsequent speed measurement) improves significantly as displayed in Figure 4-14.

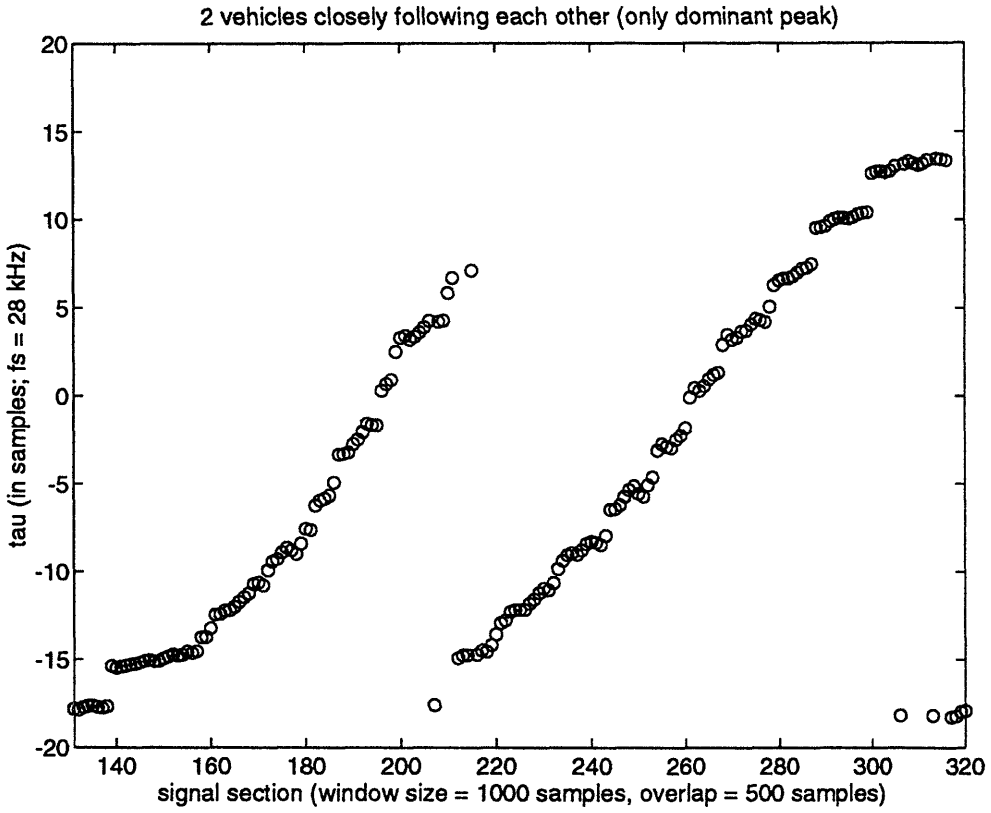

Figure 4-13: τ vs. time for two vehicles following each other closely (using only dominant peak)

The greatest difficulty arises when multiple vehicles are traveling alongside each other in the same direction but in different lanes. Considering the case of two vehicles for simplicity, if one vehicle passes the other in front of the array, the τ vs. time curve fluctuates near the inflection point, then once again reflects the dominant source's motion. When vehicles are traveling at different speeds, there is usually enough of a distinction that the curves for each vehicle can be separated and the method of

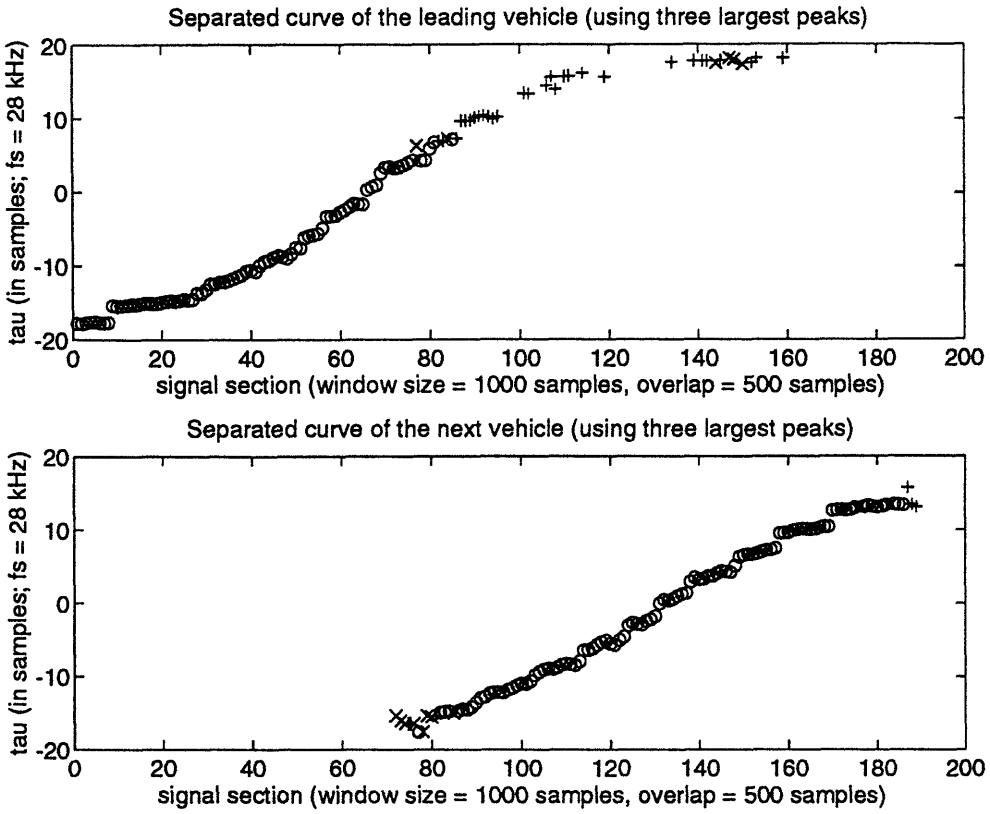

Figure 4-14: Separated curves for two vehicles following each other closely (after addition of supplemental points)

adding supplemental points can be applied.

Two examples of this are demonstrated. In both scenarios, a car in lane 3 overtook a tractor-trailer (semi) in lane 4. In the curve of Figure 4-16, τ estimates from the second largest peak were included to supplement values from the dominant peak. In Figure 4-18, estimates from the three largest peaks were combined. In both cases, the calculated speeds agreed with the verification system measurements.

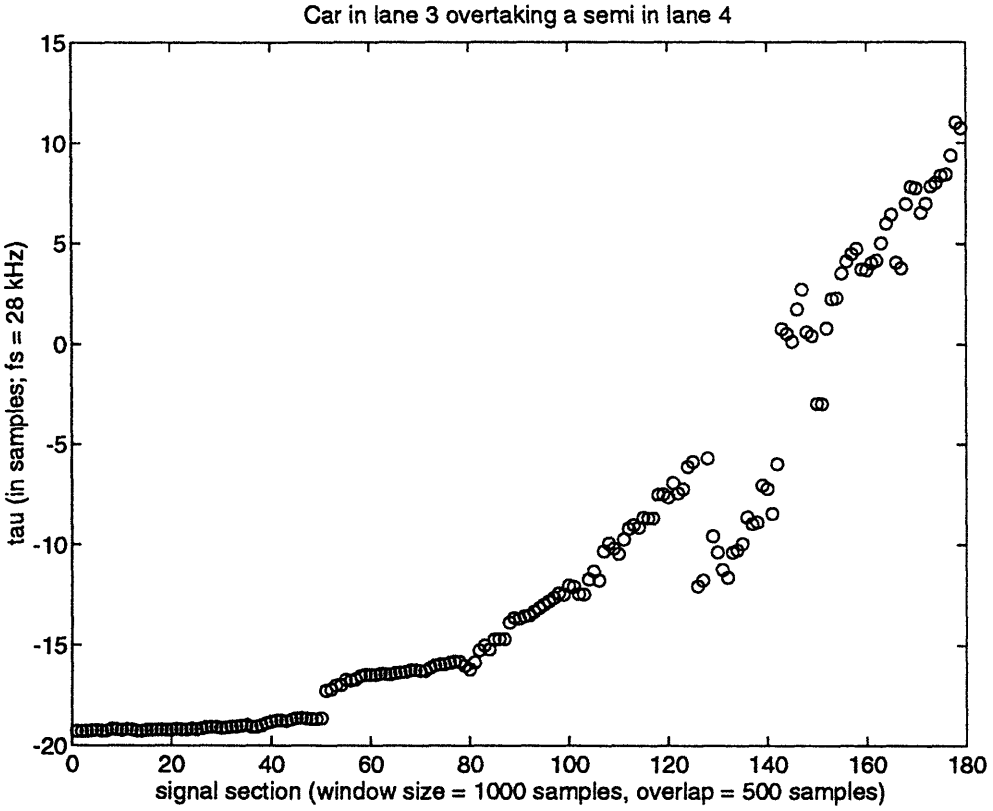

Figure 4-15: τ vs. time for a car in lane 3 overtaking a semi in lane 4 (Case 1) (using only dominant peak)

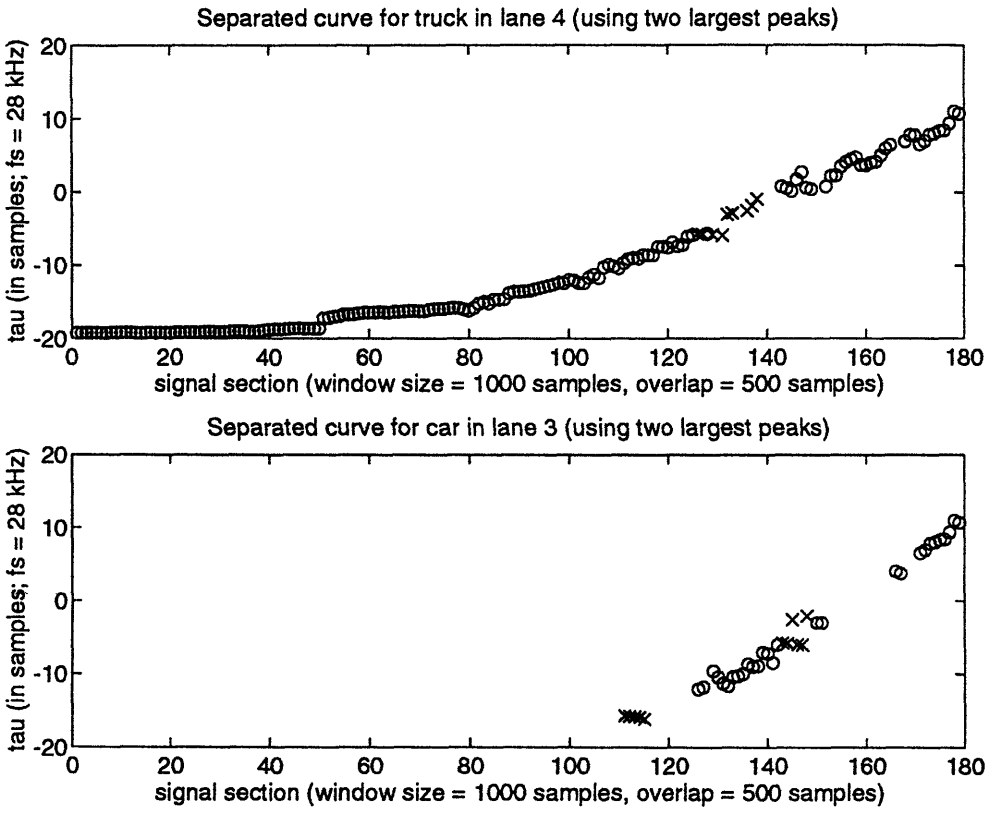

Figure 4-16: Separated curves for car overtaking semi (Case 1)
(after addition of supplemental points)

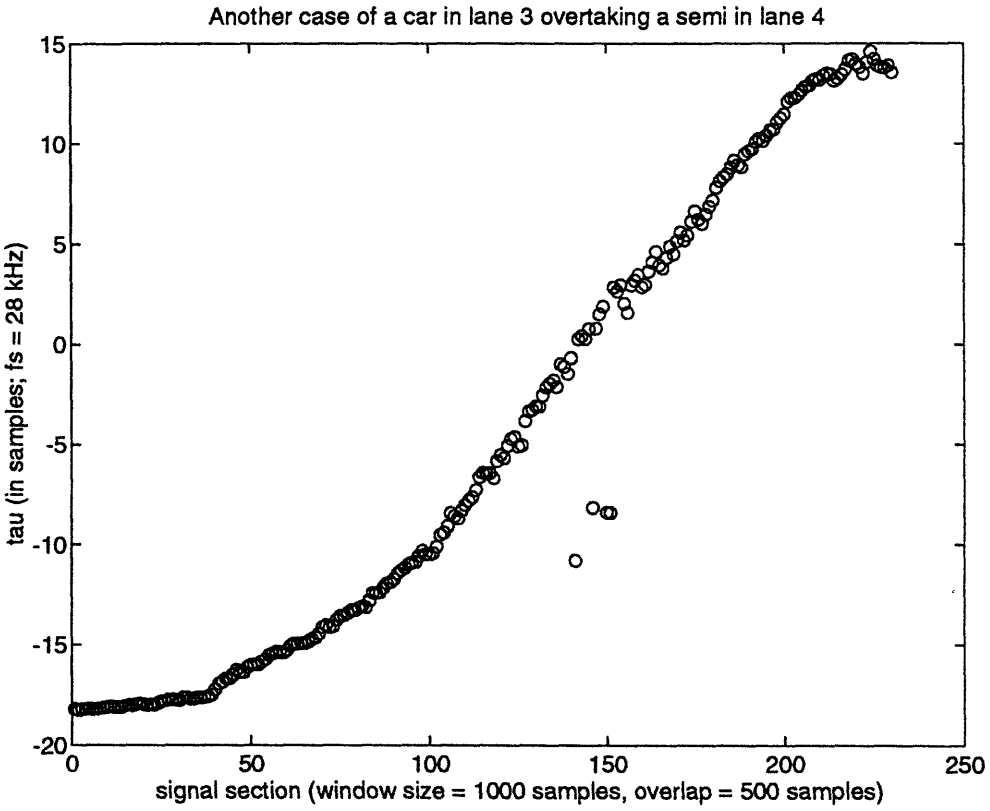

Figure 4-17: τ vs. time for a car in lane 3 overtaking a semi in lane 4 (Case 2) (using only dominant peak)

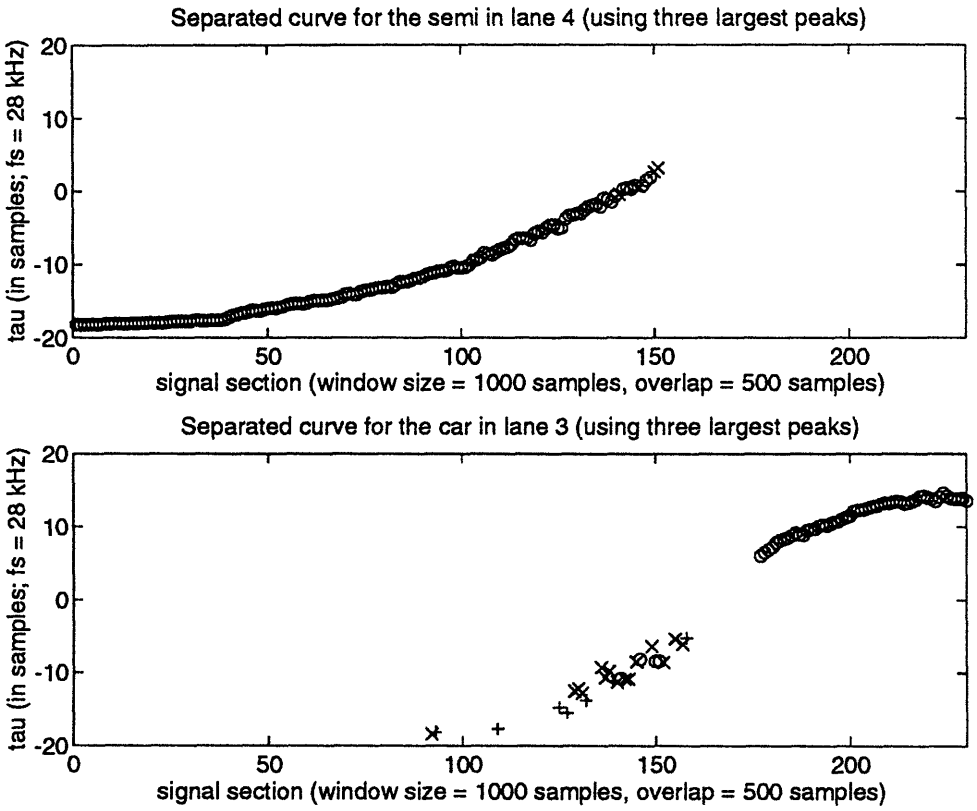

Figure 4-18: Separated curves for car overtaking semi (Case 2) (after addition of supplemental points)

However, when two vehicles are traveling in the same direction side by side at similar speeds, the observed τ vs. time curve is very similar to one from a single vehicle! A plot of τ vs. time (using the four largest peaks) for a case where two cars were traveling at the same speed in lanes 3 and 4 appears in Figure 4-19. Their common speed can be determined using the current algorithm. However, the fact that there are two vehicles present is difficult to detect. A reliable means of determining the *presence* of more than one vehicle in the detection zone must be formulated if the sensor is to be used for monitoring multi-lane roadways. This remains a problem to be handled in the future, possibly with frequency domain techniques.

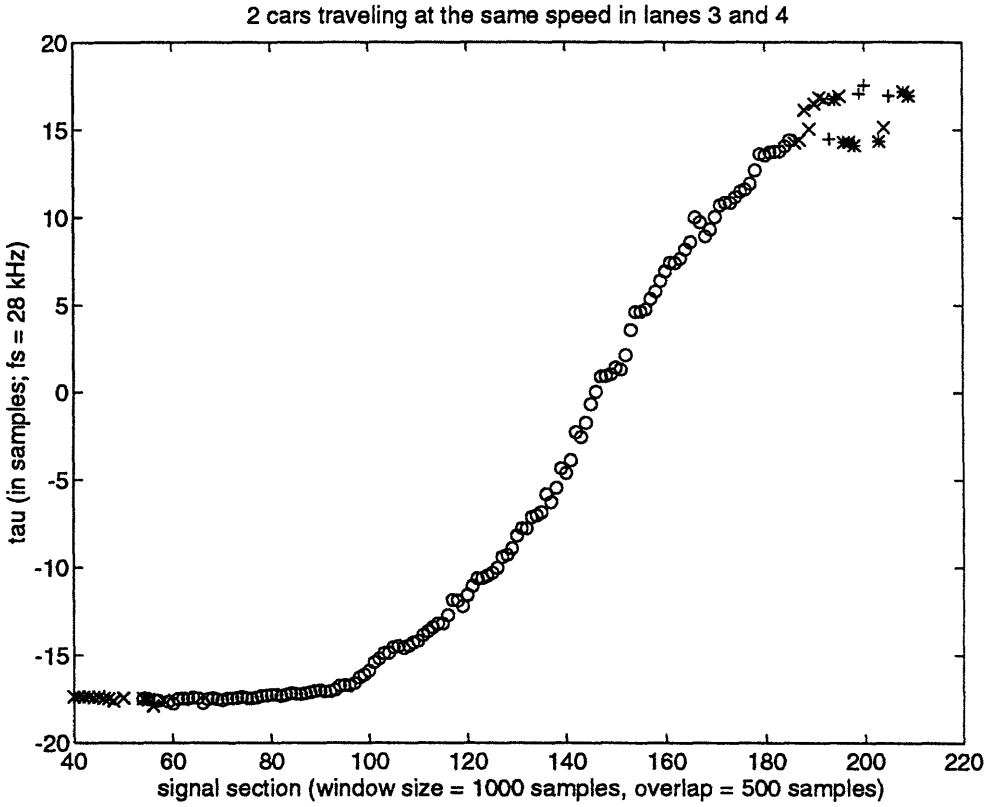

Figure 4-19: Two cars traveling at the same speed in the same direction side by side (using the four largest peaks)

4.7 Algorithm Performance

Tables 4.1 and 4.2 compare speed estimates returned by the algorithm (when R_y is given) with actual speed values obtained from the verification system during Road Test Two. Except in certain multiple vehicle cases which are highlighted in Table 4.1, the algorithm appears to work quite well.

Table 4.1: Algorithm speed estimates for multiple vehicle cases

Case	Lane	Vehicle #	Type	R_y[a]	Actual Speed[b]	Speed Estimate[c]
Passing	2	29	car	24	40.91	34.14[d]
from	4	30	car	43	28.64	28.21[d]
opposite	1	31	car	23	40.91	36.00
directions	4	32	pickup	43	32.73	38.23
Passing	3	33	car	36	28.64	28.98[e]
from	4	34	semi	44	24.55	26.41[e]
same	3	35	car	37	32.73	32.00[f]
direction	4	36	semi	46	20.45	23.64[f]
Same speed	3	37	pickup	38	36.82	35.92[g]
& direction	4	38	car	46	36.82	35.92[h]

[a] R_y (in feet) is approximated by visually inspecting the video data. The total width of Hartwell Avenue at the data collection point is 40 feet.

[b] Once again, it is emphasized that the speed measures (in mph) from the verification system are *approximate*, especially for lanes (3 and 4). The estimates from the verification system are likely within ± 5 mph of the true speed. More accurate speed measurements will probably be obtained with a radar gun in the future. However, current comparisons are an indication of algorithm potential.

[c] $\hat{\tau}$ from the three largest peaks were used to estimate vehicle speed (in mph).

[d] Speed estimates from Figure 4-12.

[e] Speed estimates from Figure 4-16.

[f] Speed estimates from Figure 4-18.

[g] Speed estimates from Figure 4-19. In this situation, the τ vs. time curve reflected the motion of the vehicle in lane 3. The presence of an additional vehicle in lane 4 is not indicated by the plot.

[h] It is assumed that if the presence of two vehicles is determined and the τ vs. time plots for individual vehicles cannot be separated, then they must be traveling at the *same* speed. The τ vs. time plots and the range measurement should reflect the motion of the closer vehicle.

Table 4.2: Algorithm speed estimates for single vehicle cases

Lane	Vehicle #	Type	R_y[a]	Actual Speed[b]	Speed Estimate[c]
1	1	car	23	38.18	36.86
	2	pickup truck	23	38.86	39.17
	3	car	24	28.64	29.03
2	4	pickup truck	25	38.86	35.07
	5	car	26	36.82	34.97
	6	semi (front axles)	26	28.64	27.92
		semi (rear axles)	26	28.64	30.32
	7	car	26	40.91	38.42
	8	car	29	40.91	40.29
3	9	car	38	35.80	38.69
	10	car	38	32.73	33.50
	11	van	39	46.02	44.91
	12	car	40	32.73	34.21
	13	car	41	30.68	37.00
	14	motorcycle	42	40.91	48.47
4	15	car	42	40.91	44.10
	16	car	42	27.27	26.70
	17	car	43	32.73	33.88
	18	car	43	28.64	32.80
	19	car	43	32.73	38.17
	20	car	43	35.80	39.62
	21	US Mail truck	43	32.73	34.39
	22	car	46	32.73	33.38
	23	car	46	32.73	34.16
	24	car	46	30.68	35.70
	25	car	46	36.82	41.80
	26	car	46	27.27	32.04
	27	car	46	40.91	45.45
	28	van	46	26.59	31.60

[a] R_y is specified in feet.
[b] The actual speed is specified in mph.
[c] The speed estimate is specified in mph.

4.8 Sensor Design Issues

Now that the basic algorithm has been outlined, design issues involving sensor hardware and the processing scheme will be addressed. Hardware-related parameters involve the choice of sensor components (number and type) and array placement (Y_0, which is the distance to the road edge, and sensor geometry).[19] User-defined algorithm parameters include, but are not limited to, the sampling rate (f_s), the correlation window size (W_{size}), the width of the correlation peak search (Δ), the fractional overlap between correlation windows (α), the type and order of curve fits, and the number of peaks to track for supplemental points (N_{peaks}). The ultimate objective is measurement precision in the largest number of traffic situations while minimizing cost, computation, and array size. Many of the effects from design choices are coupled and can be traded off against each other. These tradeoffs are discussed in this section.

4.8.1 Hardware Considerations

Each "acoustic center" in the triple aperture array is comprised of microphones which determine its range and directivity. An acoustic center could be either a single directional microphone (which is considered in this thesis) or a group of phase-matched microphones with an effective beam width and gain (which varies with frequency). Beamforming techniques could greatly enhance the accuracy of delay estimates by focusing attention on a specific spatial and frequency region which reduces interference from noise and other vehicles. However, the cost of phased-matched microphones and the complexity of beam processing makes the idea unattractive. In this investigation, single directional microphones proved quite effective as acoustic centers. Their use will be continued in forthcoming studies.

Currently, the algorithm has relied only on audible range microphones to generate

[19]The dimension s will refer to the separation between a pair of microphones which is parallel to the road whose τ vs. time curve provides the speed estimate. Even for the noncolinear arrays used with the LOCA technique in Road Test Three, triads were chosen where one of the microphone pairs was parallel to the road.

$\hat{\tau}$. In general, the Sennheiser microphones seemed to exhibit better performance than the Radio Shack microphones. However, this might have resulted from increased stationarity during the road tests (due to larger R_y), the continuous flow of traffic (which yielded few $\hat{\tau}$ attributed entirely to noise), and the inclusion of anti-aliasing filters. It would be interesting to determine if cardioid microphones from Radio Shack[20], which cost about $3 apiece, could perform as well as the Sennheiser microphones, which cost about $30 each. This may be pursued in the future. Likewise, additional research may be directed toward incorporating ultrasonic microphones for improving τ estimates.

The choice of array position (Y_0) defines limits for quasi-stationarity. In this problem, quasi-stationarity imposes constraints on source motion observed by a pair of microphones over a given time interval. Since vehicle motion is reflected in the change in time delays over time, quasi-stationarity limits $\frac{d\tau}{dt}$ *over the length of the correlation window*. Actually it is the *relative* change in τ over the correlation window, $\frac{\tau'}{\tau}$ (where $\tau' = \frac{d\tau}{dt}$), which should be kept small. Equations 4.1 and 4.2 indicate that increasing R_y (which is equal to Y_0 plus a constant) reduces the ratio of $\frac{\tau'}{\tau}$. Consequently, correlations can be performed over longer windows while still satisfying quasi-stationarity. In the same vein, for correlations over a fixed window size, the mean squared-error (MSE) of the $\hat{\tau}$ will decrease as R_y is increased. The drawbacks for lengthening R_y are reduced gain and SNR, a broadened detection zone (allowing greater interference from other vehicles), and increased range and bearing estimate bias (as discussed in the next paragraph). For ultrasonic microphones, R_y should be kept as small as possible due to their limited range.

For both colinear and noncolinear arrays, sensor spacing influences the performance of localization methods and affects the size of τ estimates. With triangulation, when R_y>>s, the baseline of the triangle is very short and estimates of R_y will exhibit bias. Likewise, for the LOCA technique, when R_y is much larger than the array spacing, small errors in determining a line of position can lead to large localization errors since the sensor positions which determine the conic are closely spaced.

[20]Instead of the omnidirectional ones from the field tests.

In both situations, the smaller the array spacing is, the greater the bias on source position estimates. A lesser motivation for keeping sensor spacing large is to reduce the effect of quantization noise on $\hat{\tau}$. For wider intersensor separation, the ratio of $\frac{\hat{\tau}}{T_s}$ is increased, so the effect of quantization is diminished. In most situations, however, R_y is much greater than the array dimensions because it is preferable to minimize array size.[21] Furthermore, it is desirable to keep intersensor spacing small so that the acoustic environment surrounding each microphone is as similar as possible.

Expected τ vs. time curves (using Equation 4.1) for varied speeds ($\frac{dx}{dt}$), R_y, and spacing (for a pair parallel to the road) were generated using Matlab. For $Y_0 = 16$ feet, $f_s = 28$ kHz, $W_{size} = 1000$ samples, and $\alpha = 0.5$, an intersensor spacing of 10 inches yielded $\hat{\tau}$ which ranged between $\pm$ 20 samples. Furthermore, for the worst case where a fast vehicle is traveling in lane 1, even at a speed of 85 mph, more than thirty τ estimates are generated while the vehicle is within $\beta = \pm 45°$, which is enough for a reasonable curve fit. The ratio of $\frac{\hat{\tau}'}{\hat{\tau}}$ is not very large (except near the inflection point where this is usually true), so theoretically good speed estimates are attainable. In the interest of keeping the array small while maintaining the flexibility of measuring nearby high speed vehicles, a spacing of 10 inches (for a total length of 20 inches) for the colinear array of Road Test Two proved a good compromise in light of other parameter settings.

4.8.2 Algorithm Parameters

Most of the algorithm parameters (f_s, W_{size}, α, Δ, type and order of curve fits, and N_{peaks}) have coupled effects on stationarity and the accuracy of the $\hat{\tau}$ and $\frac{d\hat{\tau}}{dt}$. The price for precision in these cases is often increased processing time and complexity.

The sampling rate (f_s) is the first factor which limits the accuracy of τ and $\frac{d\tau}{dt}$ estimates. Because of the discrete nature of the problem, $\hat{\tau}$ generated from cross-correlating the data will exhibit quantization noise of $\pm\frac{T_s}{2}$ (as previously mentioned). Moreover, it is important that the ratio of $\frac{f_s}{f}$ (or samples per cycle) over the frequen-

[21] This may not be true in a tunnel since R_y will be small due to limited space.

cies of interest be large so that distinct correlation peaks can be identified. Choosing a high f_s helps alleviate these problems, but increases computational load. Since IVHS requires sensors to monitor traffic in real-time, the sampling rate should be kept relatively low to reduce the average processing time per vehicle. However, due to the wide availability of inexpensive, high-speed processors, limitations on the sampling rate are minimal, especially since the current algorithm is not computationally intensive.

Since most of a vehicle's acoustic energy in the audible range is concentrated in frequencies below 8 kHz, a two-pole anti-aliasing filter with a cutoff frequency of 12 kHz was applied to the microphone outputs of Road Test Two before sampling. A sampling rate of 28 kHz was chosen to avoid aliasing problems, reduce the effects of quantization error, and maintain a high samples per cycle ratio over most of the frequency band.[22] The slow multiplexed sampling scheme employed by LabWindows did not permit consideration of higher sampling rates; however, $f_s = 28$ kHz proved sufficient for analyzing the audible range microphone data from Road Test Two.

A more significant algorithm design issue is the selection of the correlation window size (W_{size}) and the fractional overlap between successive windows (α). W_{size} directly influences the precision and mean squared error (MSE) of the delay estimates, while α affects the smoothness of the $\hat{\tau}$ vs. time curve. Both help specify processing requirements.

There are various tradeoffs associated with choosing an appropriate window size. Over each correlation interval, quasi-stationarity conditions are related to the ratio of $\frac{\tau'}{\tau}$, which is a measure of the MSE of the delay estimates.[23] $\frac{\tau'}{\tau}$ depends on several factors: W_{size}, Y_0, s, and vehicle speed. For a *fixed* W_{size}, $\hat{\tau}$ from intervals where a vehicle is near the edges of the detection zone exhibit less MSE than those from segments where the vehicle is closer to the array. In general, choosing shorter correlation windows reduces the MSE on *all* τ estimates, while adaptive window sizing

[22] When *four* channels of data from Road Test Three were required for evaluating the LOCA algorithm, the cutoff frequency of the anti-aliasing filters was lowered to 10 kHz and a sampling rate of 22.5 kHz (per channel) was employed.

[23] The exact relationship between $\frac{\tau'}{\tau}$ and the MSE of $\hat{\tau}$ has not been explored in this thesis.

(longer at the edges of the detection zone and shorter near the center) keeps the MSE of individual $\hat{\tau}$ values more balanced. The negative aspect of choosing short correlation windows is that the signals being correlated become less distinct. For shorter sample windows, the frequency resolution (Δf_{res}) which is *inversely* proportional to the length of the time window ($T_{win} = \frac{W_{size}}{f_s} = W_{size}T_s$), worsens, making τ estimates more prone to error. Adaptive window sizing is a possibility to consider in the future, but it requires more complex processing (and bookkeeping).

The fractional overlap (α) specifies the time difference between the instantaneous τ estimates, Δt, where:

$$\Delta t = (1 - \alpha)T_{win} \tag{4.13}$$

Essentially, it defines an effective temporal sampling rate for the τ vs. time curve, where the $\hat{\tau}$ from the cross-correlations are the "samples". α should be chosen large enough so that a good curve fit can be achieved. A method for obtaining a lower bound on α follows.

Given that the microphones have a directivity of β°_{max}, the time a vehicle spends in the detection zone is:

$$T_{zone} = \frac{2R_y tan(\beta_{max})}{\frac{dx}{dt}} \tag{4.14}$$

The number of $\hat{\tau}$ values obtained in this time interval is:

$$N_x = \frac{T_{zone}}{\Delta t} \tag{4.15}$$

Assuming that at least N_{min} samples are needed for a reliable curve fit [24], a lower bound for α can be found by considering the worst case of a fast car traveling at M_{max} ft/sec (the maximum $\frac{dx}{dt}$ expected) in the closest lane ($R_y = Y_0$). In this case,

[24] A formal procedure for selecting the value of N_{min} is not presented because it depends on the method of curve fitting.

the minimum time a vehicle will spend in the detection zone [25] is:

$$T_{zone,min} = \frac{2Y_0 tan(\beta_{max})}{M_{max}} \tag{4.16}$$

Since at least N_{min} samples are desired, this implies that:

$$N_{min} \leq N_{x,min} \left(= \frac{T_{zone,min}}{(1-\alpha)T_{win}} \right) \tag{4.17}$$

Solving for α yields:

$$\alpha \geq 1 - \frac{2Y_0 tan(\beta_{max})}{N_{min} T_{win} M_{max}} \tag{4.18}$$

In practice, α should be set conservatively if possible. During the analysis of the data from Road Test Two, an α of 0.5 was employed. For $M_{max} = 125 \frac{ft}{s}$ (= 85 mph), $Y_0 = 16$ feet, and $\beta_{max} = 60°$, this corresponded to a minimum of 24 delay estimates which is reasonable.

The processing time per vehicle also varies with window size and fractional overlap. Once the array's physical parameters (Y_0, s, and the geometry) are set, the boundaries of the detection zone in which the vehicle will spend a fixed amount of time (T_{zone}) are established. The number of cross-correlations performed is also the number of τ estimates obtained, N_x. An efficient method of computing the cross-correlation entails two FFTs and one inverse FFT, for a computational requirement on the order of $N_{corr} = 3Nlog_2(N)$ multiplications, where N is the next power of 2 greater than W_{size}.[26] The total amount of computations required for a single vehicle's τ vs. time curve is on the order of:

$$N_{comp} = \frac{T_{zone}}{\Delta t} N_{corr} = \frac{2R_y tan(\beta_{max})}{(1-\alpha)W_{size} T_s \frac{dx}{dt}} [3Nlog_2(N)] \tag{4.19}$$

[25] Assuming that $R_y tan(\beta_{max})$ for the farthest lane of interest is within the range of the microphones. If this is not true, a vehicle in the farthest lane might spend the less time in the detection zone than one in the closest lane.

[26] Technically, since the peak search is only conducted within $\pm\Delta$ samples of the center, only $2\Delta + 1$ samples of the cross-correlation function need to be found. Direct computation of these values requires $(2\Delta + 1)W_{size}$ multiplications. For large W_{size}, it would be more efficient to use direct computation if $(2\Delta + 1)W_{size} < 3Nlog_2(N)$.

As this equation suggests, as long as W_{size} is a power of 2 (or close to it, but below it), the difference in the number of computations for different window sizes depends on a factor of $log_2(N)$.

If $(2\Delta + 1)W_{size} < 3Nlog_2(N)$, the number of computations becomes:

$$N_{comp} = \frac{2R_y tan(\beta_{max})}{(1-\alpha)T_s \frac{dx}{dt}}[(2\Delta + 1)] \tag{4.20}$$

In general, the gate Δ should be set just large enough to accomodate the expected τ value corresponding to the farthest point in the detection zone. Keeping Δ narrow reduces computation and rejects spurious values. While generating the $\hat{\tau}$ for the data from Road Test Two, Δ was set conservatively at 30 samples.

All things considered, $W_{size} = 1000$ samples was chosen to provide a reasonable number of $\hat{\tau}$ when tracking fast vehicles, while maintaining good frequency resolution (Δf_{res}) for precision. The window was narrow enough that the assumption of quasi-stationarity held for most of the correlation windows (except perhaps near the inflection point).

Once the τ estimates for a single vehicle are isolated, they should be smoothed using curve fitting methods before the slope at the inflection point is found. This is especially critical because $\hat{\tau}$ around the inflection point will exhibit *higher* MSE and are therefore more unreliable. This arises because $\frac{\tau'}{\tau}$ is much larger as the vehicle approaches the point directly in front of the midpoint of the microphone pair. Since the $\hat{\tau}$ values around the inflection point can be relied on only in a general sense, smoothing should be performed using as many values as possible from the overall $\hat{\tau}$ vs. time curve. So far, only polynomial curve fitting has been considered due to its simplicity. A fifth-order polynomial fit returns good results when the $\hat{\tau}$ vs. time plot is dense (i.e. there are no large gaps of missing $\hat{\tau}$ values). When there is a large gap around the inflection point, the accuracy of the slope estimate suffers. Needless to say, alternative forms of curve fitting should be compared in the future. A form of parameterized curve fitting would certainly improve the accuracy of $\frac{d\tau}{dt}$ estimates, but so far has not been examined.

Finally, for cases involving multiple vehicles, the total number of peaks to track (N_{peaks}) must be selected. Once the length of the correlation interval ($T_{win} = \frac{W_{size}}{f_s}$) is established, if the signal from a single vehicle in the gate ($\pm\Delta$ samples) appears distinct (i.e. the autocorrelation has a high, narrow mainlobe and small sidelobes), then tracking the first two or three peaks should be sufficient. Experimental results indicate that for $N_{peaks} = 3$, fairly accurate speed estimates were obtained for most of the multiple vehicle cases studied.

Chapter 5

Conclusions

5.1 Future Work

This thesis describes a passive acoustic traffic sensing scheme based upon measuring differences in signal arrival time with a three-element microphone array. Continuing efforts will focus on several goals which can be divided into four areas: exploring new ideas, formalizing the current algorithm, improving estimates, and evaluating sensor performance under varied traffic and weather conditions.

In order to increase sensor versatility, new investigations will be directed toward enhancing its capabilities. An immediate research focus is the development of an accurate means of determining R_y. It was shown experimentally that the hyperbolic RDL technique returned extremely biased $\hat{R}$ and $\hat{\beta}$ when given noisy time delay estimates. Likewise, the LOCA algorithm, which also generated biased position estimates[1], appeared somewhat less sensitive to measurement noise. Determining source location from the intersection of conic axes from two widely separated triads may prove more robust. Conceivably, implementation of an extended Kalman filter could improve position estimates from *both* the hyperbolic RDL and LOCA ranging methods by compensating for noisy $\hat{\tau}$. Once a dependable ranging technique is found, a means of ascertaining the number of sources in the detection zone will be sought for han-

[1] When source position was pinpointed as a conic focus using a single triad or by the intersection of conic axes specified by two triads in a group of four microphones.

dling multiple vehicle situations. Furthermore, a method of classifying vehicles from their acoustic signatures is desired. Analyses using short-term Fourier transforms (STFTs) or wavelets could provide an approach for attacking these problems. Applications of STFT theory and wavelet analysis to vehicle sensing are briefly discussed in Appendix D. An additional topic for discussion is the incorporation of new sensor elements such as ultrasonic microphones, parabolic reflectors, or acoustic identifiers (described in Appendix A). Finally, processor architectures enabling real-time operation should be examined. The availability of inexpensive, powerful, "off-the-shelf" hardware enables even complex processing algorithms to be implemented cheaply, offering a great deal of flexibility for algorithm improvements.

Before processor implementation can be considered, details of the current algorithm must be formalized. Up until now, separation of the overall τ vs. time curves into segments reflecting individual vehicle motion was done visually. Likewise, selection of supplemental points for inclusion required human intervention. An objective procedure for performing these operations will be formulated in the future.

Algorithm performance would improve given more precise measures of intermediate parameters ($\hat{\tau}$ and $\frac{d\hat{\tau}}{dt}\,|_{\tau=0}$). Analyses which quantify tradeoff issues would permit optimization of sensor parameter settings. In addition, the inclusion of statistical prefilters would increase SNR by reducing the effects of sensor and background noise yielding better $\hat{\tau}$. An alternate means of computing τ which was not examined in this thesis involves the complex cepstum [2]. It remains to be seen if cepstral methods will generate more precise $\hat{\tau}$ than the cross-correlation technique. Lastly, for better measurements of $\frac{d\hat{\tau}}{dt}\,|_{\tau=0}$, parameterized curve fittings should be attempted and the results compared with those from polynomial curve fitting.

Once the sensor algorithm has been refined, road data reflecting a broader variety of traffic and weather conditions will be collected for evaluating sensor performance. Radar guns may be incorporated to verify vehicle range and speed. Additional data should be obtained from different multiple lane roads (such as highways) under heavier traffic conditions (such as stop and go traffic). Furthermore, there is particular interest in assessing the feasibility of using acoustic sensors in tunnels given the pres-

ence of multipath echoes. Sensor effectiveness in adverse weather conditions such as rain and wind should also be studied. Windscreens and moisture protection will be incorporated into the design of the sensor package.

5.2 Summary

In this thesis, the ground work has been laid for the development of a passive acoustic traffic sensor for measuring vehicle speed, range, and heading (direction) on multiple lane, bidirectional roadways. An algorithm has been proposed for processing time delay estimates from a triple-aperture microphone array to extract the desired information, and experimental work has been conducted to assess its potential using real traffic data.

For "dense" individual $\hat{\tau}$ vs. time plots, the algorithm returns excellent results. Once again, a dense plot implies that there are few large gaps in the $\hat{\tau}$ vs. time curve, especially around the inflection point. Once the curves are separated[2], it is a trivial matter to determine a vehicle's heading by examining the sign of the slope of the $\hat{\tau}$ vs. time curve. Furthermore, if an accurate range estimate (R_y) can be found, the algorithm provides excellent speed estimates in instances where only one vehicle is in the detection zone. In multiple vehicle cases, simple situations involving the simultaneous detection of two vehicles were analyzed. For vehicles traveling closely in the same lane or those which *pass* each other (headed in the same or opposite directions), it appears that the τ vs. time curves for individual vehicles are visually separable and can be augmented with τ estimates from subpeaks to generate sufficiently dense plots. When vehicles travel side-by-side in the same direction at similar speeds, it is difficult to distinguish them from a single vehicle by just viewing the $\hat{\tau}$ vs. time curve. In the future, multiple vehicle situations will be examined in greater detail.

Techniques for determining R_y include hyperbolic range difference location (RDL),

[2] A nonvisual procedure for partitioning overall τ vs. time plots into segments reflecting individual vehicle motion has not been investigated at this time.

the LOCA algorithm, and model-based estimation with the extended Kalman filter (EKF). For hyperbolic RDL, location is computed from the intersection of hyperbolic lines of position specified by τ estimates from microphone pairs. At least two pairs are necessary for determining a source's position. For an equally-spaced colinear array, range (R) and bearing (β) can be calculated from two simple nonlinear equations. In practice, however, noisy $\hat{\tau}$ return strongly biased $\hat{R}$ and $\hat{\beta}$ which makes hyperbolic RDL unreliable. Alternatively, the LOCA algorithm is an RDL technique where source location on a *linear* line of position is fixed by time delays between three *noncolinear* microphones. Experimental results from several three-element configurations suggest that determining source position as the focus of a conic is also sensitive to measurement noise. However, when a single vehicle's position was tracked through the detection zone, *some* of the R_y reported were accurate.[3] Improved results may be obtained by adjusting the microphone configuration, moving the array closer to the road, or by considering the intersection of conic axes for two widely separated triads (i.e., by using six microphones). A third alternative for determining vehicle position is the EKF, which is a standard technique for tracking parametric changes using sensor measurements and a model of system dynamics. A well-designed Kalman filter will potentially yield reliable R_y and speed estimates because it accounts for measurement errors in the $\hat{\tau}$. EKF methods will be explored in the future once statistical analyses of time delay estimation noise have been conducted.

Despite the current lack of a reliable range-finding algorithm, the proposed acoustic sensor shows great promise for future IVHS applications. The sensing technique evaluated in this thesis has proven quite powerful. Even without a means of measuring R_y, a sensor comprised of only two microphones can monitor a bidirectional roadway with a single lane of traffic in each direction.[4] Current efforts are directed toward

[3]It is difficult to determine which values are correct from the plot. For single triads where the conic focus is sought, most of the accurate $\hat{R}_y$ values were returned while the vehicle was close to the center of the detection zone (presumably where the conic determined by the three locations is an ellipse).

[4]For this type of roadway, R_y for the near lane and the far lane are known. Since direction of travel is determined from the slope of the τ vs. time curve, speed can be calculated using the appropriate value of R_y.

developing an accurate means of measuring R_y. Once a suitable localization method has be found, continuing research will focus on expanding the sensor's capabilities. The ultimate objective is the design of a low-cost, reliable sensor for monitoring *multiple* lane, bidirectional roadways. With this passive acoustic traffic sensor, that goal no longer seems an impossibility.

Appendix A

Acoustic Identifiers

Processing could be greatly simplified by equipping vehicles with acoustic identifiers. The term acoustic identifier will refer to an object which emits acoustic energy at a known frequency or frequencies. These identifiers could be either passive or active.

A passive acoustic identifier which could be useful is an ultrasonic whistle. Ideally, the whistle should resonate at a single or double frequency above the audible range of both humans and animals and have a measurable transfer function between air speed through the whistle (which is essentially the vehicle speed) and its acoustic intensity. Different vehicle types could be equipped with acoustic identifiers which resonate at distinct frequencies (allowing classification). An active alternative to the mechanical whistle is an electronic transmitter. It would provide similar benefits, but would be fundamentally more difficult to implement.

Ultrasonic whistles are attractive because the cost of manufacturing and installing the identifier would be extremely low, yet their use could yield substantial savings from the reduced number of sensors and simplified processing scheme. The sensor could be a single microphone whose output is passed through a matched filter. If the total power in the resulting signal exceeds a threshold, the vehicle is "detected". Its speed can be determined from the whistle's transfer function or by measuring the Doppler shift using STFTs (since there isn't much ultrasonic background noise). It remains to be seen if it is possible to design such a whistle.

Despite savings in sensor complexity, there is a major cost issue if acoustic iden-

tifiers are incorporated. Although a large number of sensors will be employed by IVHS to collect traffic data, there are significantly more vehicles than sensors. Even if the identifiers only cost a few cents apiece, the expense of placing them on *every* vehicle might outweigh the savings offered by the simplified sensors. For this reason, an algorithm which did not rely on acoustic identifiers was pursued.

Appendix B

Circuit Diagrams

This Appendix includes circuit diagrams for the microphone amplifiers, the ADXL50 amplifier, and the anti-aliasing filters.

The amplifier circuit designs for the Radio Shack microphones, the Sennheiser microphones, and the ADXL50 accelerometer are provided in Figures B-1, B-2, and B-3 respectively. They exhibited the same general structure: ac coupling, gain, then filtering with two-pole Sallen-Key circuits.

The circuit diagram for the ultrasonic microphone amplifier is a modified version of the one suggested in the specification sheet. The final design appears in Figure B-4.

Simple lowpass filters served as anti-aliasing filters. The circuit diagram for a standard two-pole Sallen-Key filter is shown in Figure B-5. The cutoff frequency (f_c) is determined by the RC product. For the audible range microphones, f_c was set at 12 kHz for the data from Road Test Two and 10 kHz for the data from Road Test Three.

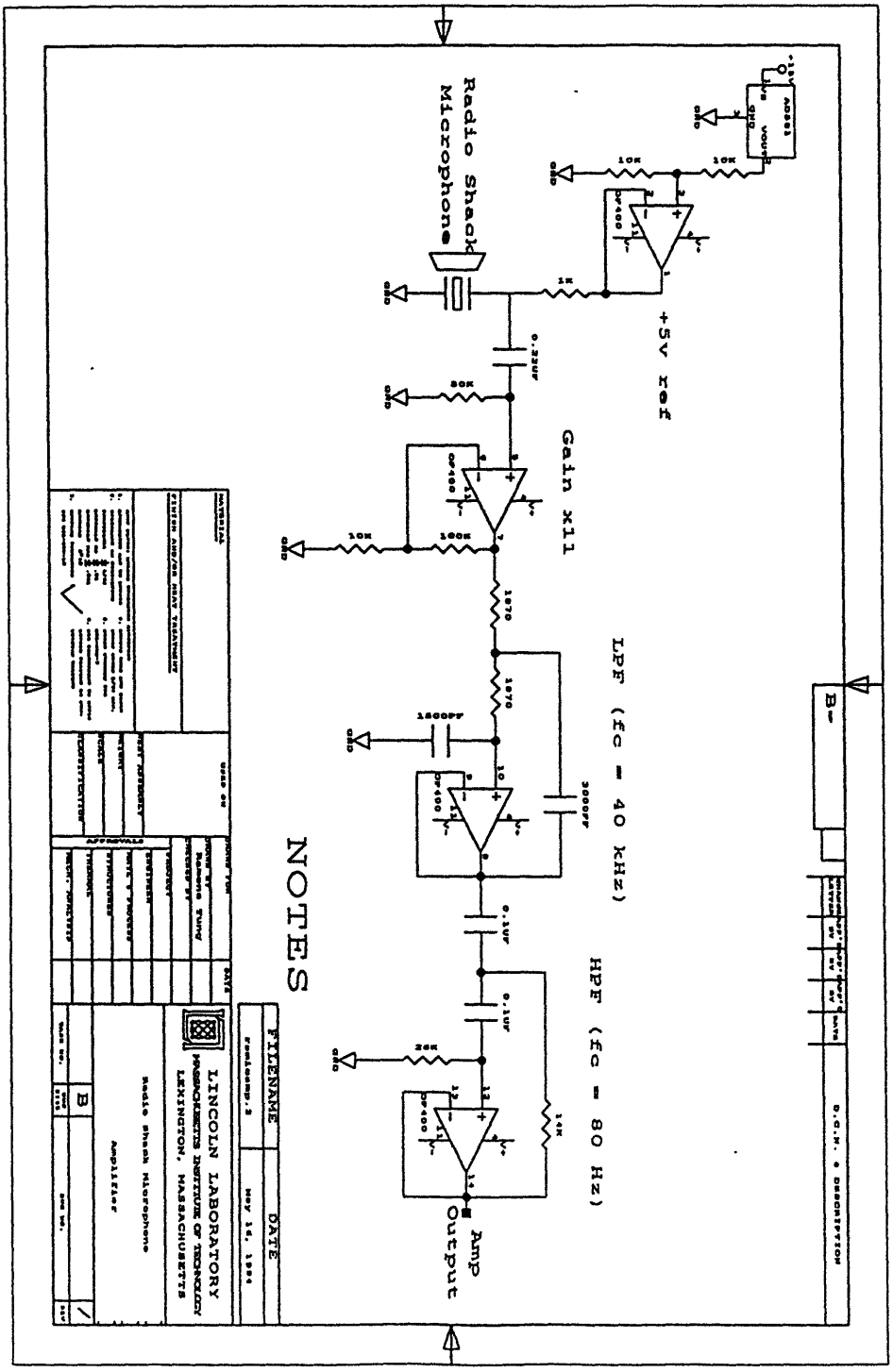

Figure B-1: Circuit diagram for Radio Shack microphone amplifier

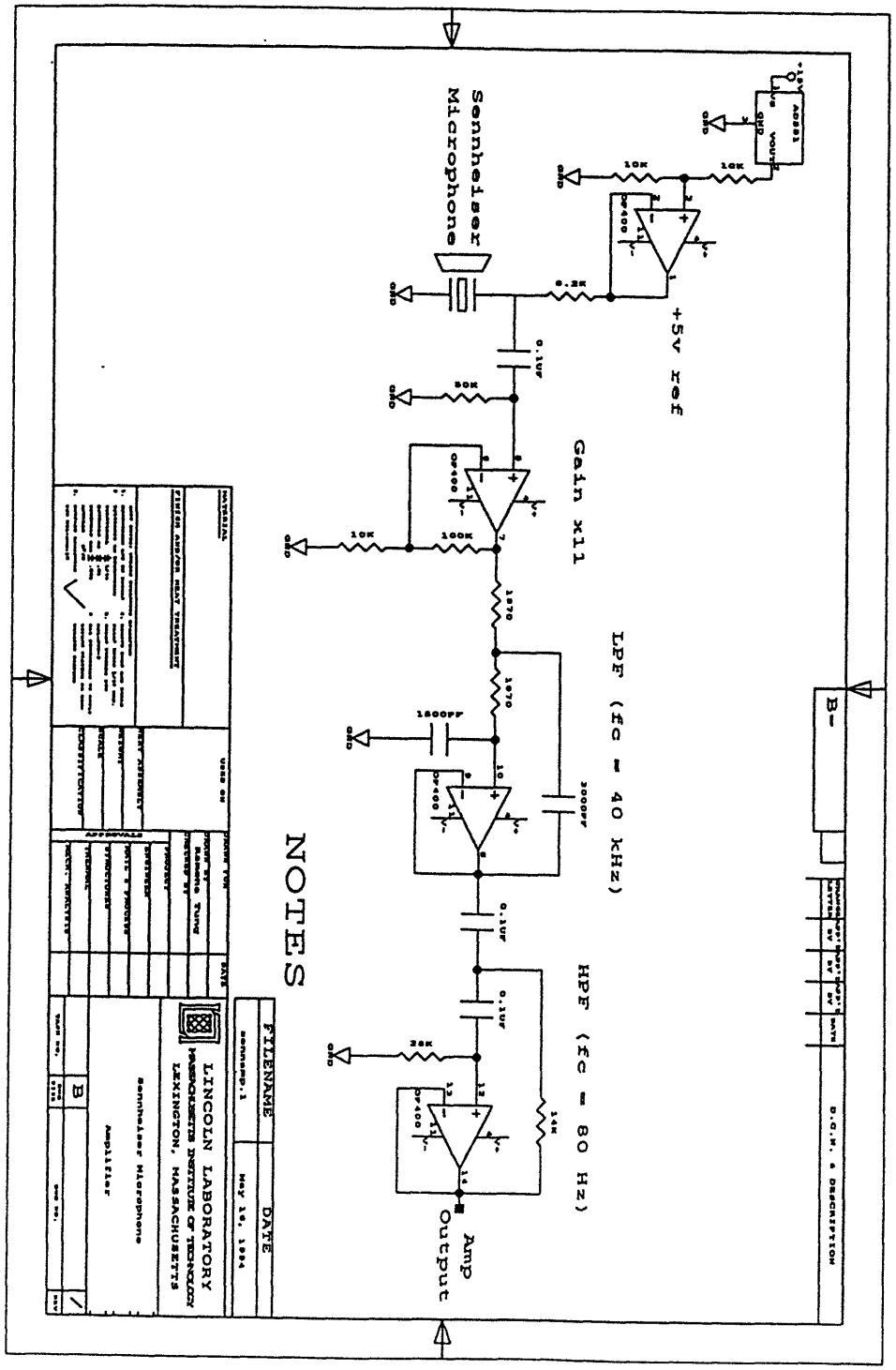

Figure B-2: Circuit diagram for Sennheiser microphone amplifier

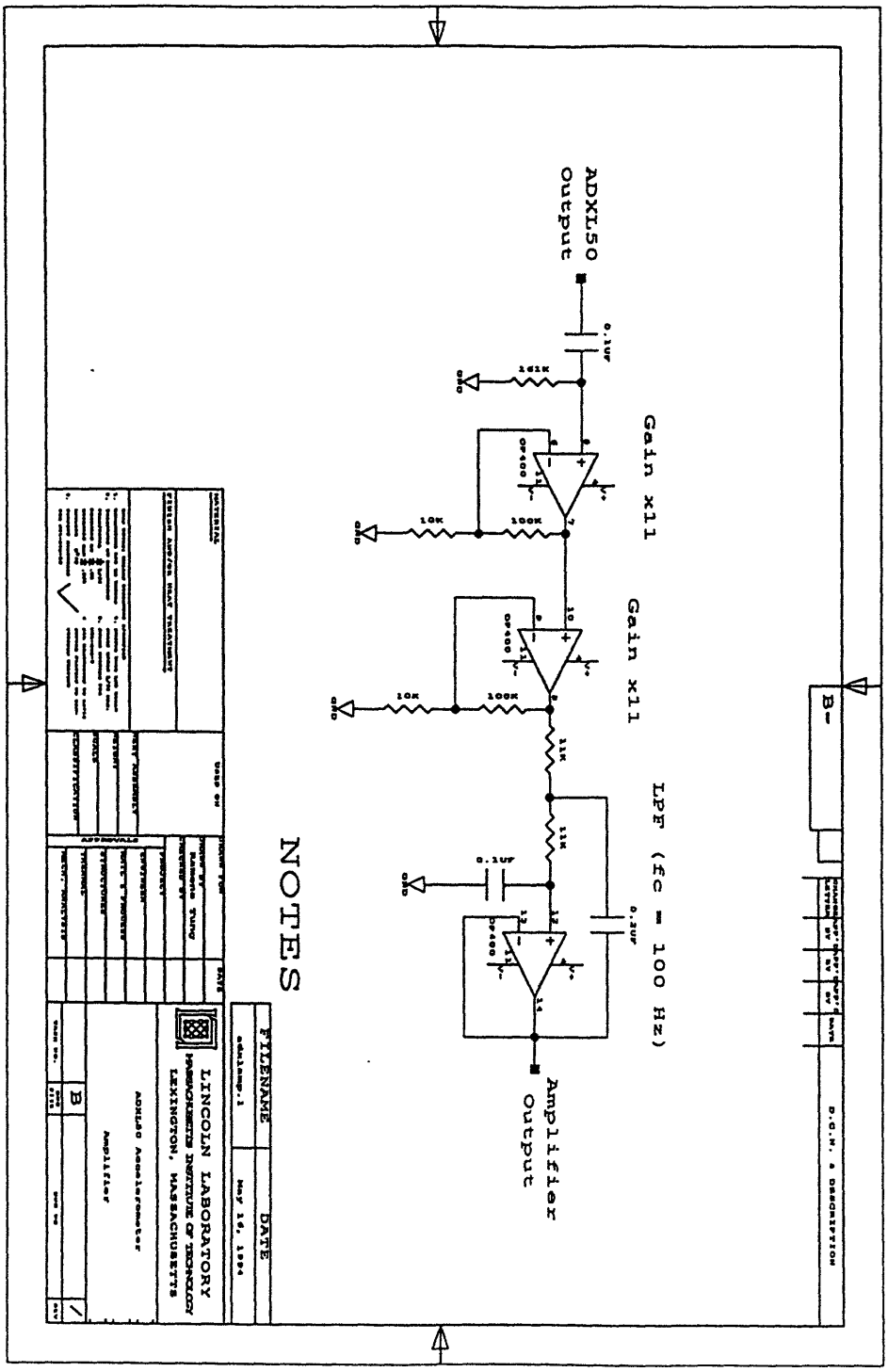

Figure B-3: Circuit diagram for ADXL50 accelerometer amplifier

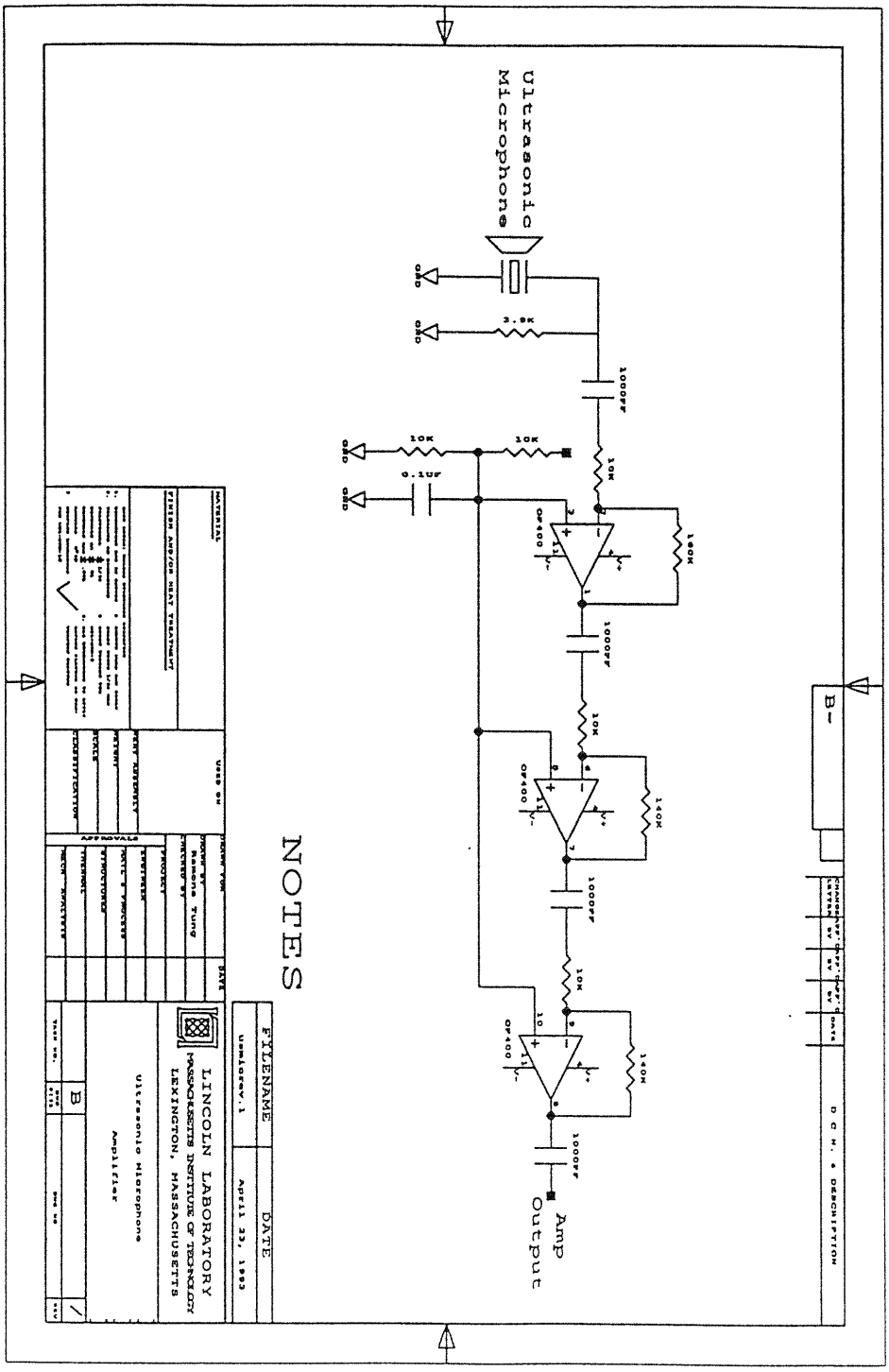

Figure B-4: Circuit diagram for Murata-Erie ultrasonic microphone amplifier

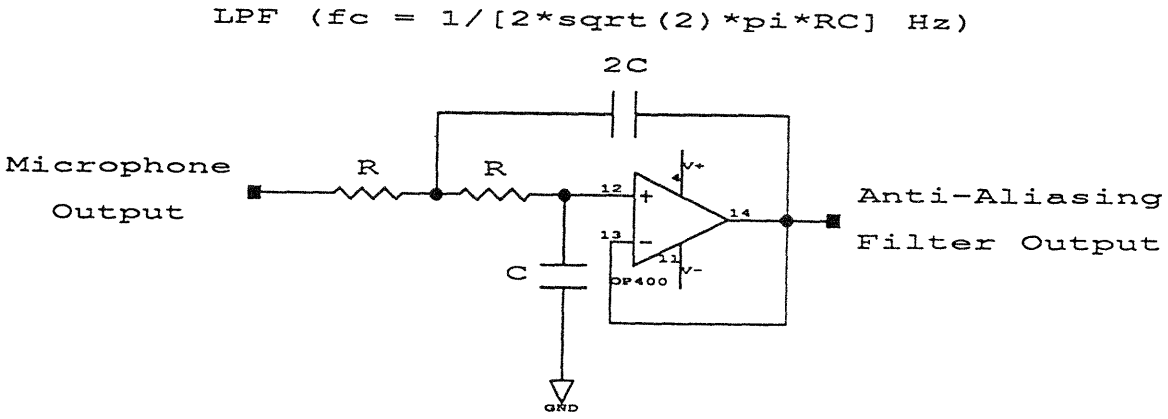

Figure B-5: Circuit diagram for anti-aliasing filter

Appendix C

Verification System

In Field Test One, speed verification was supplied by two air hoses spaced one meter apart and associated digital circuitry. The first hose the vehicle encounters is designated "A" and the second, "B". When a vehicle's wheels run over a hose, a "pulse" of air is generated which causes an air switch at the end to generate a low TTL pulse. The air switch outputs are first debounced using a simple finite state machine (FSM) before being sent to another FSM which provides control signals for supporting digital hardware. Both FSMs were realized by programmable array logic (PAL) devices.

Since the air switches are sensitive to pulses of air, they must be debounced to avoid false triggering by reflections from the ends of the hose. The simple four-state FSM which performs the debouncing operation appears in Figure C-1. Whenever a transition occurs at a switch output, the FSM determines whether it is a true pulse by setting a timer realized by an RC circuit. If the signal reverts to its original state before the timer runs out, the pulse is considered a transient. If the timer expires before the signal transitions again, the output is considered a true pulse.

The control PAL implements a simple nine-state FSM which is described by the flow chart in Figure C-2. Upon receiving a true pulse from A indicating that vehicle's front wheels have crossed, a digital counter is started. The next pulse from B stops the counter and allows the value (which is a multiple of the circuit clock period) to be stored in memory. While the FSM "waits" for the rear wheels to cross both hoses (another set of two pulses), the memory address register (MAR) is incremented and

the counter is reset. When the next experiment is ready, the FSM is reset and the process repeats. If the memory fills up (which only happens after 256 tests), a flag stops the FSM from overwriting values from earlier tests. Once testing is completed, manual address switches are set to access stored count values. When the count values are converted to seconds by dividing by the clock rate, the reciprocal corresponds to vehicle speed in meters per second (since the hoses were separated by one meter).

Circuit diagrams for the debounce and verification control circuitry are provided in Figures C-3 and C-4 respectively. A photograph of the actual hardware appears in Figure C-5.

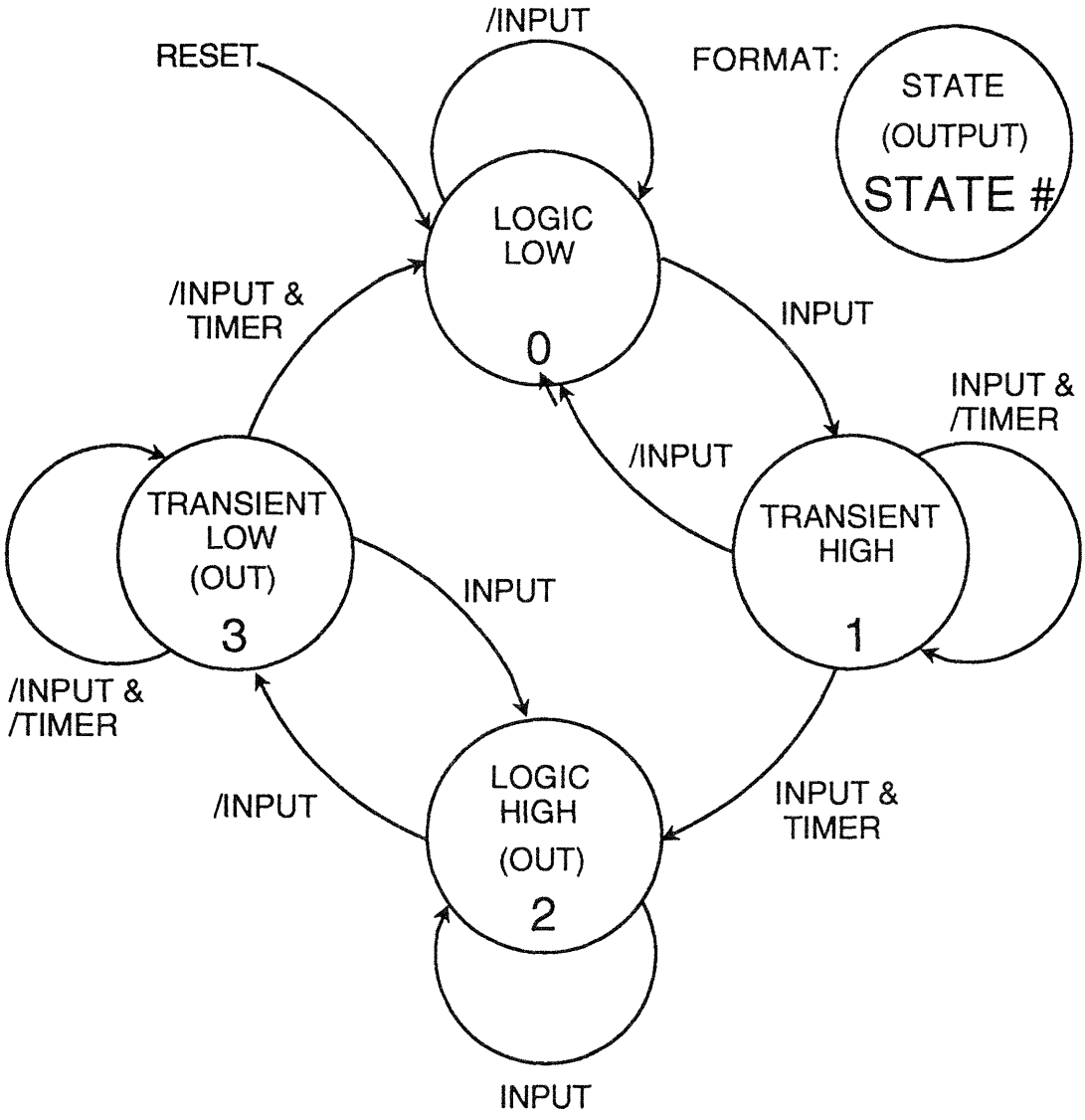

Figure C-1: Debounce PAL finite state machine

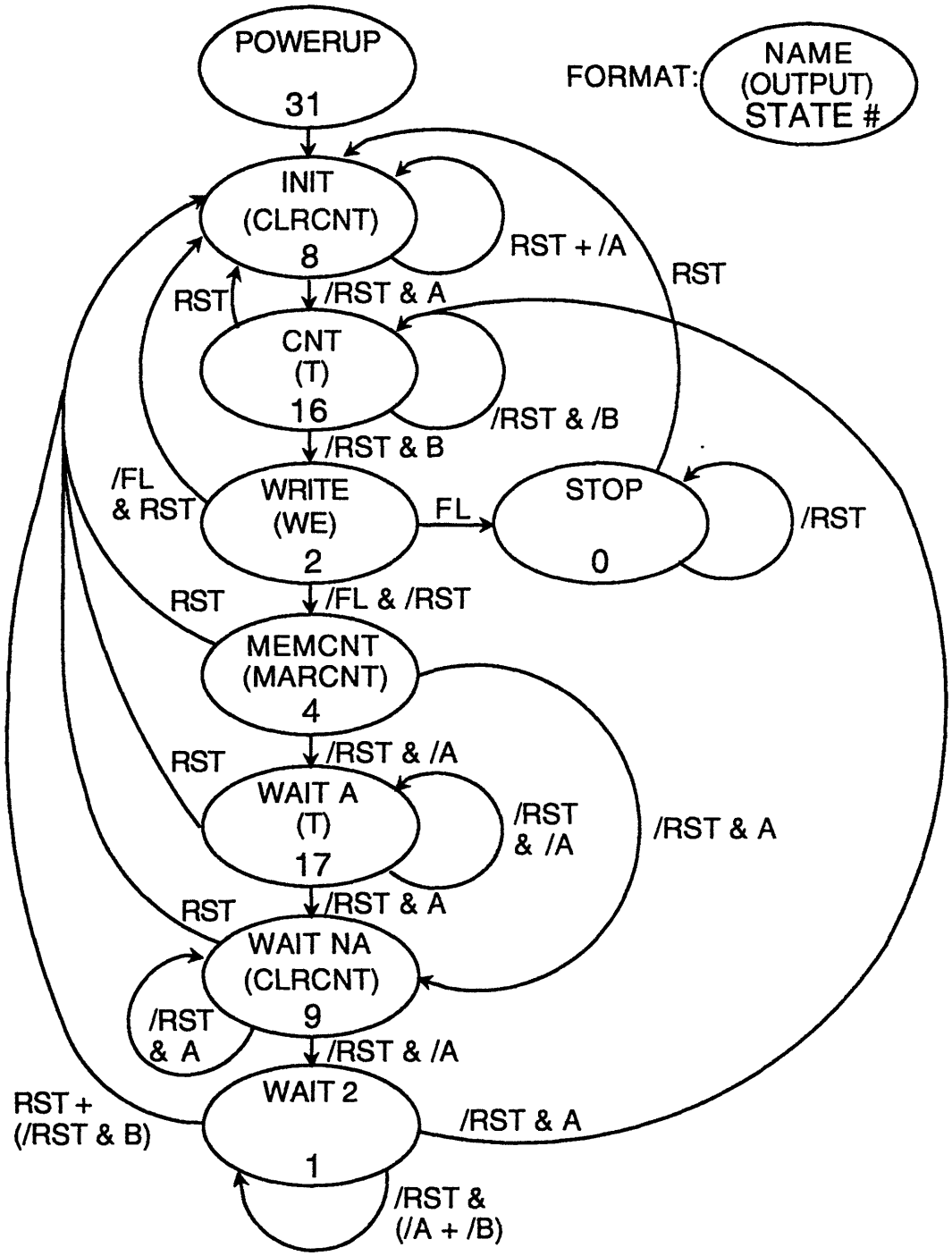

Figure C-2: Control PAL finite state machine

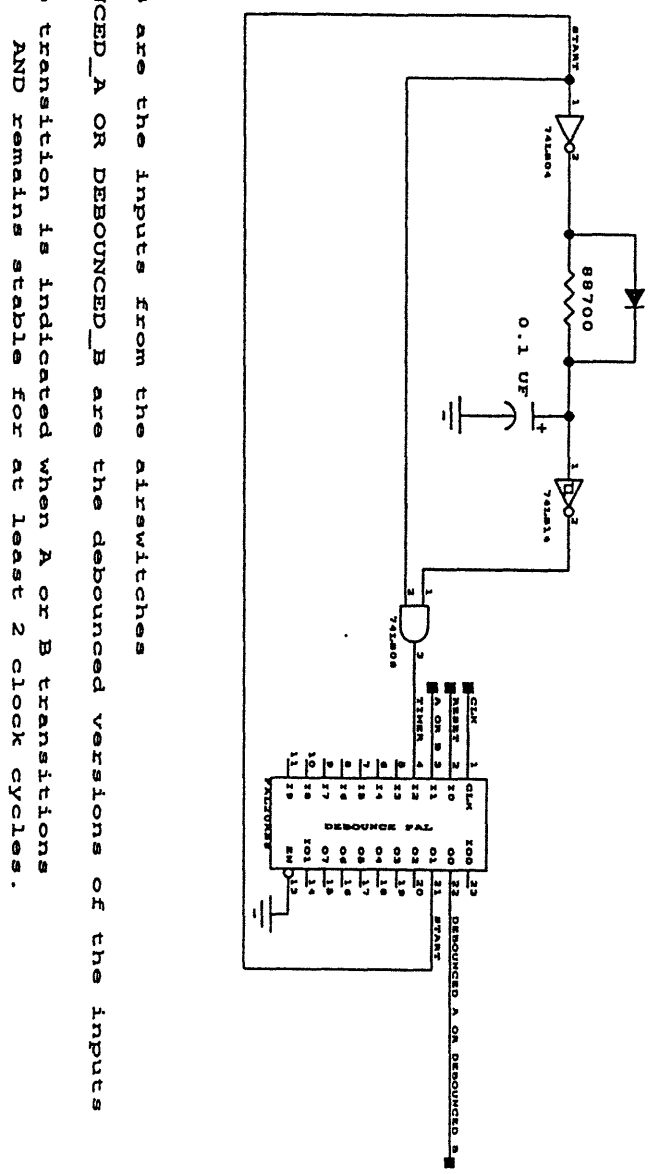

A OR B are the inputs from the airswitches

DEBOUNCED_A OR DEBOUNCED_B are the debounced versions of the inputs

A true transition is indicated when A or B transitions
AND remains stable for at least 2 clock cycles.

Figure C-3: Diagram of the debounce circuit for Field Test One

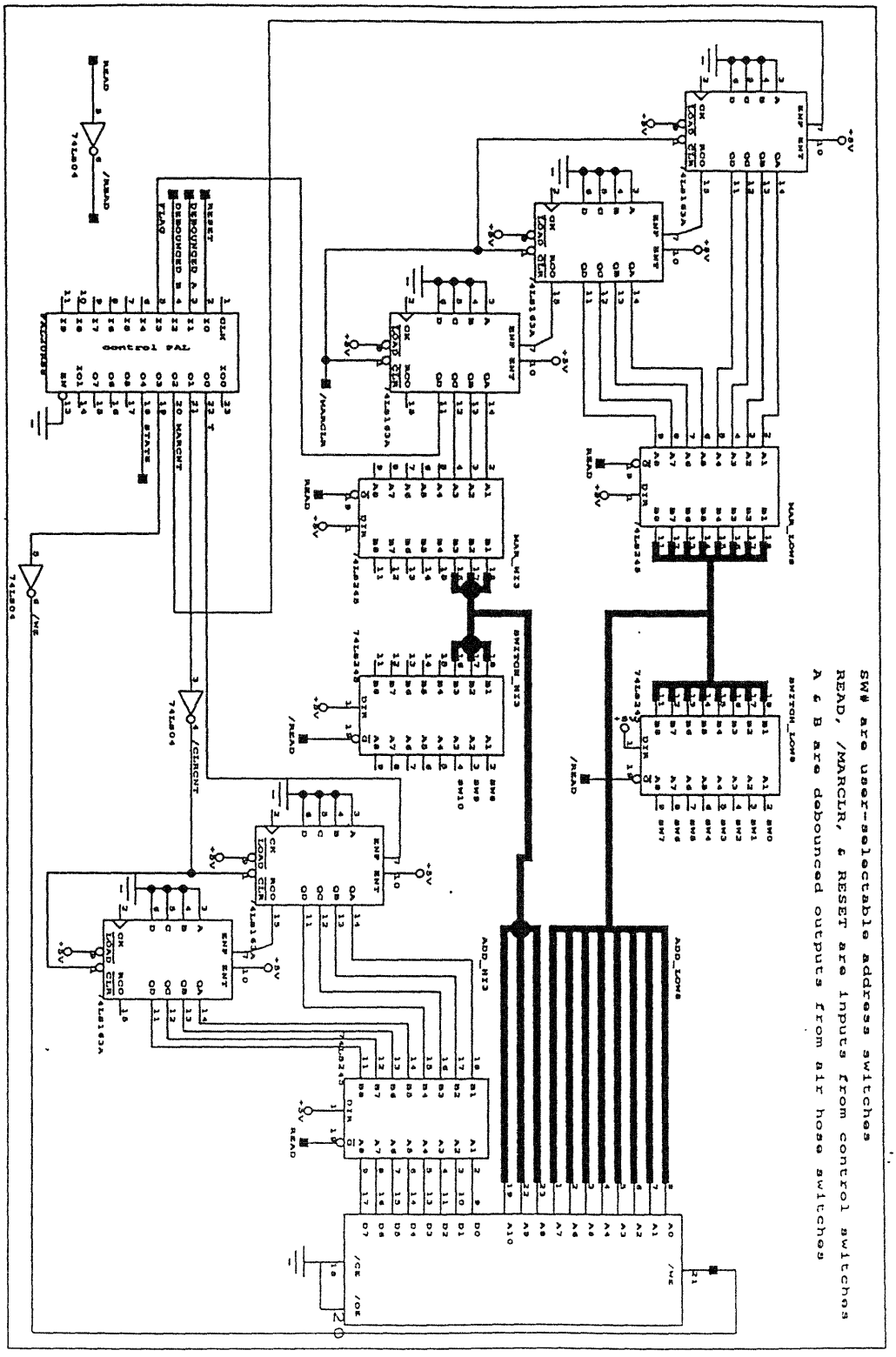

Figure C-4: Diagram of the verification control circuit for Field Test One

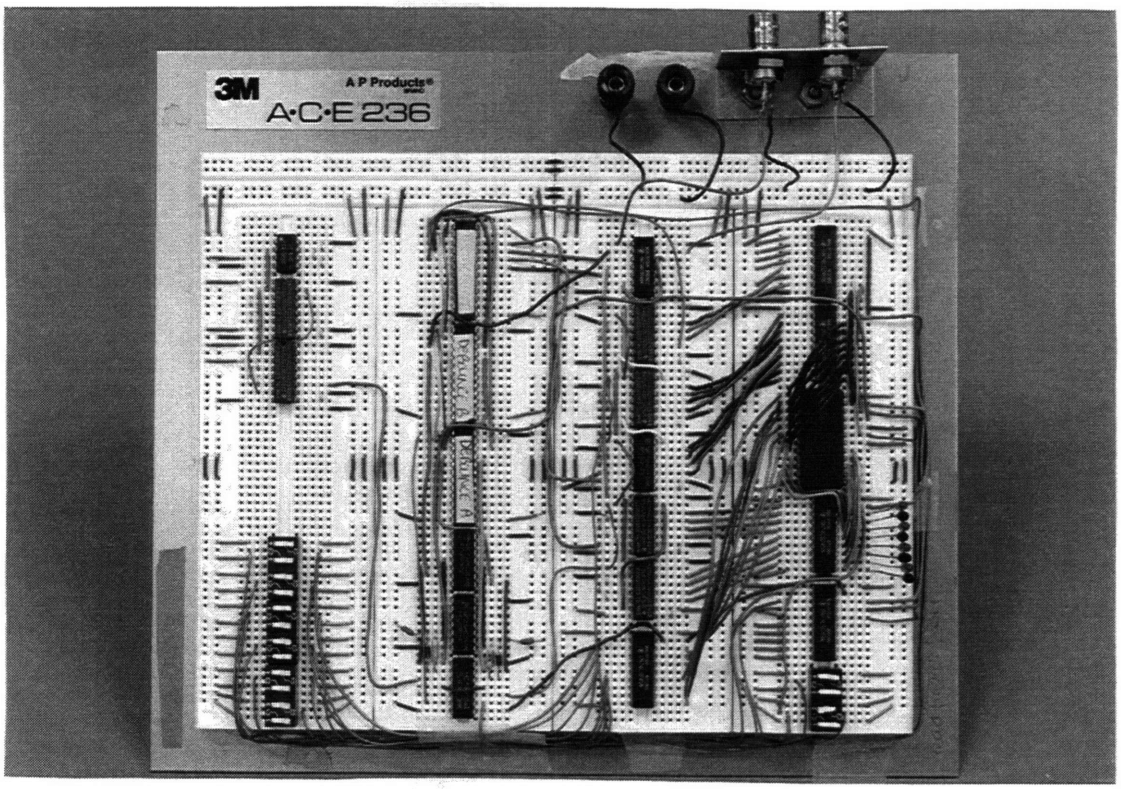

Figure C-5: Photograph of hardware for the verification system of Field Test One

Appendix D

Alternative Algorithm Approaches

The current traffic variable estimation algorithm is based upon tracking the change in time delays between pairs of microphones over successive correlation windows. Because of the non-stationarity of the acoustic source signal, time/frequency processing methods were also considered, including short-term Fourier transforms (STFTs) and wavelet analysis. STFT and wavelet theory as applied to the traffic sensing problem are discussed briefly below. Though presently rejected, these methods (and others) will be reconsidered in the future when addressing the vehicle classification problem.

D.0.1 Short-Term Fourier Transforms

Short-term Fourier transforms (or spectrograms) emphasize frequency domain analysis of short consecutive windowed data segments. In addition to signal frequency content, *trends* observed over a series of windows provide important clues for identifying source parameters. Theoretically, Doppler shifts can be observed by tracking dominant peaks if the frequency resolution (Δf_{res}) is fine enough.

Both the STFT and cross-correlation window size are subject to the same quasi-stationarity constraints. Once again, frequency spectrum resolution ($\Delta f_{res} = \frac{f_s}{W_{size}}$) is inversely proportional to the length of the observation interval. However, for STFTs, *fine* resolution is desired since the content of the frequency spectrum is important. This requires a large W_{size} which adversely affects stationarity. The

stationarity/resolution tradeoff is one of the major limitations of using STFTs.

Another factor which discourages the use of the STFT is the computational requirement. Disregarding the fractional overlap between windows (α), the number of operations needed to compute the spectrogram of a signal is comparable to the number required for generating the time delay record. However, the *processing* necessary for each STFT will be more involved than the simple peak searches over $2\Delta+1$ values required by delay estimation. Likewise, if parameter trends over successive windows must be tracked, STFTs will demand a great deal of memory (and organized indexing).

Analysis of the audible range spectrograms of different vehicles revealed wideband spectra without apparent universal peaks which could be tracked for Doppler shifts.[1] STFTs and frequency domain analysis are definitely under investigation for vehicle classification. However, for speed estimation, they were set aside in favor of the current algorithm for its simplicity.

If acoustic identifiers (see Appendix A) are employed in the future, the Doppler shift of the narrowband signal could be measured using STFTs for speed determination. Returning to τ estimation, once the speed is known, R_y is found directly using Equation 4.3 for lane discrimination. Depending on its performance, this approach could reinforce (or replace) the current speed/range estimation algorithm.

D.0.2 Wavelet Analysis

Application of wavelet theory was also proposed as an alternative to time delay tracking. Wavelets are especially interesting for wideband signal analysis because of their variable resolution properties. Furthermore, they are useful for modeling space and/or time-varying (STV) systems. This section briefly describes wavelets and their possible applications to the traffic sensing problem. Deeper discussions of wavelet theory can be found in [1] [8].

A wavelet (or "little wave") is a special oscillatory signal whose envelope decays

[1] Except for the possible low frequency spike mentioned in Section 3.2.1.

quickly to zero. Signals or systems are represented by coefficients associated with a *particular* wavelet set where each element is a scaled (dilated or compressed) and translated (shifted) version of the original wavelet (termed the *mother wavelet*). All wavelets in a set are normalized to have the same energy and can be expressed in the form:

$$s(t) = \frac{1}{\sqrt{a}} g\left(\frac{t-b}{a}\right) \tag{D.1}$$

where g(t) is the original mother wavelet with "a" representing the scale[2] and "b" the translation. For a *specific* mother wavelet, wavelet coefficients, W_gf(a,b), are generated by correlating the signal with corresponding scaled (a) and translated (b) versions of the original. The coefficient represents the degree of correlation between the signal and the scaled, translated wavelet. Depending on the choice of mother wavelet, different information about the signal f(t) can be extracted.

A primary advantage of using wavelets over STFTs is their variable frequency resolution. Namely, for wavelet transforms, the *relative* frequency resolution ($\frac{\Delta f_{res}}{f}$) remains constant, whereas for STFTs the *absolute* frequency resolution (Δf_{res}) is the same for all frequencies. Wavelets offer flexibility in the tradeoff between resolution and processing time. In general, for a vehicle's wideband acoustic spectrum, wavelets provide fine resolution at low frequencies where it is needed and coarse resolution at high frequencies where it is not as critical.[3] On the other hand, for the same processing interval (T_{win}), STFTs exhibit a constant average resolution over the entire spectrum. In order to achieve high resolution, the observation interval must be lengthened by increasing W_{size}, which affects stationarity and increases processing time.[4]

Because the Doppler effect is directly proportional to frequency (i.e. small for low frequencies and large for high frequencies), the wavelet domain (where resolution is also proportional to frequency) seems a more appropriate choice for analysis than the Fourier domain. Ideally, a wavelet set which maps wideband, nonlinear Doppler

[2] $\frac{1}{\sqrt{a}}$ is the normalization term.

[3] Fine resolution at high frequencies can be achieved by using "sophisticated" mother wavelets which have a time-bandwidth product that is significantly greater than one.

[4] Technically, since $T_{win} = \frac{W_{size}}{f_s}$, the same effect could be realized by reducing the sampling rate, but doing this has other repercussions.

shifts in the frequency domain into measurable linear shifts in the wavelet domain is sought for speed determination. However, other wavelet sets could be equally informative. Along with possibilities for speed measurent, viewing various wavelet transforms (using different mother wavelets) of a microphone's output may provide insight toward the vehicle classification problem.

Another potential application of wavelets is toward modeling the distortion experienced by the source signal with a space/time-varying (STV) system. System modeling using wavelets is discussed in [8]. An STV system representation could account for the distortion introduced by source motion where the input is the vehicle's actual acoustic spectrum and the output is the signal received by the microphone. It seems conceivable to approximate the Doppler shift as some form of time-scaling operation. Further research may be conducted to evaluate the feasibility of this theory.

Bibliography

[1] Ingrid Daubechies. *Ten Lectures on Wavelets.* Society for Industrial and Applied Mathematics, 1992.

[2] Joseph C. Hassab. *Underwater Signal and Data Processing.* CRC Press, 1989.

[3] *Surface Transportation and the Information Age: Proceedings of the 1992 Annual Meeting of IVHS AMERICA*, May 1992.

[4] A Revolutionary Solution for Traffic Sensor Needs. AT&T, December 1993.

[5] AT&T SmartSonic^{TM} Traffic Surveillance System. AT&T, January 1994.

[6] Intelligent-Vehicle Highway Society of America. Strategic Plan for IVHS in the United States. Technical Report IVHS-AMER-92-3, IVHS America, May 1992.

[7] Ralph O. Schmidt. A new approach to geometry of range difference location. *IEEE Transactions on Aerospace and Electronic Systems*, 8(6):821–835, November 1972.

[8] Randy K. Young. *Wavelet Theory and Its Applications.* Kluwer Academic Publishers, 1993.